MECHANISMS OF CHEMOTHERAPEUTIC RESISTANCE IN GLIOMA: MATHEMATICAL MODELING AND GENE EXPRESSION PROFILING

by

SALAHELDIN S. HAMED

A Dissertation submitted to the

Graduate School-New Brunswick

Rutgers, The State University of New Jersey

and

The Graduate School of Biomedical Sciences

University of Medicine and Dentistry of New Jersey

in partial fulfillment of the requirements

for the degree of

Doctor of Philosophy

Graduate Program in Biomedical Engineering

written under the direction of

Charles M. Roth

and approved by

_____

_____

_____

_____

New Brunswick, New Jersey

May, 2010

ABSTRACT OF THE DISSERTATION

MECHANISMS OF CHEMOTHERAPEUTIC RESISTANCE IN GLIOMA:

MATHEMATICAL MODELING AND GENE EXPRESSION PROFILING

By SALAHELDIN S. HAMED

Dissertation Director:
Charles M. Roth

Gliomas are refractory to chemotherapy because of acquired resistance, which is associated with changes in important cellular processes, such as cell cycle kinetics and cell death. The mechanistic relationship between resistance markers and failure of chemotherapy remains to be elucidated. To that end, identification of biological systems and their interactions is of great promise.

We characterized the pharmacological response of glioma cell lines to chemotherapeutic drugs, carmustine and etoposide. We developed a cell cycle structured mathematical model that reproduces the dynamics of dose response of cells to the two chemotherapeutic agents based on two parameters relating to cell cycle arrest and cell death. We have shown that the model can provide a quantitative distinction between the influence of these two processes on tumor cells simply from pharmacological dose response curves, from which mechanism is not obtained using traditional analyses. The model suggests that carmustine elicits its effect via cell death, while etoposide primarily

induces cell cycle arrest. We have also applied this methodology to track acquisition resistance to chemotherapy.

We have generated a panel of glioma cell lines resistant to carmustine by incremental stepwise exposure to sublethal doses of the drug. To characterize molecular events underlying response of resistant and parent cell lines to carmustine, we performed gene expression profiling using micaroarrays followed by functional network analysis. We found that NFκB activation is implicated in the response to carmustine, and resistant cells exhibit increased survival mediated by inflammatory responses. In addition, resistant cells induce genes promoting cell cycle arrest and repress genes implicated in cell cycle phase transitions and proliferation. In agreement with gene expression results, we found that resistant cells exhibit decreased cell death and rapid and efficient arrest. We have characterized the DNA repair capacity, which is known to modulate cell cycle arrest and apoptosis.

Our results provide insights into molecular pathways involved in resistance to carmustine *in vitro*. If they prove to hold for gliomas in human patients, these results can point the way towards improved therapeutic regimens that act upon NFκB mediated cell survival module in concert with cell cycle checkpoint abrogators.

ACKNOWLEDGEMENT

I would like to acknowledge Professor Charles M. Roth, Charlie, who has been an outstanding mentor throughout my years at Rutgers University, both as an undergraduate and graduate at the Biomedical Engineering program. I am deeply indebted to his support, insight and, patience. I would also like to thank former members of the Roth lab: Dr. Joseph L. Vitolo, who was a constant source of inspiration through his youthful and resilient personality, Dr. Li Kim Lee and Dr. Sumati Sundaram, whose work ethic is a model to emulate, and Michelle Burley. I would also like to acknowledge current members of Roth Lab: Aina Andrianarijoana, who taught me great deal of molecular biology, Lavanya Peddada, Carolyn Waite, Dominik Naczynski, Dr. Hong Yang, and Dr. Vidya Iyer, all of whom made life much more enjoyable around the lab.

I would like to thank my committee members who always made themselves available whenever I requested help or advice. I would also like to thank the larger BME family for their help throughout my years at Rutgers: Dr. Prabhas Moghe, Dr. Linda Anthony, Dr. Marianthi Irapetritou and BME administrative staff.

I would like to thank Theresa Choi at EOHSI Flow Cytometry Lab, Dr. Emmanuel Zachariah at UMDNJ Tumor Biology Lab, and Dr. Paul Van Hummelen at EOHSI for help with various assays.

I would like to thank my friends who made my graduate school experience much more rewarding and enriching: Dr. Mohamed D. Arafa, Dr. Yahia M. Tokal, Dr. Mohamed H. Nazier, Ahmed Turk, Dr. Ashish Misra, Dr. Gary Monteiro, and Dr. Michael Wininger.

Finally, I would like to dedicate this work to my family who consistently supported and inspired me. No words can ever express my gratitude to my father (Sobhi Hamed), my mother (Samiha Hammouda), my sister (Dr. Lamiaa Hamed), my brother (Mohamed Hamed) and my Aunt (Nawal Hammouda). I would also like to dedicate this work to my wife, Dr. Rania S. Younes, for her support and encouragement through the last phase of my studies and to my newborn son Mohamed, who has brought much joy and happiness to our life.

TABLE OF CONTENTS

LIST OF TABLES

LIST OF FIGURES

CHAPTER 1

INTRODUCTION

1.1 Significance

Prognosis and Classification of Gliomas

More than 41,000 people are afflicted with primary central nervous system (CNS) tumors per year in the USA. These tumors account for 2.2% of all cancer related deaths [1]. Gliomas represent 42% of primary CNS tumors, 75% of which are malignant [1]. The survival of patients diagnosed with glioblastoma multiforme (GBM), the most malignant form, reaches 6 months for 42.4% of the patients, 1 year for 17.7% of patients, and 2 years for only 3.3% of the patients [1]. Gliomas are one of the main challenges in the field of oncology because of their malignancy, poor prognosis, and failure of treatment modalities [1].

Diffuse astrocytomas are the most common type of primary brain tumors in adults. In terms of pathological classification, they are divided into lower grade astrocytomas (WHO grade II), anaplastic astrocytomas (WHO grade III), and glioblastoma multiforme (WHO grade IV) [2]. Lower grade astrocytoma is the least aggressive but it is still highly infiltrative and possesses a high potential for malignant progression [2]. Gliomas, in general, exhibit characteristics of malignant tumors: aberrant proliferation, evasion of apoptosis, avoidance of external growth control and immunoregulation, and high degree of intrinsic and acquired resistance to therapeutic intervention [2]. The malignant phenotype of gliomas has been linked with a wide range of genetic aberrations; these aberrations have been identified in primary GBM, tumors arising *de novo*, and secondary GBM, tumors arising from lower grade lesions [2,3]. These mutations have been shown

to affect main aspects of cell physiology, such as genomic stability, cell cycle control, apoptosis, and other signaling pathways [2].

Treatment Modalities of Gliomas

Surgery, radiation, and chemotherapy are the three modalities utilized in the treatment of malignant gliomas. The main aim of surgery is resection of the tumor; however, the benefits of resection are limited—in the majority of cases—to reduction of the tumor bulk and obtaining tumor biopsies for pathological analysis. Total resection is not attainable due to the infiltrative nature of gliomas, where they spread several centimeters into surrounding normal brain tissue [2]. In a similar fashion, the infiltrative nature of gliomas limits the effect of radiation on patient outcome [2]. Normally, the volume exposed to radiation includes the enhancing volume (region containing actual tumor tissue), surrounding edema (region containing normal brain tissue infiltrated by microscopic tumors), and a region of normal brain tissue [2]. Thus, a significant portion of normal brain tissue is exposed to radiation, which limits the amount of exposure and, ultimately, tumor control [2].

Chemotherapy, as a treatment modality in addition to surgical intervention and radiotherapy, has the advantage of reaching tumor cells regardless of anatomic location [2]. In addition, many chemotherapeutic agents are not associated with neurotoxic effects; thus, toxicity is only a problem at the systemic level [2]. Most importantly, brain tissue in composed of differentiated cells with limited proliferative capacity; theoretically, chemotherapeutic agents selectively target tumor cells, which have a high proliferative capacity [2].

1.2 Chemotherapeutic Resistance

Similar to other tumors, gliomas are not responsive to chemotherapy because of a high degree of intrinsic and acquired resistance to chemotherapeutic agents. Intrinsic resistance is characterized by lack of initial response to chemotherapy as a result of the presence of some mechanisms in the tissue of origin of the tumor (e.g., P-glycoprotein, which is an ATP-dependent efflux pump) or genetic alterations (e.g. mutations in p53) that render cells resistant to chemotherapy [3]. On the other hand, acquired resistance is marked by an initial response to treatment followed by relapse in the form of a more aggressive tumor that is no longer responsive to the original chemotherapeutic agent [3]. There are, at least, two possible hypotheses for acquisition of resistance *de novo*. First, there may exist a fraction of tumor cells with genetic mutations that result in a resistant phenotype prior to the start of therapy. With prolonged exposure to cytotoxic agents, sensitive cells respond to therapy and resistant ones proliferate to form a tumor mass by monoclonal expansion [3]. Second, exposure to therapy upregulates some resistance pathways or some stress survival mechanisms that enable a fraction of cells to survive during the course of treatment [3].

Several markers of resistance to chemotherapy have been characterized in glioma models. First, ATP-dependent efflux pumps transport cytotoxic agents out of cells by means of transmembrane proteins encoded by multi-drug resistance genes and multidrug resistance- associated proteins (MDR1, ABCB1, MRP, and ABCC1). Second, increased activity of glutathiones and glutathione-related enzyme systems, namely, glutathione-S-transferase increases the detoxification of alkylating agents. Third, increased activity of protein kinase C (PKC) family changes phase transitions in the cell cycle. In addition,

resistance has been linked to the presence of some enzymes that counteract the cytotoxic effect of specific chemotherapeutic agents. For example, O^6-methylguanine methyl transferase (MGMT) removes alkyl groups added to the O^6 position in guanine nucleotides by DNA alkylating agents. Other enzymes such as hydrofolate reductase and thymidilate synthase have been found to contribute to resistance of gliomas to chemotherapy. However, none of these individual markers of resistance is sufficient to explain the complexity of the resistance phenotype. Alternatively, resistance to chemotherapy in glioma models has been attributed to alterations in key cellular processes such as deficiency in DNA repair mechanisms, which renders tumor cells tolerant to methylation; alterations in cell cycle dynamics, which minimizes the fraction of cells in the vulnerable phase; or dysfunction in apoptotic pathways that ensures cell survival upon exposure to chemotherapy regardless of drug-target interaction. Reference [3] provides a comprehensive overview of mechanisms of resistance in gliomas.

1.3 DNA Alkylating Agents: Standard of Care in Glioma Treatment

Alkylating agents: Damage and Repair

The mainstay of chemotherapy in the treatment of malignant glioma is DNA alkylating agents; namely, 1,3-bis (2-chloroethyl)-1-nitrosourea (BCNU) and temozolomide. They elicit their effect by adding chloroethyl (in the case of BCNU) or methyl groups (in the case of temozolomide) to DNA resulting in the formation of O^6-alkylguanine, N^7-alkylguanine, N^3-alkyladenine, and N^3-alkylguanine. In addition, alkylation results in the formation of critical secondary DNA damages [4]. O^6-alkylguanine lesions are repaired by the enzyme MGMT, which transfers an alkyl group from guanine to its cysteine residue (cys 145), while nucleotide excision repair (NER),

base excision repair (BER), and translesion DNA synthesis (TLS) repair N^7-alkylguanine, N^3-alkyladenine, and N^3-alkylguanine lesions [5]. Failure to repair these lesions results in the formation of DNA double strand breaks (DSB), which initiates cell cycle arrest and apoptosis [6]. Resistance to DNA alkylating agents in gliomas, as well as other tumors, has been attributed to either tolerance of tumor cells to damage or increased capacity to repair DNA lesion, i.e., enhanced MGMT activity, BER, NER, and TLS [6].

Cell Cycle Deregulation and Resistance to Alkylating agents

Cell cycle deregulation is one of the hallmarks of cancer and tumorigenesis [7]. Checkpoints are signaling pathways that restrain cells from progressing through phases of cell cycle upon exposure to stress [8]. The goal of checkpoints is to monitor the proliferative capacity of cells and ensure proper replication of DNA prior to division. However, gliomas, as well as other tumors, exhibit a high degree of unrestrained growth as result of increased activity of cyclins and cyclin-dependent kinases (CDK), which accelerate progression through the cell cycle; decreased activity or total loss of CDK inhibitors; or alterations in key components of checkpoints signaling, such as p53 and DNA damage response genes (e.g., ATM, Chk1 and Chk2) [9].

At the level of cellular processes, DNA damage repair is directly related to cell cycle arrest and apoptosis. Upon exposure to chemotherapy, cells arrest transiently at cell cycle checkpoints in order for DNA damage repair to take place. In the case of sustained or irreparable damage to DNA, cells undergo apoptosis as well as other forms of cell death [9-12].

At the molecular level, DNA damage is sensed by ATM (ataxia telangiectasia mutated) and ATR (ATM and Rad3-Related) proteins, which leads to activation of G1-S

checkpoint through p53 signaling or G2-M checkpoint activation through Chk1 and Chk2 signaling [9]. The exact role of checkpoint activation and cell cycle arrest in response to DNA alkylating agents is not clear. On the one hand, a group of studies suggest that the ability of tumor cells to undergo cell cycle arrest subsequent to drug exposure is correlated with resistance because of increased DNA damage repair. These studies suggest that abrogation of checkpoints increases sensitivity to alkylating agents because cells undergo mitotic catastrophe as a result of progression through cell cycle with damaged DNA. This hypothesis has been supported by many studies on glioma cell lines in response to DNA damage [13-15]. The alternative hypothesis is that cell cycle arrest is an end goal of therapy and increased arrest, or decreased proliferation, is a sign of response to treatment. This has also been shown in many glioma cells lines upon exposure to chemotherapy [16, 17].

Cell Death and Resistance to Alkylating Agents

DNA repair pathways, at the molecular level, are also connected to many modes of cellular demise: apoptosis, necrosis and, autophagy [6]. The most investigated mode, however, is apoptosis. Upon exposure to DNA alkylating agents, DSB are detected by DNA repair proteins, through an unknown sequence of events, which leads to activation of p53 signaling. Activation of p53 signaling results in death receptor-mediated apoptosis and, in the case of mutant p53, mitochondria-mediated apoptosis [6]. In addition, cell survival pathways—such as NF-κB signaling, AKT/Protein Kinase B (PKB) and JNK—have been shown to be modulated in response to exposure to DNA damaging agents [6]. Thus, alterations in the activities of any of these pathways, many of which are common in gliomas [18], result in chemotherapeutic resistance.

From a therapeutic perspective, resistance to alkylating agents is dependent on the outcome of three interacting events: DNA damage repair, cell cycle arrest and cell death. As previously discussed, a consistent model for resistance, involving the regulation of these three processes, is currently lacking.

Cell Cycle Modeling: Analytical Approach to Characterize Drug Effects

Thus far we have established that the outcome of chemotherapy is dependent upon the magnitude of cell cycle arrest and/or induction of apoptosis as a result of damaging DNA—of the highly proliferative—tumor cells. Thus, resistance to chemotherapy could be analyzed quantitatively utilizing parameters related to cell cycle regulation. Several aspects of cell cycle kinetics such as cell cycle time, quiescent fraction, S-phase fraction, and apoptosis rates have an effect on the response to chemotherapy and patient prognosis [19]. For example, cell cycle time varies from 30 to 60 hours, apoptotic index varies from 0.1% to 4%, S-phase fraction ranges from 1% to 40%, and proliferation index ranges from 1% to 70% [19]. As such, variations in cell kinetics are distinct from one tumor to another and result in disparate responses to chemotherapy. Thus, we may gain important insights into chemotherapeutic response using mechanistic models integrating parameters of cell cycle kinetics in addition to other factors such as drug pharmacokinetics and development of genetic resistance in order to enhance response to chemotherapy.

Several mathematical models have been proposed to maximize efficacy of chemotherapeutic intervention, especially in clinical trials. These models have been developed to maximize the efficacy of treatment (model output) by means of manipulating dosing and/or scheduling (model input). Norton and Simon formulated a model that exploits resistance due to changes in cell cycle kinetics [20]. The model

predicts that moderate initial doses of cell cycle specific drugs followed by escalating doses leads to more cell kill compared to intense initial doses followed by constant doses. This model, however, ignores the effect of acquired genetic resistance. In another attempt, Coldman and Goldie proposed a model centered around the development of genetic resistance; their model predicts that intense initial doses are more effective as the likelihood of developing resistance is minimized [21].

Modified Hill models have been used to describe dose response curves and extract some important parameters such as the concentration needed to kill a given percentage of total cell population and maximum cell kill. These parameters are fairly important in characterizing response to a given chemotherapeutic agent; however, they do not provide insights about the mechanism of action of drugs. This model is a statistical fit to data, not predictive, and different from one cell line to another.

Mechanistic models have been developed as well to predict the efficacy of drugs on tumor cells. Gardner developed an exponential kill model that predicts the shape of the dose response curve based on the mechanism of action of drug (i.e. whether the drug is cell cycle specific or non specific)[22]. There are few input parameters, measured experimentally, required for constructing the model: drug concentration; duration of drug exposure; cell cycle phase distribution, namely fraction of cells in the vulnerable phase of cell cycle; and level of sensitivity to drug. The output of the model is a predicted dose response curve which can be used to estimate IC_x, concentration of drug that kill x % of cell population, and maximum cell kill.

A cell cycle-structured model has been developed by Sherer et al to optimize scheduling of cell cycle specific chemotherapeutic agents [23]. The main goal of the

model is to maximize cell kill of tumor cells with minimal damage to normal tissue. Model inputs are cell cycle phase distribution, rates of transitions between phases, drug concentration and duration of drug exposure. The model proposes that initial treatment with a cell cycle specific agent causes oscillations in the fraction of cells in each phase of the cell cycle; thus, a consequent treatment when a high fraction of cells are in the vulnerable phase of cell cycle would maximize cell kill. The model assumes that drug effects are independent of each other when multiple drugs are used.

A cell cycle structured model was developed by Panetta et al to elucidate the effect of mercaptopurine on the cell cycle dynamics of three acute lymphoplastic leukemia cell lines with different degrees of sensitivity [24]. Input parameters needed to construct the model are distributions of cells among phases of the cell cycle before and after treatment. The model estimates the rates of transition between phases of the cell cycle before and after treatment of the different cell lines. The model shows that, after incorporation of mercaptopurine, resistant cells arrest in S-phase efficiently and their commitment to apoptosis is much slower compared to sensitive cells. Thus, cell cycle deregulation is one of the resistance mechanisms implicated in resistance to chemotherapy.

1.4 A Systems View of Resistance

The presence of one or more of the resistance mechanisms stated above does not provide a detailed understanding of the resistant phenotype; that is, the molecular systems biology behind the development of resistance phenotype is not yet understood. The presence of any of the aforementioned mechanisms is only correlative with response to treatment and there is no detailed mechanistic view. Thus, characterization of the molecular events and cellular processes implicated in resistance is required for more

effective chemotherapy regimens.

Genome-Wide Characterization of Intrinsic Resistance

Large scale monitoring of molecular changes, especially gene expression profiles, has acquired a central role in understanding resistance to chemotherapy. Microarrays have been used to measure genome-wide changes in gene expression of many cancer cell lines and tumor xenografts. In many studies, it was found that basal expression profiles of several groups of genes exhibit strong correlation with response to various classes of chemotherapeutic agents [3]. In addition, microarrays have been used to compare changes in gene expression profiles of cells resistant to a given chemotherapeutic agent and those that are sensitive in order to elucidate biological pathways implicated in resistance development [3]. Numerous studies were performed on a panel of 60 cell lines, known as NCI60, representing tumors from various organ tissues [25-29]. The response of each individual cell line to thousands of chemotherapeutic agents was determined. Microarray technology was used to compare gene expression profiles of cell lines resistant to a given chemotherapeutic agent and their sensitive counterparts. The same methodology was applied to tumor xenografts, which represent a more clinically relevant model compared to *in vitro* testing of cell lines [30].

Similarly, it was found that the expression patterns of certain groups of genes dictate the response of tumor xenografts to chemotherapeutic agents. The goal of these studies is to select a group of genes that serve as predictors of response to a given therapeutic agent, which is an important step toward personalizing cancer treatment.

Gene expression data from the panel of the 60 cell lines and sensitivity to chemotherapeutic agents were used to construct functional relationships between genes

and chemotherapeutic agents [31, 32]. Statistical analysis techniques were applied to these datasets, gene expression and drug sensitivities, to constructs networks that relate the expression pattern of certain genes to the effect of chemotherapeutic agents. Relevance networks, based on statistically significant correlations between pairs of genes and sensitivity measures, identify relationships between genes and chemotherapeutic agents. Other techniques were developed to achieve the same goal; however, the relationship between genes and chemotherapeutic agents are statistical, not based on biological mechanisms, subject to change based on the stringency of statistical threshold applied.

Resistance: An Acquired Phenotype

To understand the molecular mechanisms implicated in acquiring resistance to chemotherapeutic agents, gene expression profiles of parental cell lines and "modified" subclones that are resistant to a specific group of chemotherapeutic agents were compared. The resistant subclones were developed by prolonged exposure of sensitive cell lines to sublethal doses of chemotherapeutic agents [33, 34] or by transfecting cells with a given gene or an expression sequence tag that has been shown to confer resistance [35, 36].

The goal is to elucidate the changes in gene expression that confer cell lines with resistance to specific classes of chemotherapeutic agents, such as DNA damaging agents and topo I inhibitors. These studies were performed to confirm the role of specific resistance mechanisms to chemotherapeutic agents, such as the role of MGMT in resistance to BCNU and ATP-binding transporters to topoisomerase I inhibitors. These studies have shown that aberrant expression is usually associated with genes involved in

critical processes such as DNA mismatch repair, DNA excision repair, cell cycle progression, apoptosis and stress response pathways.

Genome-Wide Characterization of Resistance in Gliomas

Similar studies have been carried out on various glioma models. Gene expression profiles of glioma biopsies, and cell lines, have been used to identify genes correlated with poor prognosis and, consequently, to determine potential therapeutic targets [37, 38]. Another group of studies were aimed at identifying the role of certain genes in determining the response to a given class of chemotherapeutic agent [39-42]. In addition, induction of resistance *in vitro* by prolonged exposure to sublethal doses of cytotoxic agents—and comparison with the parent cell line at the gene expression level—was used to identify mechanisms of resistance [33, 34, 43].

The main drawback with these studies is that basal gene expression profiling is performed rather than monitoring changes in gene expression upon exposure to drug. It could be more beneficial, from a therapeutic perspective, to characterize the response of resistant cells upon exposure to chemotherapy in comparison to the more sensitive counterparts. Thus, instead of having a list of genes that are found to be differentially expressed between resistant and parent cell lines, there is a need to characterize the cellular events that differentiate the response of resistant cell lines in comparison to that of sensitive ones.

CHAPTER 2

MATHEMATICAL MODELING TO DISTINGUISH CELL ARREST AND CELL KILLING IN CHEMOTHERAPEUTIC DOSE RESPONSE CURVES

ABSTRACT

Dose response curves are utilized widely to characterize the response of tumor cell lines to chemotherapeutic drugs, but the assay methods are non-standardized and their analysis is based on phenomenological equations. To provide a framework for better interpretation of these curves, we have developed a mathematical model in which progression through the tumor cell cycle is inhibited by drug treatment via either cell cycle arrest or entrance into cell death pathways. By fitting dose response data, preferably over a dynamic range, the contribution of these mechanisms can be delineated. The model was shown to fit well experimental data for three glioma cell lines treated with either carmustine or etoposide. In each cell line, the major mechanism of tumor cell inhibition was cell death for carmustine in contrast to cell cycle arrest for etoposide. U87 cells with acquired *in vitro* resistance to carmustine were shown to have attained a greater ability to enter cell cycle arrest and thus to avoid cell death. This approach will aid in understanding better the action of chemotherapeutic agents on tumor cells and can be incorporated into tumor growth models for the selection of dose/timing regimens *in vivo*.

2.1 INTRODUCTION

Pharmacological dose response curves are used to derive basic information regarding the amount of a drug needed to achieve a particular biological response. Often the entire dose response is distilled into a single EC_{50} value, without consideration to the shape of the curve, whether all the values of a response are attainable, or the dynamics of the process. Considerable information regarding the therapeutic mechanism remains hidden in such an analysis of the dose response, information that could be brought to light upon careful experimental design and data analysis and through the consideration of a mechanistic model.

A specific area where improved understanding of molecular pharmacology is critical is in cancer therapeutics, especially tumors with high level intrinsic or acquired resistance as is the case with gliomas. DNA damaging agents exert their activity by a combination of growth arrest and cell killing, both apoptotic and necrotic. However, a detailed molecular characterization of these events is currently lacking even for clinically well-established agents, which further complicates the task of overcoming resistance. In spite of the incomplete characterization of these molecular events, it may be possible to improve the efficacy of DNA damaging agents—and overcome resistance—through understanding their contribution to cell cycle arrest and cell death. Improved efficacy of cell cycle specific drugs could be achieved through proper dose scheduling or by combination with the correct second drug.

In order to provide a framework for improved understanding of the molecular pharmacology of DNA damaging agents on glioma cell lines, we have developed a mathematical model describing the contribution of cell cycle arrest and cell death on the

proliferation of these tumor cell lines. The effect of model parameters on the pharmacological dose response is detailed. The model is validated by its correspondence to dose response curves for the DNA damaging agents BCNU, which the standard of care in glioma treatment, and etoposide (VP-16), which a cell cycle specific DNA topoisomerase II inhibitor. This approach allows us to ascribe mechanistic interpretations to the dose response curves for each of these drugs.

In order to develop a preliminary understanding of events implicated in acquisition of resistance to BCNU, we have applied the modeling approach to glioma cell line U87 that have acquired resistance *in vitro* through prolonged sublethal exposure. In the future, the model may be useful in selecting dose schedules or drug combinations for improved efficacy.

2.2 MATERIALS AND METHODS

2.2.1 Chemotherapeutic Agents

BCNU and Etoposide were purchased from Sigma-Aldrich (St. Louis, MO), and dissolved in DMSO (Sigma-Aldrich, St. Louis, MO) and stored at -20 ^{o}C at a stock concentration of 100 mg/ml.

2.2.2 Cell Lines

Human Glioblastoma cell lines A172 and U87 and astrocytoma cell line SW1088 were purchased from American Type Culture Collection (Rockville, MD). A172 and SW1088 were cultured in DMEM (Invitrogen, Carlsbad, CA) supplemented with 10% FBS (GIBCO-BRL, Gaithersburg, MD), 4 mM L-glutamine (GIBCO, Gaithersburg), and 100 U/mL Penicillin/Streptomycin. Human glioblastoma cell line U87 was cultured in

MEM (GIBCO-BRL) supplemented with 10% FBS, 4 mM L-glutamine, 100 U/mL penicillin/streptomycin. Cells were cultured at 37 ^{o}C and 5% CO_2 atmosphere.

2.2.3 Resistant Cells

Resistant cell lines were developed by sublethal exposure to incremental doses of carmustine. U87 cells were exposed to an initial concentration of 15 μg/mL for 48 hours. Subsequently, cells were incubated in drug free media. Increments of 5 μg/mL were used when cells show increased survival. U87 cells underwent 11 cycles of treatment over a period of 8 months. Maximum concentration to which cells were exposed was 40 μg/mL. After cells achieved a significant level of resistance, as evidenced by viability assay, cells were pulsed with 10 μg/mL of carmustine every 4 weeks to maintain resistant phenotype.

2.2.4 Viability Assays

Cells were resuspended in culture medium at a concentration of 10^5 cells/ml. 100 μL of cell suspension (10000 cells) were seeded in wells of a 96-well plate. Cells were cultured for 18 hours to assure proper attachment. Dilutions of BCNU and etoposide, along with DMSO (Sigma-Aldrich, St. Louis, MO) as vehicle control, were prepared in culture media and added to cells for 72 hours or designated time-points. 20 μL of MTS solution (Promega, Madison, WI) was added to every well and left to incubate for two hours. Absorbance plate reader (Bio-Rad, Hercules, CA) was used to measure absorbance at 490 nm. Average of six wells per single drug concentration was normalized to vehicle control (cells treated with DMSO). Empirical fitting of dose response curves was performed using the following equation:

$$f = f_{resist} + \frac{1 - f_{resist}}{1 + \left({}^{[D]}\!/\!_{IC50} \right)^{n}} \qquad (1)$$

where f is the fractional viability (relative absorbance), [D] is the drug concentration, and the three fitting parameters f_{resist}, IC_{50} and n are interpreted as a fraction of resistant cells, the standard pharmacological IC_{50} value, and a cooperativity (Hill) coefficient, respectively. Empirical fits were performed using the software package KaleidaGraph v. 4.03 (Synergy Software, Reading, PA).

2.2.5 Propidium Iodide (PI) Exclusion

To determine extent of cell death, cells were incubated with 100 μg/mL carmustine or etoposide and harvested at 12, 24, 48 and 72 hours. Floating dead cells were collected as well as viable cells and were washed with PBS. Cells were suspended in a 20 μg/mL solution of propidium iodide in PBS and immediately analyzed by flow cytometry, described below.

2.2.6 Flow Cytometry

Propidium Iodide (PI) (Molecular Probes, Eugene, OR) staining was performed to determine cell cycle phase distribution based on DNA content. Cells were seeded a density of $2x10^5$ cells and were left for 16 hours. Subsequently, cells were exposed to 5μg/mL of etoposide or 25μg/mL of carmustine and harvested at 0,8,12, 24, 48 and 72 hours. At designated time-points, cells were washed with PBS (GIBCO-BRL) and fixed in 70% ice-cold ethanol. Cells were centrifuged at 300 rcf for 6 minutes at 4 ^oC. Cell pellet was washed twice with PBS then stained with 20 μg/mL PI (Molecular probes, Eugene, OR) in 0.1% (V/V) Triton X-100 (Bio-Rad Laboratories) PBS solution with 0.2 mg/mL RNaseA (Qiagen, Valencia, CA) in PBS for 15 minutes at room temperature in the dark. Analysis was performed with FACScan flow cytometer (Becton-Dickinson, Mansfield, MA). Cell cycle distributions, generated by CellQuest (Becton-Dickinson),

were imported into ModFit software (Verity Software House, Topsham, ME) to quantify the fraction of cells in each phase of cell cycle. Triplicate samples were used for every time-point.

2.2.7 Mathematical Model

A population balance model was used to follow the distribution of cells through the various phases of the cell cycle. Each phase of the cell cycle is treated as a compartment, except that the G_2 and M phases are lumped together as they are indistinguishable by DNA content in flow cytometric analysis. First-order rate constants (k_1, k_2, k_3) parameterize the rates of transition among successive phases. In addition, cells in the G1 and G2/M phases may be directed to the death compartment (D) as a result of chemotherapy treatment; this is also treated as a first-order process, with rate constant γ. Cell cycle arrest is modeled by introduction of a parameter, f_a, which is the fractional probability that a cell will pause rather than proceed with mitosis. The model is shown schematically in Figure 2.1. The balance on cells in each compartment is as follows.

$$\frac{dG_1}{dt} = 2\left(1 - f_a\right)k_3 G_2 - \left(\gamma + k_1\right)G_1 \tag{2}$$

$$\frac{dS}{dt} = k_1 G_1 - k_2 S \tag{3}$$

$$\frac{dG_2}{dt} = k_2 S - \left[\left(1 - f_a\right)k_3 + \gamma\right]G_2 \tag{4}$$

$$\frac{dD}{dt} = \gamma\left(G_1 + G_2\right) \tag{5}$$

In these equations, G_1, S and G_2 are the numbers of cells in the G_1, S and G_2/M phases of cell cycle, respectively; D is the number of cells that have died. The

experimental quantity of interest is the total number of live, viable cells, which is obtained in the model by summing over the number of cells in each phase of cell cycle:

$$\{\text{Viable cells}\} = G_1 + S + G_2 \tag{6}$$

Assuming that cells untreated with drug are in a steady-state growth condition, the rate parameters (k_1, k_2, k_3) can be determined from the initial fraction of cells in each phase ($f_{G1}^0, f_S^0, f_{G2}^0$) and the growth rate, μ, each of which was measured experimentally, according to the following relations:

$$k_1 = \mu \frac{2 - f_{G1}^0}{f_{G1}^0} \tag{7}$$

$$k_2 = \mu \frac{1 + f_{G2}^0}{f_S^0} \tag{8}$$

$$k_3 = \frac{\mu}{f_{G2}^0} \tag{9}$$

These steady-state values form a set of initial conditions for the system before perturbation by drug treatment. Given a set of parameters and initial conditions, the model (equations 2-5) was integrated using the ode15s solver in MATLAB (Mathworks, Natick, MA).

The effect of drug on cell cycle arrest was modeled with a saturation equation without any cooperativity parameter. Since the maximum fraction of cells in arrest is one, f_a maps onto a single parameter characterizing the dose effect, K_a. The cell death rate, γ, is assumed to be proportional to drug concentration, with an effect that decays exponentially with time, with time constant τ, due to spontaneous deactivation of the drug. That is,

$$f_a = \frac{[D]}{K_a + [D]} \tag{10}$$

$$\gamma = k_g [D] e^{-t/\tau} \tag{11}$$

To determine the best fit of the model parameters (K_a, k_g, τ) to experimental data, a simulated annealing algorithm was used [44] as implemented in the MATLAB function simann.m (http://isbweb.org/~tgcs/software/simann.m). The parameters were bounded such that $0.0 \leq \log(K_a) \leq 3.0$, $-6.0 \leq \log(k_g) \leq -3.0$ and $0 \leq \log(\tau) \leq 2$ h^{-1}, where K_a is in units of μg/mL, k_g is in units of μg/mL/h, and τ is in units of hours.

2.2.8 Statistics

Experiments were performed that there are at least three replicate populations of cells for each measurement. Each data point is reported as mean of populations and error bars represent standard deviations. When possible, statistical significance was determined using single-tailed Student's t-test. Results were deemed statistically significant for confidence levels of 95% ($p < 0.05$)

2.3 RESULTS

2.3.1 Dose Response Signatures

To characterize the pharmacological dose response, several glioma cell lines (A172, U87, and SW1088) were each exposed to varying concentrations of carmustine and etoposide for 48 hours, and their viability (metabolic activity) was determined using the MTS assay (Figure 2.2). The three different cell lines showed qualitatively similar responses to carmustine and etoposide. For each cell line, low concentrations of carmustine do not inhibit cell viability; however, as the concentration of carmustine increases, viability drastically decreases and cells are completely destroyed at high doses

(~ 250 μg/mL). The response to etoposide is fundamentally different from that of carmustine, as cells show a gradual decrease in viability with increasing concentration of etoposide. Using the conventional paramcological dose response fits to the data (Equation 1), all of the cell lines exhibited a lower EC_{50} value and higher Hill (cooperativity) coefficient for carmustine treatment as compared to etoposide (Table 2.1).

To characterize dynamics of dose response, the metabolic activity of U87 cells exposed to etoposide and carmustine for varying duration (18, 24, 48 and 72 hours) was quantified (Figure 2.3). Carmustine was found to exert significant effects on cell viability by 18 hours, and its effects were only increased slightly at later time points. Etoposide, on the other had, exerted an effect on U87 metabolic activity that was quite weak at early times (18 and 24 hours) and pronounced only by 72 hours. Similar dynamics in the response to both drugs were observed in other cell lines (data not shown).

2.3.2 Cell Cycle Model

Mathematical models structured on cell cycle have been used to describe chemotherapeutics previously, particularly to predict dose timing regimens that might take advantage of the cell cycle phase specificities of many drugs [23, 45, 46]. We hypothesized that a cell cycle structured model could highlight the distinct dynamics and dose response to etoposide and carmustine exhibited by multiple cell lines (Figure 2.2). The model is described in detail in the previous section and summarized schematically in Figure 2.1.

The two parameters acting to alter the proliferation of tumor cells are cell cycle arrest (f_a) and cell death rate (γ). In order to see how each parameter affects cell growth

in the model, we varied the magnitude of each of these parameters individually with the other set to zero. When cells are arrested with increasing frequency as they pass through the G2 phase, the fraction of cells in each phase redistributes with an increasing fraction stagnated in G2/M phase (Figure 2.4). While this effect on cell cycle appears quite moderate at an arrest fraction of 0.5, this fraction is sufficient to induce a marked decrease in cell number after 48 hours (Figure 2.4c). In the extreme case where all cells are blocked from mitosis (f_a = 1.0), then the final cell number is equal to the initial cell number.

Cell death after DNA-damaging chemotherapeutics including carmustine and etoposide can occur from both apoptotic and non-apoptotic pathways [47]. In the framework of the model, the transition from G1 or G2/M phases to a death program redistributes the population of cell cycle phases, giving rise to a transient enrichment of S phase cells (Figure 2.5). The redistribution is more rapid than for cells undergoing cell cycle arrest. A strong effect of death rate on cell number is observed (Figure 2.5c), with high rates allowing for complete cell elimination, in contrast to the cell cycle case where the cells were merely inhibited from growing.

The effect of drug on cell cycle arrest and apoptosis was modeled as simply as possible, with a one-parameter equation for arrest where the parameter, K_a, is an indication of the dose at which arrest is significant, and a two-parameter (k_g, τ) equation indicating the rate of entry into cell death pathway and the time scale of chemotherapeutic killing action (Equations 7-8). In this way, the effect of a drug acting only via growth arrest vs. one acting only via cell killing could be determined. Growth arrest leads to a gradual slowing down of growth as drug concentration increases,

resulting in a "soft" dose response curve (Figure 2.6a). In contrast, when cells are killed rather than arrested, the dose response curve is sharper in shape and more evident at early times (Figure 2.6b). The intracellular half-life of drug, τ, does not alter the basic appearance of cell killing dose response but tunes its sharpness and dose range (Figure 2.6c).

2.3.3 Comparison with Experiment

The shapes of the simulated dose curves for growth arrest or cell death appear similar to the experimental curves for cells treated with etoposide or carmustine, respectively. In order to provide a more quantitative link between mechanism and dose response curves, we fit the dose response data for each cell type to the model, where both growth arrest and apoptosis were allowed to contribute. A comparison between experimental data and model predictions is shown in Figure 2.7 for U87. A single set of parameters (K_a, k_g, and τ) is fit to the ensemble of data for each drug. While there are some features of the data, most notably hormesis (stimulation of cellular metabolic activity at low concentrations of drug), that are not described by the model, overall the combined dose and time dependencies are fit well.

The model was fit to time course, dose response data for A172, SW1088 and U87 cells (Figure 2.8). The model parameters show a distinct difference between the two drugs and a marked similarity among the cell type for a given drug. For all three cell lines, the fit value of K_a is lower for etoposide treated cells as compared with carmustine treated cells, indicating a greater propensity for cell cycle arrest following etoposide treatment (Figure 2.8a). The increased k_g values in each cell line indicate a much greater entry into cell death programs following carmustine treatment (Figure 2.8b). The fit

values of τ indicate an intracellular half-life on the order of a day for carmustine, whereas the values for etoposide are less meaningful due to the very low rate of entry into cell death (Figure 2.8c).

The model was also used to characterize changes in glioma cell responses in cells that acquired resistance to chemotherapeutics. Resistance was induced in U87 cells by treatment with an escalating but sublethal dose schedule of carmustine for 11 cycles. These cells, denoted as U87C, are less sensitive to carmustine exposure with an increase in EC_{50} from 48 μg/mL to 135 μg/mL. The U87C cells do not differ from U87 cells in their entry into cell death but increase their overall survival by entering into cell cycle arrest to a greater extent and thus avoiding further damage leading to death (Figure 2.8)

The distinction between cell cycle arrest and cell death was measured experimentally. For cell cycle analysis, U87 cells treated with drugs were harvested at varying times, fixed, stained with propidium iodide (PI), and subjected to flow cytometry followed by software quantification of cell cycle distribution. Treatment with either drug results in transient S phase accumulation followed by a redistribution with a majority of cells ending up in G2/M phase by 72 hours (Figure 2.9). However, treatment with etoposide produced a greater final distribution in G2/M phase with essentially no cells completing mitosis and reaching G1 phase, whereas cells treated with carmustine retained a percentage (~20%) of cells in G1 phase as would be expected for cells completing the cell cycle and dividing. To determine the number of dead cells, drug treated cells were stained with PI without prior fixation, identifying only those cells whose membrane barrier have been compromised. A much higher percentage of cells were killed by

carmustine treatment as compared with etoposide (Figure 2.10). Results for A172 and SW1088 cells are similar (data not shown).

2.4 DISCUSSION

Mathematical models structured on cell cycle have been used previously to describe the growth dynamics of tumor cells. The effect of a chemotherapeutic drug has typically been incorporated as a fitted change in the rate parameters governing transitions among the states (cell cycle phases) of the model [24, 46, 48]. Cellular level models of drug response can be incorporated modularly into tissue models of tumors that account for three-dimensional restrictions on growth and drug penetration [49, 50]. Given a set of fitted parameters and assuming the system will perform the same under repeated administration, predictive strategies for improved scheduling of chemotherapeutic regimens can be identified [23].

Previous models have not incorporated multiple modes of drug action or allowed distinction among mechanisms of action. By assuming knowledge of the cell cycle phase dependencies of growth arrest and death rate, we were able to use the model in simulation mode to explore the differences in dose response and dynamics for these two primary mechanisms of chemotherapeutic action. The model elaborates quantitatively how death leads to a rapid reduction in cell number, whereas growth arrest causes a more gradual lag of the cell population compared to non-arrested ones. Furthermore, the shape of the dose response curve depends critically on the mechanism, with a steeper response in the case of cell killing compared to cell cycle arrest. The shape of the dose response curve is a manifestation more of the dynamics of the cell cycle processes occurring rather than the

pharmacological equations (eqn. 7 and 8) employed, as these do not employ Hill coefficients, which is the usual method of describing sharp dose response.

We had observed in the response of glioma cell lines to etoposide and carmustine that the former more closely resembled the simulations of cell cycle arrest and the latter resembled more closely the simulations of cell killing. We sought to incorporate both mechanisms simultaneously into the model and to use parameter fitting to determine the relative contribution of each to the observed pharmacological data. We included the effect of drug concentration on cell cycle arrest using a saturation-response curve without a Hill coefficient (Equation 7) and for cell killing using a simple linear expression. In the latter case, a saturation expression was also investigated, but the additional parameter relative to a linear model did not improve the fit significantly. On the other hand, incorporation of an intracellular half-life, τ, did improve the fit significantly (p value < 0.01, as determined by an F-test). An exponentially decaying kill rate has been applied previously to model cancer drug pharmacodynamics [22, 23].

Each of the mechanisms incorporated into the model – cell cycle arrest and cell killing through apoptotic and necrotic pathways – has been ascribed to each of these drugs[51-54]. Carmustine, or 1,3-bis(2-chloroethyl)-1-nitrosurea (BCNU), is a monofunctional alkylating agent that creates alkylguanine adducts requiring DNA repair and can also produce interstrand cross-links [55]. These processes can lead to cell death via both apoptotic and necrotic mechanisms [47]. On the other hand, saturation of the DNA damage pathway can lead to signaling along the ATM and ATR signaling and cell cycle arrest. Etoposide, or VP-16, is a topoisomerase-2 inhibitor that incurs DNA damage and can lead to cell cycle arrest or apoptosis depending on the status of tumor

suppressors such as p53 or PTEN or the presence of other pharmacological agents such as valproic acid [51, 56]. Thus, the mechanism and effectiveness of these drugs depends intricately on the molecular composition of the particular tumor. In this light, it is somewhat surprising that the pharmacological profiles for each drug were similar across each of the cell lines tested, which have been shown to posses disparate molecular composition (see Appendix Tables A.7-A.9 for list of genetic and molecular changes of cell lines). The similarities may reflect genetic similarities among the cell lines selected; for instance, all three have deletions in chromosome 19q [57].

Treatment decisions for gliomas—as well as other malignant tumors—will increasingly be made with the aid of molecular (e.g., DNA microarray) or cellular (e.g., *in vitro* drug sensitivity testing) testing using tissue from an individual's tumor [58]. In addition to the caveats associated with using cell culture as a surrogate for *in vivo* tumor growth conditions[59], the measurement and representation of pharmacological response are also issues. Typically, drugs are evaluated using a cell culture assay similar to that employed here, but at a single time point, and the data are represented using a saturation response with cooperativity (Hill) coefficient (Eqn. 1). Dynamics are not included in such a representation, and thus the pharmacological parameters will depend on the time at which the assay is completed. Indeed, an assessment of the relative potency of carmustine and etoposide would be influenced by whether an early or late time point is chosen (Figure 2.3). Use of the structured, dynamic model employed here allows the drug responses to be characterized by parameters that are mechanistic and reflect behavior over a prescribed period of drug treatment. Furthermore, hypotheses regarding treatment dose/timing schedules or combinations can be simulated *in silico* and validated

experimentally. This can be particularly useful when first-line chemotherapy fails and a second course of treatment can be selected. The modeling approach employed here allows facile interpretation of the cellular changes occurring as cells become resistant, information that can be useful in selecting a complementary treatment. In light of this model, U87 cells acquire resistance to carmustine through enhanced arrest in G2/M. This could be valuable information from the therapeutic perspective. For example, the use of checkpoint abrogators, such as caffeine or pentoxyfilline (PTX), may sensitize cells to carmustine and overcome resistant phenotype. However, this hypothesis warrants further molecular characterization of resistant phenotype and response of cells upon exposure to chemotherapy.

In this work, tumor cells are treated as homogeneous and are described at the level of cell cycle. While this level of details appears to describe *in vitro* pharmacological assays reasonably well, application to *in vivo* data will require incorporation of population heterogeneity, which could be of drug exposure or DNA repair response [60]. In addition, molecular level models have been developed to describe DNA damage responses and cell cycle arrest [61-64]. Integrating molecular details into cellular models and then to tissue models that account for tumor tissue morphology and transport will provide a much more comprehensive description of tumor response to chemotherapy in a fashion that can serve as a framework for understanding the responses of individual tumors. While parameterizing integrated, multiscale models in a way that reflects human tumor physiology accurately will be a challenge, the reward will come in the ability to test various treatment regimens *in silico* and to predict which is best suited based on the genetic composition of the tumor being treated.

2.5 TABLES AND FIGURES

Cell Line	Drug	f_{resist}	EC_{50} *	n
A172	Carmstine	-5±2	82±2	4.3±0.4
A172	Etoposide	24±3	7±1	0.9±0.1
SW1088	Carmustine	-25±25	97±33	1.5±0.4
SW1088	Etoposide	23±9	15±7	0.6±0.1
U87	Carmustine	-1±4	48±4	1.9±0.2
U87	Etoposide	-1±77	47±174	0.4±0.3

Table 2.1: Pharmacological parameters of glioma cell lines
*units of μg/mL

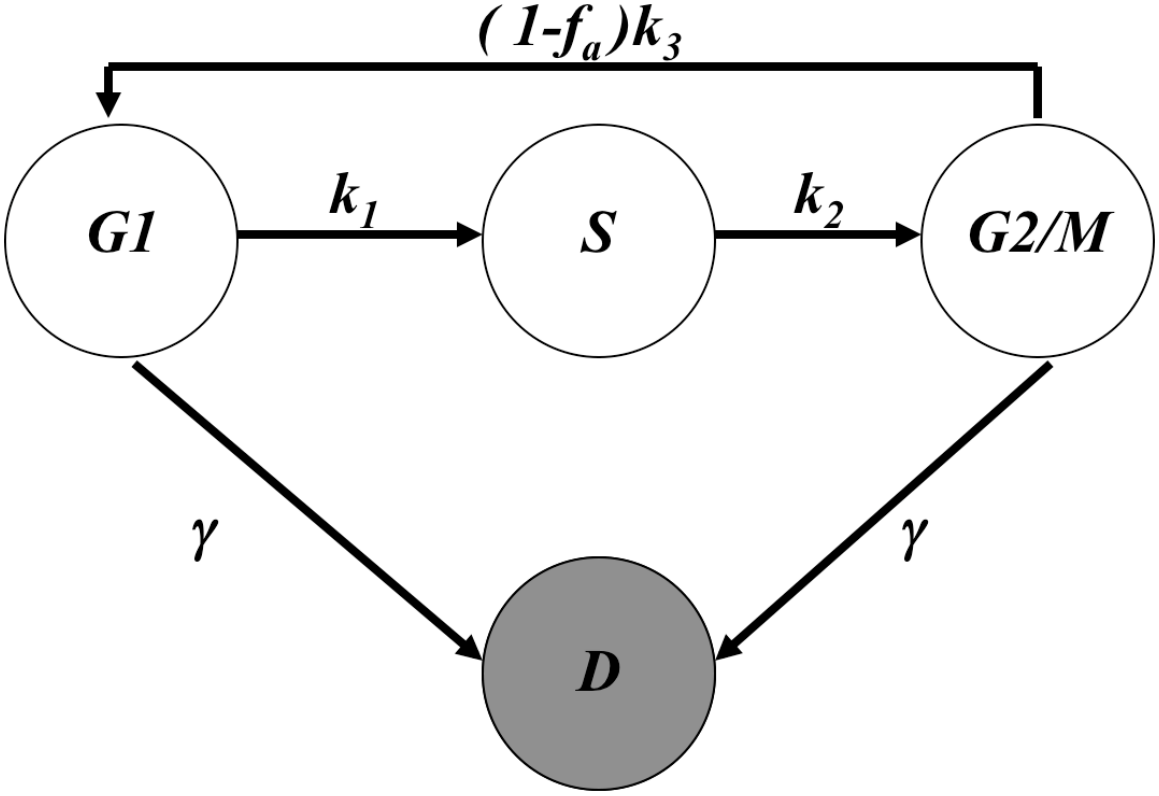

Figure 2.1: Compartmental Model of Cell Cycle. G1, S and G2/M represent phases of cell cycle that are distinguishable by flow cytometry. k1, k2 and k3 represent rates of transition between phases of the cell cycle, each of which is treated as a compartment. fa represents that fraction of cells arrested in G2/M, while γ represents the rate of entry into cell death, denoted as D compartment.

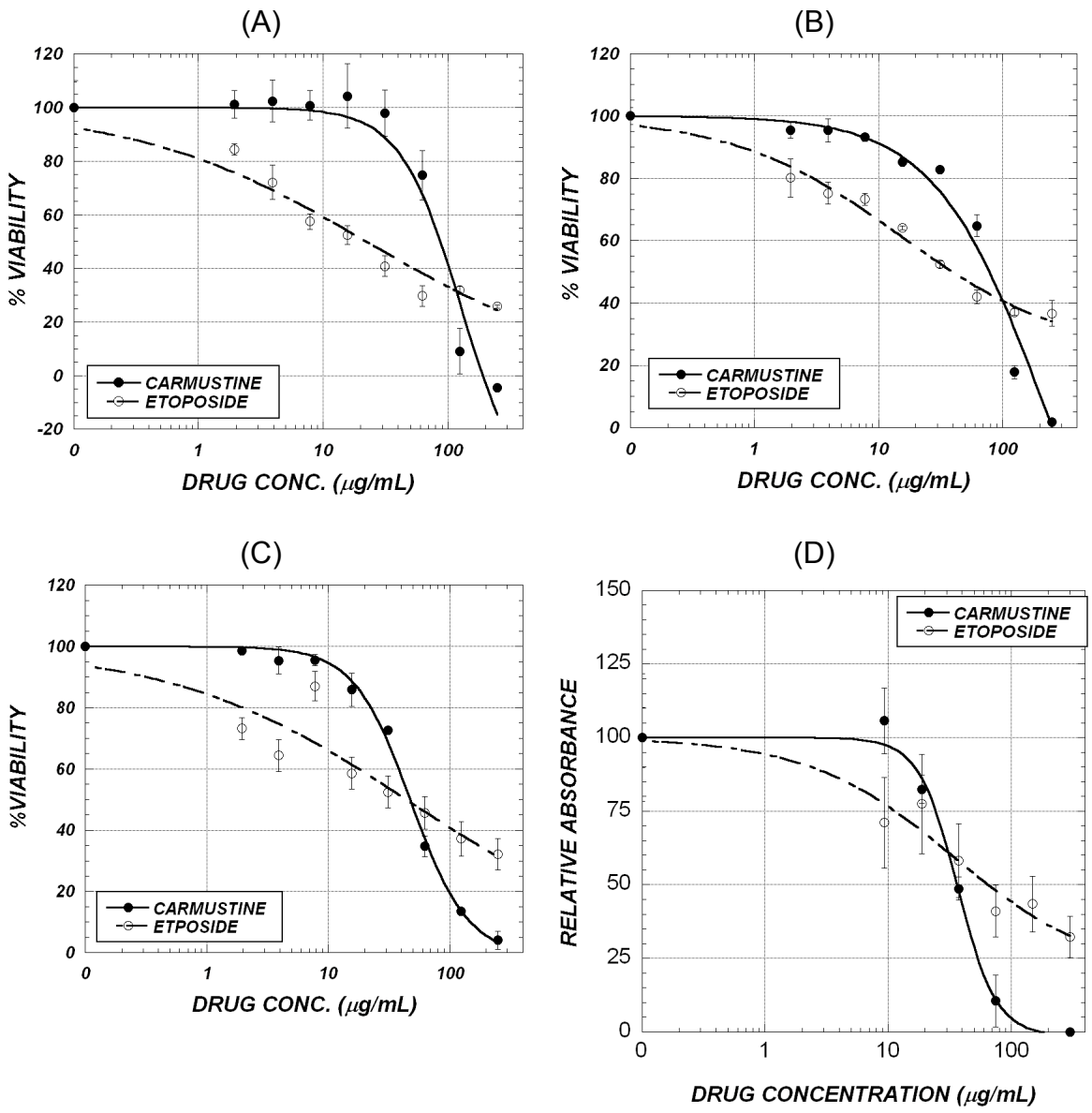

Figure 2.2: Response of Different Cell Lines. (a) A172, (b) SW1088, and (c) U87 to carmustine and etoposide at 72 hours. Cell viability was determined by MTS assay, which measures metabolic activity of viable cells. (d) Response to A172 to etoposide and carmustine was also determined by calcein staining at 72 hours.

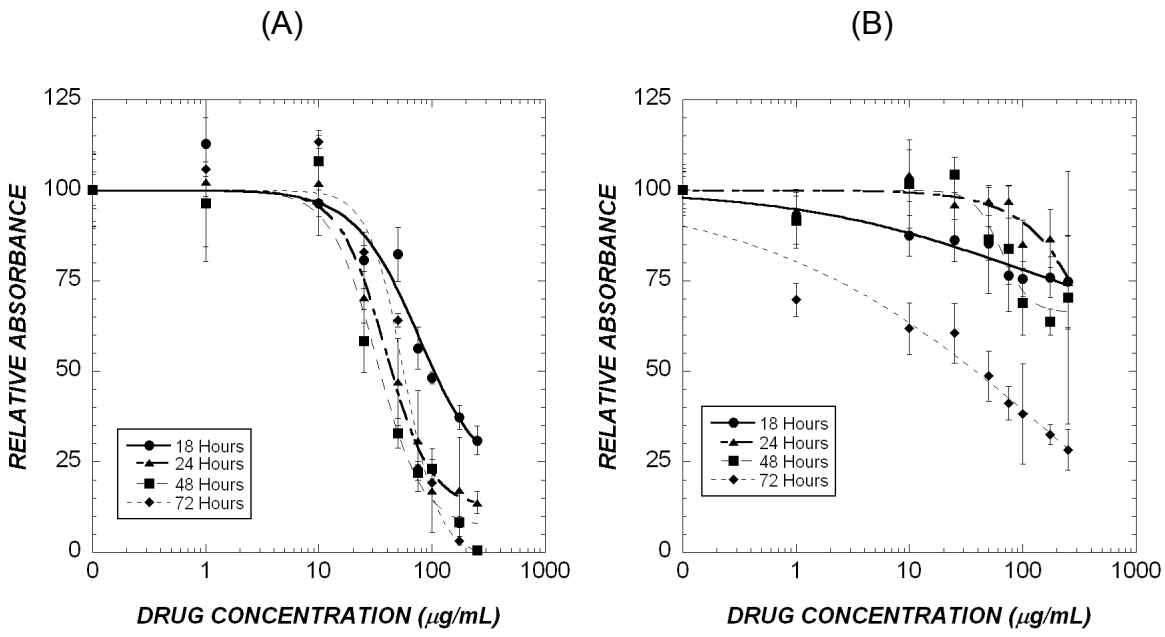

Figure 2.3: Response Dynamics of U87 to (A) carmustine and (B) etoposide at 18, 24, 48 and 72 hours. Cell viability was determined by MTS assay.

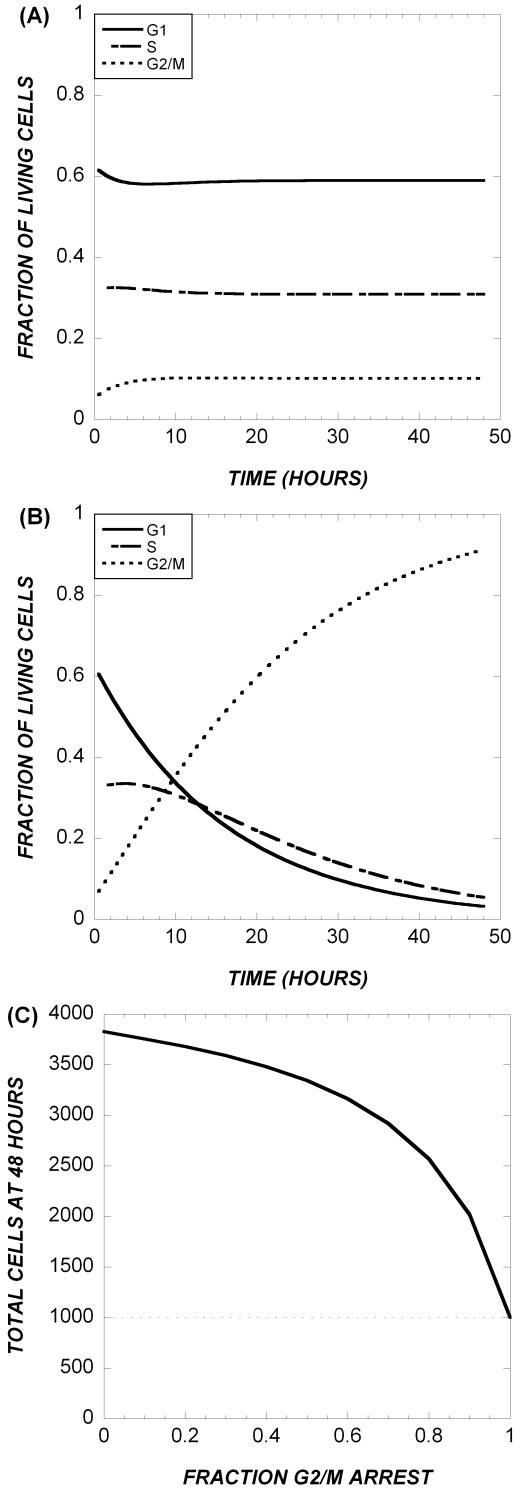

Figure 2.4: Effect of fraction of transitioning cells arrested (f_a) on cell cycle dynamics: (A) f_a = 0.5; (B) f_a = 1.0. (C) Decrease in cell number as a function of f_a. There is a slow redistribution among phases of the cell cycle with increased values of f_a, which corresponds with a marked decrease in cell growth at 48 hrs. When f_a = 1, total number of cells at 48 hrs equals initial number of cells. Shape of dose response curve due to cell cycle arrest is "soft".

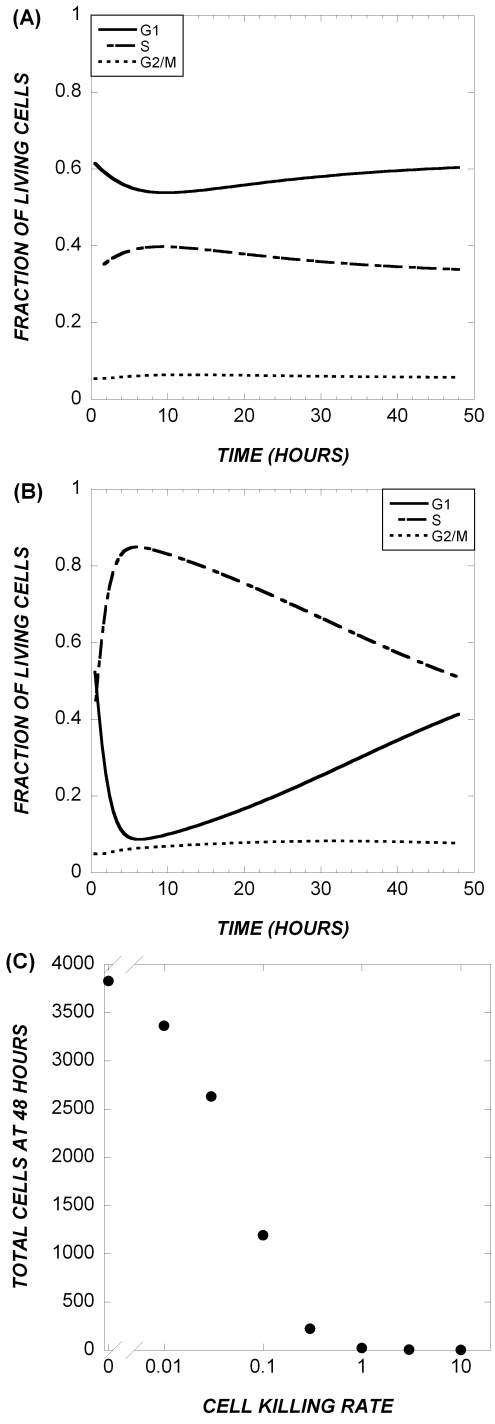

Figure 2.5: Effect of Cell Killing Rate (γ) on Cell Cycle Dynamics. (A) $\gamma = 1.0\ h^{-1}$; (B) $\gamma = 2.0\ h^{-1}$. (C) Decrease in cell number as a function of γ. There is a rapid redistribution among the phases of the cell cycle with increasing value of γ. This increase in γ correlates with rapid decrease in total cell count at 48 hrs, with total elimination of cells, and a "sharp" dose response curve.

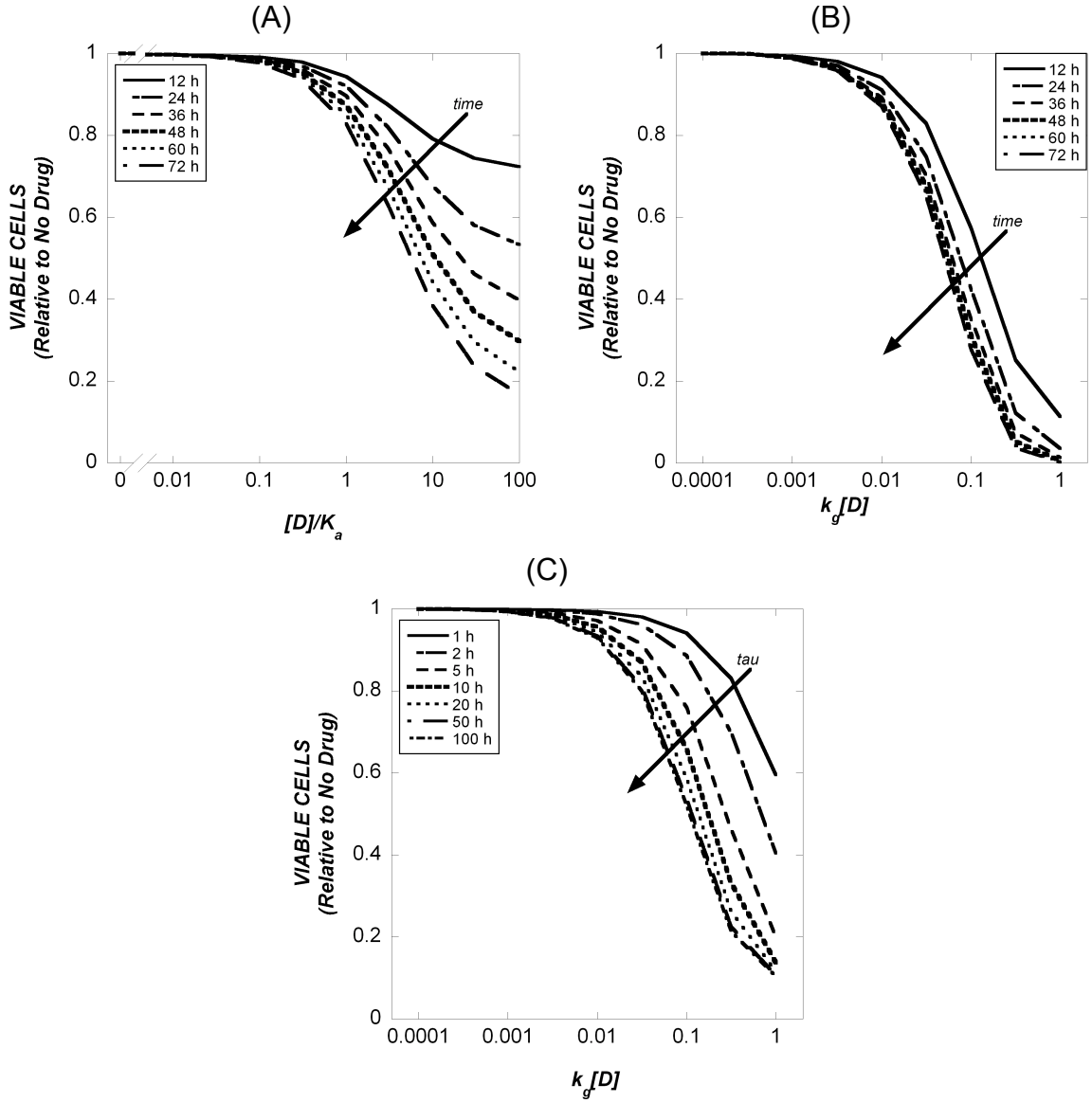

Figure 2.6: Effect of Pharmacological Parameters on Cell Viability Curves. (A) Effect of cell cycle arrest across time from 12-72 h, (B) Effect of cell killing across time from 12-72 h (with tau fixed), (C) Effect of cell killing across various values of tau (with time fixed).

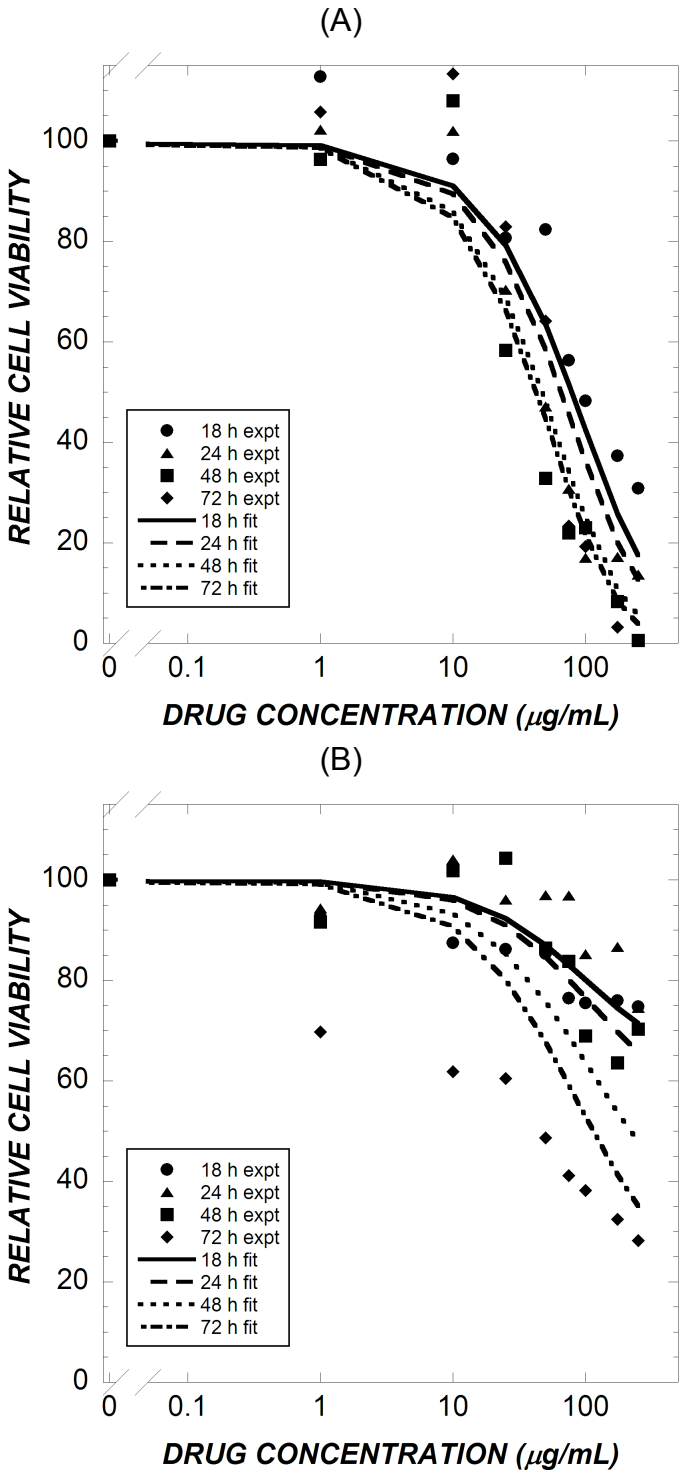

Figure 2.7: Model and Experiment Comparison. Response of U87 to (A) carmustine or (B) etoposide at 18, 24, 48 and 72 hours, along with corresponding model fits.

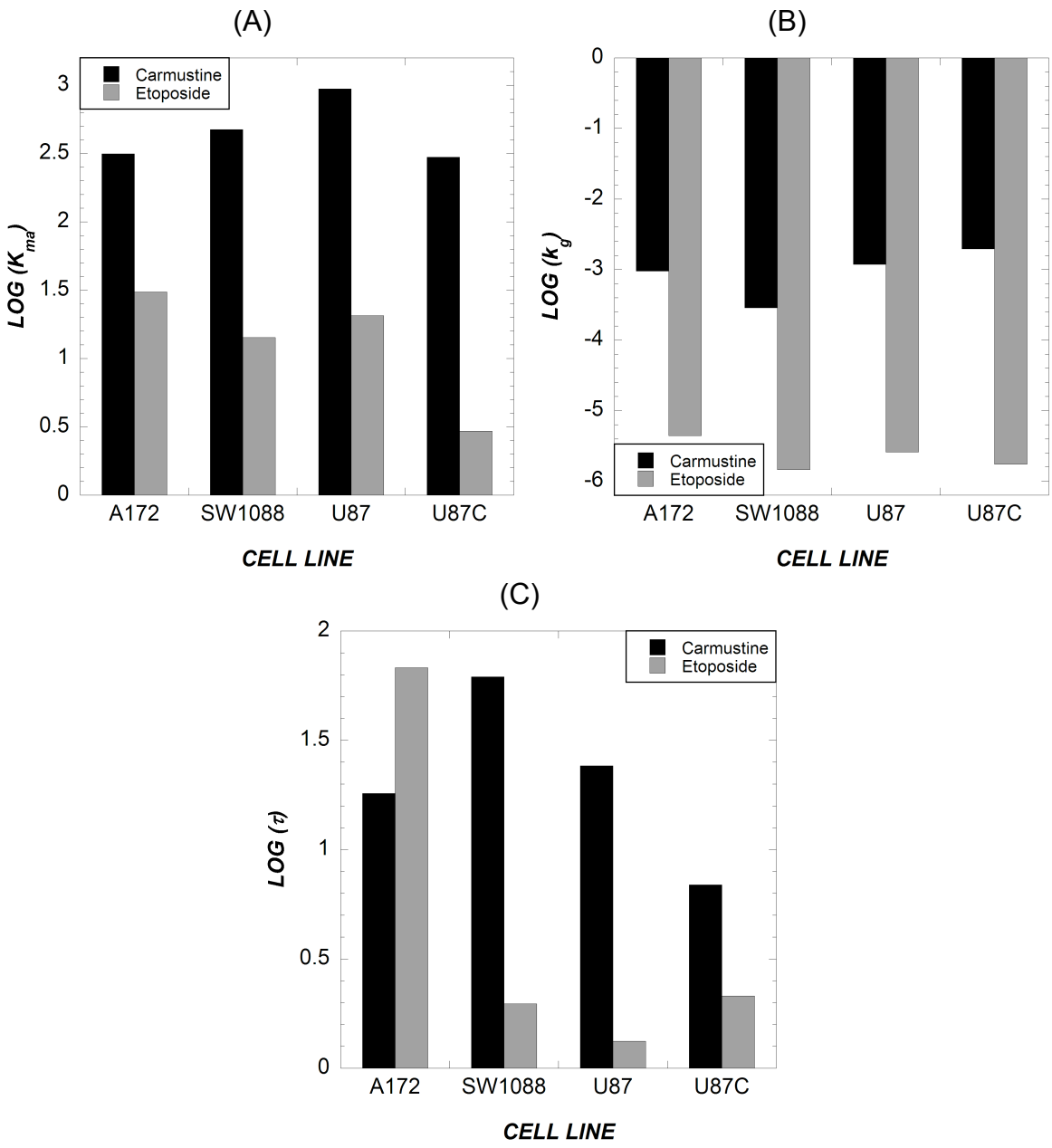

Figure 2.8: Parameters Fit to The Cell Cycle Structured Pharmacodynamic Model Described. (A) effective conc. for cell cycle arrest, K_{ma}, units of μg/mL, (B) rate parameter for entry into cell death pathway, k_g, units of $(\mu g/mL)^{-1}$ h^{-1}, (C) intracellular half-life, τ, units of h.

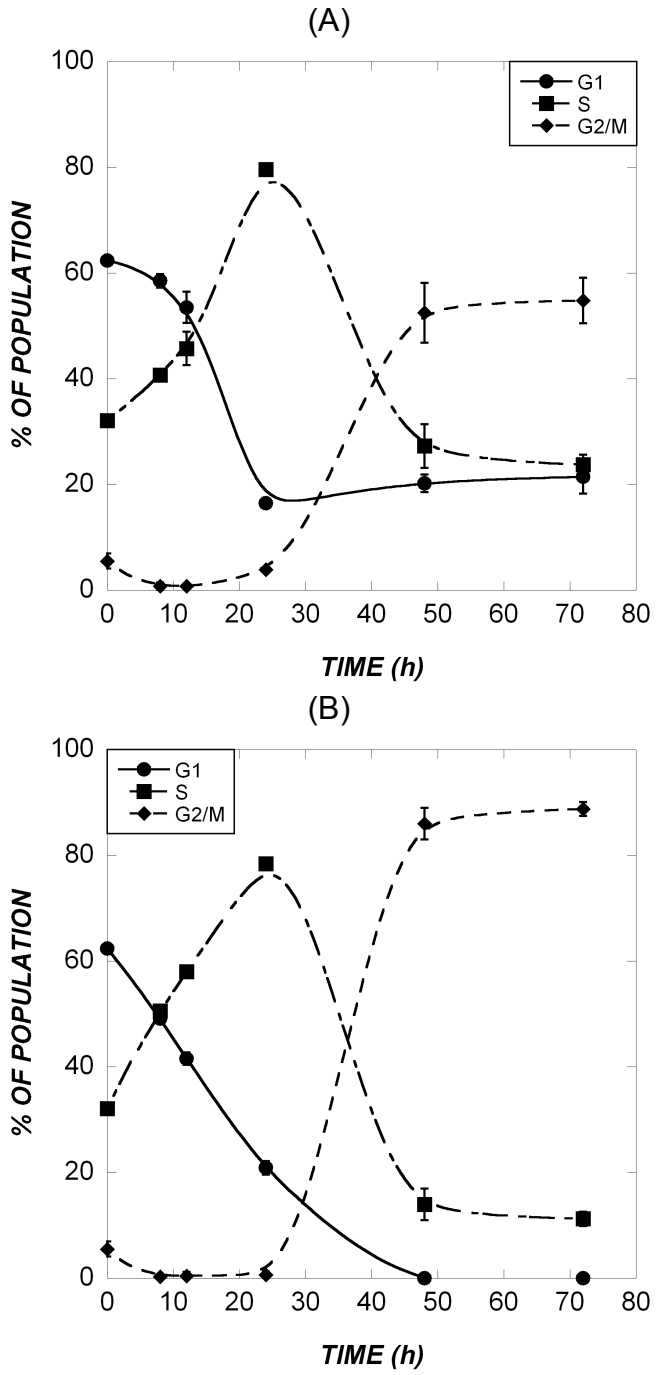

Figure 2.9: Cell cycle Changes of U87 Cells. Redistribution of cell among phases of cell cycle subsequent to exposure to (A) carmustine (25 μg/mL) or (B) etoposide (5 μg/mL)**.**

(A)

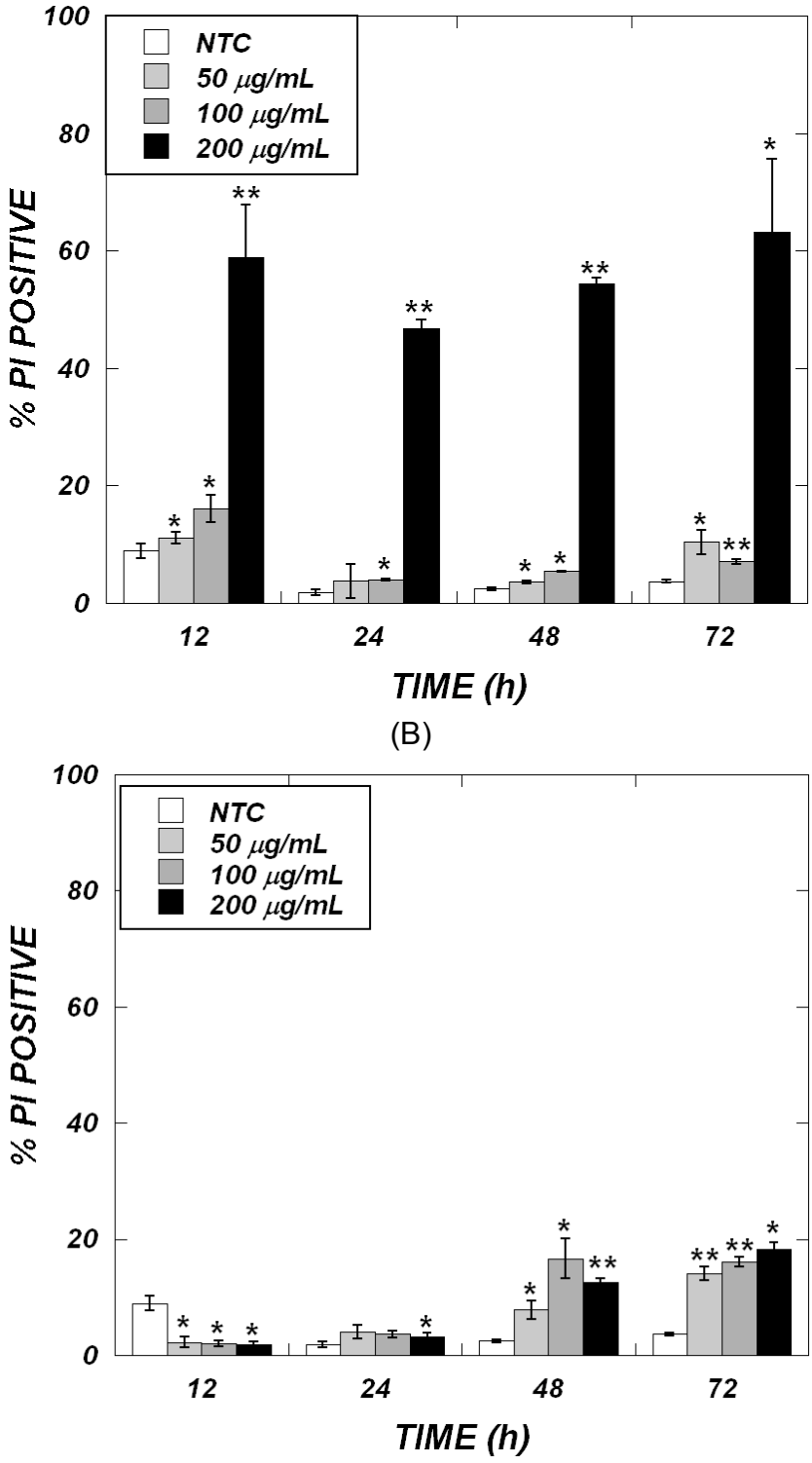

Figure 2.10: Propidium Iodide (PI) Staining of U87 Cells. (A) carmustine or (B) etoposide. * indicates $p<0.05$ and **indicates $p<0.01$ comparing drug treat and control at each time point.

CHAPTER 3

UNDERSTANDING CHANGES ASSOCIATED WITH ACQUIRED RESISTANCE TO CARMUSTINE IN GLIOMA CELL LINES THROUGH GENE EXPRESSION PROFILING

ABSTRACT

Failure of treatment because of acquired resistance to alkylating agents is one of the hallmarks of gliomas. In the current study, we have developed resistance to carmustine in a panel of glioma cell lines through prolonged sublethal exposure. To develop a more mechanistic understanding of resistance, we conducted gene expression profiling of parent versus normal cells upon exposure to carmutine. We utilized gene ontology and systems biology data analysis techniques to unravel modules and biological processes involved in resistance to carmustine. In addition, we validated gene expression results by characterizing changes in cell death and growth arrest in resistant cells and their parent cell lines upon exposure to carmustine. We also investigated the role DNA damage repair in resistance to carmustine.

We performed gene expression profiling along with gene ontology in resistant and parent cell lines upon exposure to chemotherapy. We found that the NFκB pathway plays an important role in promoting survival in resistant cells, through the induction of inflammatory response genes. In addition, we found that resistant cells induce genes promoting cell cycle arrest and repress genes implicated in cell cycle phase transitions and proliferation. DNA repair genes were not implicated in response to carmustine. In agreement with expression profiling results, resistant cells exhibit a higher level of survival upon exposure to carmustine, given by the fraction of apoptotic and necrotic cells, compared to parent cell lines. In addition, resistant cells exhibit more rapid arrest in

G2/M compared to parent cell line. We explored the status of DNA repair capacity, which is known to control both cell death and cell cycle arrest, upon exposure to carmustine. We found that resistant and parent cell line did not exhibit differential capacity to repair DNA. Our results provide insights into molecular pathways involved in resistance to carmustine *in vitro*. If they prove to hold for gliomas in human patients, these results can point the way towards improved therapeutic regimens that act upon NFκB mediated cell survival module in concert with cell cycle checkpoint abrogators.

3.1 INTRODUCTION

Gliomas are the most lethal primary tumors in the central nervous system. They are highly infiltrative, which renders surgical resection and radiation practically ineffective. In addition, prognosis is very poor because of high recurrence rate and increased resistance to chemotherapy. In order to develop more effective treatments and improve patient outcome, a better understanding the molecular basis of resistant phenotype is required.

The monofunctional alkylating agent 1,3-bis(2-chloroethyl)-1-nitrosourea (BCNU), a DNA alkylating agent, has been used in the treatment of gliomas as an adjuvant to surgical resection and radiation [2]. Carmustine is currently used in Gliadel® wafers [65], which are implanted intracranially subsequent to tumor resection. Alkylating agents result in the formation of O^6-alkylguanine, N^7-alkylguanine, N^3-alkyladenine, and N^3-alkylguanine. In addition, alkylation results in the formation of critical secondary DNA damages [4]. Carmustine has been shown to elicit its cytotoxic effects through growth arrest, apoptosis or combination thereof [6]. However, the effects of carmustine, and alkylating agents in general, have been shown to be reversed by the presence of active methyl guanine methyl transferase (MGMT), base excision repair (BER) and translesion DNA synthesis (TLS) systems [4]. In addition, alterations in cell cycle regulation and cell death pathways—which are regulated by DNA repair pathways—have been correlated with resistance [66]. A comprehensive model for resistance, involving the regulation of these three processes, is currently lacking.

A multitude of molecular pathways have been implicated in resistance to chemotherapy in glioma models [3]. However, the presence or absence of any of these

markers does not necessarily indicate a certain level of response because of the complexity of the resistant phenotype. This is further complicated by the fact that tumor cells exhibit a high degree of redundancy in survival and proliferation pathways and genetic heterogeneity within tumors and from patient to patient [18]. In addition, a mechanistic understanding of resistance in light of these markers is currently lacking. Thus, it is important to characterize biological systems, and their interactions, that are implicated in resistance, which is a multifactorial and a coordinated process [67].

A number of studies have utilized genome-wide gene expression profiling using microarrays to select a group of genes implicated in resistance or "resistance signature" to a given chemotherapeutic agent in different cancer models as well as gliomas [28-30, 34, 68-73]. These studies tend to ignore a good portion of information that is embedded in the data because of low differential expression or averaging the expression over a population with heterogeneous genetic background [74]. Thus, it is important to analyze microarray data from complex phenotype studies, such as resistance, in the context of biological processes or gene modules rather than gene lists. Using this methodology, one can obtain more meaningful and useful results from the therapeutic perspective [43].

In the current work, we have developed resistance to carmustine in a panel of glioma cell lines, with disparate molecular composition (see Appendix Tables A.7-A.9), through prolonged exposure to sublethal doses of carmustine. To develop a more mechanistic understanding for resistance, we conducted gene expression profiling of parent versus normal cells upon exposure to carmutine. We utilized gene ontology and large scale data analysis techniques to unravel modules and biological processes involved in resistance. In addition, we characterized changes in cell death and growth arrest

between resistant cells and their parent cell lines upon exposure to carmustine. In addition, we investigated the role of DNA damage repair in resistance to carmustine.

3.2 MATERIALS AND METHODS

3.2.1 Chemotherapeutic Agents

BCNU and Etoposide were purchased from Sigma-Aldrich (St. Louis, MO), and dissolved in DMSO (Sigma-Aldrich, St. Louis, MO) and stored at -20 ^{o}C at a stock concentration of 50 mg/mL.

3.2.2 Cell Lines

Human Glioblastoma cell lines A172 and U87 and astrocytoma cell line SW1088 were purchased from American Type Culture Collection (Rockville, MD). A172 and SW1088 were cultured in DMEM (Invitrogen, Carlsbad, CA) supplemented with 10% FBS (GIBCO-BRL, Gaithersburg, MD), 4 mM L-glutamine (GIBCO, Gaithersburg, MD), and 100 U/mL Penicillin/Streptomycin. Human glioblastoma cell line U87 was cultured in MEM (GIBCO-BRL) supplemented with 10% FBS, 4 mM L-glutamine, 100 U/mL penicillin/streptomycin. Cells were cultured at 37 ^{o}C and 5% CO_2 atmosphere.

3.2.3 Resistant Cell Lines

Resistant cell lines were developed by sublethal exposure to incremental doses of carmustine. Cells were exposed to an initial concentration of 15 μg/mL for 48 hours. Subsequently, cells were incubated in drug free media. Increments of 5 μg/mL were used when cells show increased survival. Cells underwent 11 cycles of treatment over a period of 8 months. Maximum concentration to which cells were exposed was 40 μg/mL. After cells achieved a significant level of resistance, as evidenced by viability assay, cells were pulsed with 10 μg/mL of carmustine every 4 weeks to maintain resistant phenotype.

3.2.4 Viability Assay

Cells were resuspended in culture medium at a concentration of 10^5 cells/mL. 100 µL of cell suspension (10000 cells) were seeded in wells of a 96-well plate. Cells were cultured for 18 hours to assure proper attachment. Dilutions of BCNU and etoposide, along with DMSO (Sigma-Aldrich, St. Louis, MO) as vehicle control, were prepared in culture media and added to cells for 72 hours or designated time-points. 20 µL of MTS solution (Promega, Madison, WI) was added to every well and left to incubate for two hours. Absorbance plate reader (Bio-Rad, Hercules, CA) was used to measure absorbance at 490 nm. Average of six wells per single drug concentration was normalized to vehicle control (cells treated with DMSO). Empirical fitting of dose response curves was performed using the following equation:

$$f = f_{resist} + \frac{1 - f_{resist}}{1 + \left({}^{[D]}\!/\!_{IC50} \right)^n} \tag{10}$$

where f is the fractional viability (relative absorbance), [D] is the drug concentration, and the three fitting parameters $f_{resis}t$, IC_{50} and n are interpreted as a fraction of resistant cells, the standard pharmacological IC_{50} value, and a cooperativity (Hill) coefficient, respectively. Empirical fits were performed using the software package KaleidaGraph v. 4.03 (Synergy Software, Reading, PA).

3.2.5 Growth Inhibition Assay

Cells were suspended in culture medium at a concentration of 2.5×10^3 cells/mL. 500 µL of cell suspension were seeded in wells of a 24-well plate. Cells were cultured for 24 hours to assure proper attachment. Dilutions of BCNU and etoposide, along with DMSO (Sigma-Aldrich, St. Louis, MO) as vehicle control, were prepared in culture

media and added to cells for 72 hours. Cells were washed twice with phosphate buffered saline (PBS) and were left to grow in drug free media for 10 days. Cells were washed twice with ice cold PBS. 250 μL of 20 mM calcein (Molecular Probes, Eugene, OR) in PBS was added to each well and cells were incubated for 45 minutes and 4 ^{o}C. Fluorescence plate reader (Beckman Coulter, Fullerton, CA) was used to measure fluorescence (485 nm excitation /535 nm emission), which results from oxidized calcein by live cells. Average of three wells per single drug concentration was normalized to vehicle control (cells treated with DMSO).

3.2.6 RNA Extraction and Hybridization

Total RNA was isolated from exponentially growing cells using RNeasy mini kit (Qiagen, Valencia, CA) according to manufacturer's protocol. The quality of RNA was assessed via Agilent bioanalyzer 2100 using the RNA nano kit (Agilent Technologies, Palo Alto, CA). cDNA synthesized from 5 mg of RNA using SuperScript® VILO cDNA synthesis kit. RNA from control (DMSO) or carmustine treated cells was labeled indirectly using a dendrimer-based [75] Genisphere 3DNA Array 350 labeling kit (Genisphere, Hatfield, PA). Remaining washing steps were performed according to manufacturer's protocols.

3.2.7 Experimental Setup and Data Analysis

Each of the six cell lines (A172, A172CR, SW1088, SW1088CR, U87 and U87CR) were treated with vehicle control (DMSO) or carmustine for one hour, 4 biological replicates were used for each treatment. Two pairs of dye swap experiments were performed for each cell line. Microarrays were scanned on a GenePix 4000B scanner (Axon Instruments, Union City, CA). GPR files containing raw data were loaded

into MATLAB (Mathworks). For each cell line, features were removed from the entire dataset (4 replicates) if one array had a negative flag or negative value after background subtraction. In addition, featured were excluded if the average expression did not exceed 2-fold change and were not found to be consistent in at least three of the four replicates. Filtered data were loaded in R statistical programming environment. Data were normalized using LOWESS algorithm. Differentially expressed genes were determined using MAANOVA (*M*icro*A*rray *AN*alysis *O*f *VA*riance) package in R [76]. The fixed-effect linear ANOVA model that accounts for dye, array and sample variation was used pick differentially expressed genes. We then tested a null hypothesis of no differential expression using F statistics computed on the James-Stein shrinkage estimates of the error variance [77]. To avoid any assumption on error distribution, the package offers the possibility of computing p-values for hypothesis tests via permutation methods (in our analyses 500 permutations with sample shuffling were carried out). Finally the false-discovery rate controlling method [78] was used to correct significance estimate for multiple testing hypothesis. We selected, as differentially expressed, the features with $p < 0.05$ for further analysis.

3.2.8 Gene Ontology and Functional Network Analysis

Ingenuity Pathway Analysis (Ingenuity Systems, Mountain View, CA) is a web delivered application that allows the discovery, visualization and exploration of molecular interaction networks in gene expression data. We used IPA to obtain gene ontology, canonical pathways and functional networks. Differentially expressed, statistically significant, genes along with GenBank (National Institutes of Health, Bethesda, MD) accession number and fold-change were uploaded to IPA. Each accession

number was mapped onto its corresponding gene product in the IPA knowledge base. These mapped focus genes were used as a starting point for generation biologic networks. A score was computed for each network according to the fit of the original set of significant genes. This score reflects the negative logarithm of the P-value that indicates the likelihood of the focus genes in a network being found together as a result of random changer. Using a 99% confidence level or $[-\log_{10}$ (P-value)$] \geq 2$ were considered significant.

3.2.9 Propidium Iodide Exclusion

To determine extent of cell death, cells were incubated with 100 μg/mL carmustine for 24 hours. Floating dead cells were collected as well as viable cells and were washed with PBS. Cells were suspended in a 20 μg/mL solution of propidium iodide in PBS and immediately analyzed by flow cytometry, described below.

3.2.10 Flow Cytometry

Propidium Iodide (PI) (Molecular Probes, Eugene, OR) staining was performed to determine cell cycle phase distribution based on DNA content. Cells were seeded a density of $2x10^5$ cells and were left for 16 hours. Subsequently, cells were exposed to 25μg/mL of carmustine and harvested at 0,12, 24, 48 and 72 hours. At designated time-points, cells were washed with PBS (GIBCO-BRL) and fixed in 70% ice cold ethanol. Cells were centrifuged at 300 rcf for 6 minutes at 4 ^oC. Cell pellet was washed twice with PBS then stained with 20 μg/mL PI (Molecular probes, Eugene, OR) in 0.1% (V/V) Triton X-100 (Bio-Rad Laboratories) PBS solution with 0.2 mg/mL RNaseA (Qiagen, Valencia, CA) in PBS for 15 minutes at room temperature in the dark. Analysis was performed with FACScan flow cytometer (Becton-Dickinson, Mansfield, MA). Cell

cycle distributions, generated by CellQuest (Becton-Dickinson), were imported into ModFit software (Verity Software House, Topsham, ME) to quantify the fraction of cells in each phase of cell cycle. Triplicate samples were used for every time-point.

3.2.11 Single Cell Alkaline Electrophoresis (Comet) Assay

The amount of DNA damage subsequent to drug exposure was quantified using a single cell alkaline electrophoresis assay (Trevigen Inc., Gaithersburg, MD). Cells were exposed to 50 μg/mL of carmustine for 2 hours. Cells were then washed and harvested (time zero) or washed and incubated in drug-free media and harvested at designated time points. Cells were washed and trypsinized in the dark and suspended in ice-cold PBS at a concentration of 10^5 cells/mL. 30 μL of cell suspension were added to 300 μL of Low Melt Agarose (LMA) (Trevigen Inc.), which had been incubated at 37 ^{o}C for at least 30 minutes. 50 μL of cell suspension in LMA were added to the sample slot of the CometSlide ^{TM} (Trevigen Inc.). CometSlides ^{TM} with samples were incubated at 4 ^{o}C in the dark for 30 minutes to allow LMA to solidify; subsequently, CometSlides ^{TM} were immersed in chilled mild lysis buffer (Trevigen Inc.) for at least two hours in the dark at 4 ^{o}C to allow for cell lysis within LMA. CometSlides ^{TM} were then incubated in an alkaline buffer of pH ~ 13 (Trevigen Inc.) at room temperature for 20 minutes in the dark. CometSlides ^{TM} were subsequently immersed in an alkaline electrophoresis buffer (200 mM NaOH, 1mM EDTA) and run in an electric field of 300 mA for 20 minutes at 4 ^{o}C. CometSlides ^{TM} were washed two times in distilled water and once in 70% ethanol for 5 minutes, subsequently slides were dried at 45 ^{o}C to bring cells into a single plane for microscopic analysis. CometSlides ^{TM} were stained with Sybr Green ® and images were captured with epifluorescence microscope. Images were analyzed in ImageJ software

[79] and amount of damaged DNA was quantified as the integrated intensity of the tail moment relative to the total intensity of DNA in the tail and nucleus, where at least 100 comets for each time-point or condition were analyzed.

3.2.12 Statistics

Experiments were performed that there are at least three replicate populations of cells for each measurement. Each data point is reported as mean of populations and error bars represent standard deviations, unless stated otherwise. When possible, statistical significance was determined using single-tailed Student's t-test. Results were deemed statistically significant for confidence levels of 95% ($p < 0.05$). For multiple comparisons, one-way ANOVA was performed and Tukey's HSD test performed for pairwise comparisons.

3.3 RESULTS

3.3.1 Acquired Resistance to Carmustine

A172, SW1088 and U87 were exposed to 11 cycles of treatment with carmustine. Population of cells surviving after 11 cycles of treatment were deemed resistant and named A172CR, SW1088CR and U87CR. To confirm the acquisition of resistant phenotype, parent cell lines (A172, SW1088, and U87) and their resistant counterparts (A172CR, SW1088CR, and U87CR) were exposed to varying concentrations of carmustine for 72 hours and their viability (metabolic activity) was determined via MTS assay (Figure 3.1 A-C). As expected, A172CR, SW1088CR and U87CR exhibit higher viability compared to their parent cell lines, at concentrations ranging from (20 to 100 μg/mL). At lower concentrations, resistant and parent cell lines exhibit similar viability.

At high concentrations (<100 μg/mL), fraction of cells surviving is minimal in both groups of cell lines.

Pharmacological dose response curves were fit to equation (9) and EC_{50} values were estimated (Table 3.1). Parent cell lines (A172, SW1088 and U87) exhibit the same level of intrinsic resistance to carmustine, given by the equal EC_{50} values. However, U87CR cells seem to possess the highest level of acquired resistance compared to SW1088CR and A172CR. In both groups of cell lines, the fraction of cells surviving at the highest dose of carmustine is close to zero as shown from the fit value for f_{resist}.

Growth inhibition assay was performed to assess the effect of drug exposure on proliferation (Figure 3.2 A-C). A172CR and SW1088CR cells exhibit higher proliferation rate subsequent to drug exposure compared to the parent cell lines. This is an indication that resistant cells have an increased capacity to overcome the effects of carmustine exposure and resume proliferation when compared to the parent cell lines. It is worth noting that A172 cell line maintains a high level of proliferative capacity compared to the other two parent cell lines, which could be interpreted as a higher level of intrinsic resistance. This is probably reflected in the decreased acquisition of resistance in A172CR cells. This is agreement with the study performed by Wolff et al., which investigated the response of a panel of glioma cell lines to a wide range of chemotherapeutic agents. It was found that A172 cells are the most resistant cell line to the range of chemotherapeutic agents tested [80].

3.3.2 Gene Expression Profiling and Gene Ontology Analysis

In order to understand the molecular basis behind acquisition of resistance to carmustine, we performed gene expression profiles using oligonucleotide arrays. To

characterize early response genes implicated in response to carmustine, we compared changes in gene expression profiles upon exposure (1 hr) to 70 μg/mL of carmustine compared to vehicle control (DMSO) in resistant and parent cell lines. The gene expression changes varied among cell lines: 182 (99 induced and 83 repressed) in A172 cells, 231 (113 induced and 118 repressed) in A172CR cells, 271 (131 induced and 140 repressed) in SW1088 cells, 320 (172 induced and 138 repressed) in SW1088CR cells, 261 (161 induced and 100 repressed) in U87 cells, and 230 (114 induced and 116 repressed) in U87CR cells.

Inginuity Pathway Analysis (IPA) tools were used to establish interactions, based on data reported in literature, among differentially expressed genes in each of the cell lines; these interactions are divided into functional networks, each of which is associated with a specific cellular function, physiological state or a given disease (see Appendix, Tables A.1-6, for detailed listings of networks and functions for each cell line).

Top scoring functions varied among cell lines (Table 3.2). However, some functions--such as cell cycle, cell growth and proliferation, and cell death--were regulated in the majority of cell lines. It is worth noting that genes associated with these functions were not common among any of the cell lines. This is an indication that each cell line has a specific carmustine response signature.

Network analysis based on predetermined, manually curated, molecular interactions show that networks centered around NFκB signaling are among the top 4 scoring networks of each cell line (Table A.1 network 1, Table A.2 network 2, Table A.3 network 3, Table A.4 network 1, Table A.5, network 1, Table A.6 network 4, and Figures 3.4-3.6). In addition, top-scoring functional networks that are implicated in cell death, cell cycle,

and DNA recombination and repair were connected to networks built around NFκB in all cell lines. This is in agreement with similar studies indicating the role of NFκB signaling in response to O^6-alkylalting agents [43, 81].

At the level of cell death and survival, top-scoring networks in A172 cells are build around cell survival and proliferation pathways such as NFκB, PI3K, MAPK and Jnk (Table A.1, network 1). That is, genes with differential expression in the dataset have direct relationships with these pathways; however, the net effect of changes in gene expression are not conclusive as some alterations result in a proapoptotic (repression of NOL3 and induction of RARB) outcome, while others result in an antiapoptotic (repression of TRAIL and induction of MAP2K) outcome (Table 3.3). In A172CR, cell survival is correlated with increased expression of inflammatory response genes (Table A.2, network 1 and 2; Table 3.3; and Figure 3.4), which is consistently correlated with increased survival in glioma models [82].

At the level of cell cycle changes, A172CR exhibit increased regulation compared to parent cell line. In A172CR, genes that are associated with transitioning between phases of cell cycle were repressed (CDC2, BIRC5, TOP2, RAD21, etc.). On the contrary, A172 cells exhibit significant induction of genes that promote re-entry into and progression of cell cycle, such as GAS6, MAP2K1, and MXD3 (Table 3.3). Both cell lines did not exhibit a high degree of regulation of DNA replication, recombination and repair; however, A172CR showed an induction of 3 genes implicated in repair of DNA strand breaks (FGF2, IL24, and SMAD3).

SW1088 cells exhibit a higher degree of regulation of cell death compared to SW1088CR (58 differentially expressed genes versus 19, Table 3.3). Nodes of the NFκB

network are repressed in the case of SW1088 (Table A.3, network 4, and Figure 3.5). This repression of NFκB is also concomitant with the presence of proapoptotic changes in gene expression, such as the induction of genes correlated with proapoptotic outcome (CDC20 and CRAPB) and repression of genes correlated with antiapoptotic outcome CYR61 and CXCL1. In the case of SW1088CR, changes in expression of genes implicated in cell death are inconclusive as some change were antiapoptotic while others were proapoptitc.

At the level of cell cycle regulation, SW1088 cells exhibit a much higher level of regulation compared to SW1088CR cells. SW1088 cells exhibit more changes that favor progression through G1/S phases and mitosis—given by increased expression of ADM, CSF, and CDC20—compared to SW1088CR cell line. The expression profile changes of genes involved in DNA repair were not significant, with genes involved in resolving DNA double strand breaks were consistently repressed in SW1088, which is counter intuitive.

At the level of cell death and survival, U87CR cells exhibit a higher level of significant changes; there is a consistent induction of gene associated with survival (CAT, CSF, IL1A, and TAF1B) and repression of genes associated with cell death (CD40, APH1B, FKBP38, WIPF1 and MET). Many of these genes are involved in mounting inflammatory response as well, which could explain the enhanced survival of U87CR cells (Figure 3.6).

U87 cells exhibit a high degree of cell cycle regulation upon exposure to carmustine. Cell cycle regulation is the top-scoring function (Table 3.3) and cell cycle regulation appears in 3 of the 5 top-scoring networks (Appendix, networks 1, 2 and 4).

Some of these changes favor arrest, such as induction of G1 arrest genes (p21 and KRAS) and repression of genes that transition into S phase (E2F3, MPG and NRG1). Other changes, however, favor progression through G1/S (induction of DTD1, ELVAL1, and HAS2). In addition, there is a consistent induction of genes that result in cell proliferation (GSK3B, KRAS, and HSPA2) that is concomitant with repression of genes that hamper proliferation (PURA, and STAT5). U87CR cells, on the other hand, exhibit sustained arrest in G1/S through repression of genes that results in G1/S transition (MET and PLAC1) or induction of genes that result in sustained G1/S arrest (IL1A and CSF2). In addition, other changes in gene expression result in sustained G2/M arrest (induction of IL1A, increases arrest in G2/M, and repression Cyclin A, which increases G2/M phase transition) and decreased proliferation (repression of EGR1 and CD40, which are involved in proliferation).

U87 exhibited a high degree of control over the expression of genes involved in DNA damage response (REV1, APBB1, RPE, MCM6 and MPG), contrary to U87CR cells where there were no significant changes in the expression of genes involved in DNA damage response.

These results indicate that resistant cells exhibit a higher capacity to induce an inflammatory response through NFκB activation compared to parent cells lines, which is indicated by the induction of interleukins in A172CR and U87CR cells. Repression of NFκB components is correlated with increased sensitivity in SW1088 cells compared to SW1088CR. Thus, cell survival pathways seem to play a central role in resistance to carmustine.

At the level of cell cycle regulation, cell cycle arrest, at G1/S and mitosis, and suppressing progression through cell cycle and proliferation is correlated with resistance to carmustine. Carmustine resistant cell lines exhibit gene expression changes that favor arrest, while parent cells exhibit profiles that are less synchronized, where expression changes favoring cell cycle arrest and progression seem to take place simultaneously.

Genes implicated in DNA damage repair processes, which are thought to play a central role in resistance carmustine, did not exhibit significant changes except in the case of U87 cells.

These results indicate that A172CR cells acquired resistance to carmustine through mounting an inflammatory response and tighter control over cell cycle progression compared to parent cell line. In the case of SW1088 and SW1088CR cells, the primary factor in resistance to carmustine is induction of apoptosis. SW1088 exhibit strong proapoptotic profile and marked repression of NFκB complex; conversely, SW1088CR exhibit a strong antiapoptitc profile. At the cell cycle level, SW1088 exhibited changes that favor progression through phases of cell cycle compared to SW1088CR. Similar to SW1088CR, U87CR exhibit a strong antiapoptotic signal, which is concomitant with induction of genes implicated in inflammatory response. In addition U87CR cells maintain a tight control over proliferation compared to U87.

3.3.3 Effect of Drug Exposure on Cell Death and Cell Cycle dynamics

Carmustine, a chloroethylating agent, elicits its cytotoxic effect by inducing cell death, which includes both apoptosis and necrosis [47]; it also includes cell cycle arrest [6]. To validate gene expression results, we utilized PI exclusion assay, which is used for the detection of compromised cells, whether cell death happens through apoptosis or

necrosis [47, 83] (figure 3.3). Cells were exposed to carmustine (100 μg/mL) or vehicle control for 24 hours. Resistant cells exhibit a smaller fraction of cell death compared to parent cells lines, given by percent of PI incorporation. It is worth noting that the A172 cell line exhibits lower level of cell death compared to SW1088 and U87 cells, which is in agreement with previous results indicating a higher level of intrinsic resistance. These results are in agreement with expression profiling experiments, which suggest that carmustine resistant cells induce changes that favor cell survival and suppress apoptosis and cell death.

We have shown previously that U87CR cells are more efficient in arresting in G2/M phase upon exposure to carmustine. These results were further supported by parameters obtained from model fits (see Chapter 2). As such, we aimed to characterize the dynamics of cell cycle distribution of cell lines (parent vs. resistant) upon exposure to carmustine (Figures 3.7-3.9). Cells were exposed to 25 μg/mL of carmustine or DMSO and harvested at designated times. In the case of A172 and U87, resistant cells exhibit an earlier arrest in G2/M phase, by 24 hours, compared to parent cell line, by 48 hours. In addition, U87CR cells have a higher fraction of cells (~70%) accumulated compared to parent cell line (~50%). On the other hand, SW1088 and SW1088CR exhibit a distinct behavior, where parent cell lines exhibit more rapid arrest in G2/M. However, the total change in accumulation in G2/M phase, which is fraction in G2/M at 72 h less fraction in G2/M at 0 h, in SW1088CR is higher than that of the parent cell line. These results are in agreement with the gene expression studies, which suggest that resistant cells exhibit a tighter control over progression through cell cycle, at least at earlier times.

Resistant cells, A172CR, SW1088CR and to a lesser extent U87CR, exhibit a higher capacity to reenter cell cycle at later times, given by the high fraction of cells in G1 and S phases. This observation is in line with the growth inhibition results, which show that resistant cells are more capable of proliferation subsequent to drug exposure. Two possible hypotheses behind the increased capacity of resistant cells to continue progressing through cell cycle after exposure to chemotherapy are: (1) resistant cells are capable of repairing DNA damage induced by carmustine through enhanced DNA repair pathways or (2) cells are capable of progressing through cell cycle, at later times, irrespective of the amount of DNA damage; that is, the amount of damage *per se* is not a determinant in cell response, rather it is the response that the cell mounts.

3.3.4 DNA Damage Repair Capacity

To investigate whether increased efficiency of G2/M arrest in resistant cell lines relative to parent cell lines is mediated by enhanced DNA damage repair in resistant cells, we exposed resistant and parent cell lines to 50 μg/mL of carmustine for 2 hours, after which cells were incubated in drug-free media and harvested at designated times. Comet assay was performed to detect the level of DNA damage (Figure 3.10).

A172 and SW1088 cells accumulated comparable levels of DNA damage subsequent to exposure to carmustine (Figure 3.11 A and C), which could be an indication that the level of DNA damage is not a factor in the increased level of intrinsic resistance of the A172 cells line. In addition, resistant cell lines, A172CR and SW1088CR exhibit increased initial DNA damage, at time zero; however the level of damage at 4 hours becomes similar to that of the parent cells lines (Figure 3.11 B and D). U87 cells have a distinct response to DNA damage in which the parent cell line

accumulates more damage (> 50%) upon carmustine exposure compared to resistant cell line (~25%); however, the damage is repaired in parent cell lines to a much lower level (<25%), while resistant cell line has a sustained level of damage (~30%) (Figure 3.11 E and F), these results are in agreement with the gene expression profiling results, where U87 cells exhibit changes in the gene involved in DNA damage response. These data, in agreement with gene expression profiles, indicate that the resistance phenotype to carmustine is not the result of enhanced DNA repair capacity. These cells are known not to express significant amounts of MGMT [84, 85]. Thus, resistance could not be the result of elevated levels of MGMT.

The status of mismatch repair determines the response to alkylating agents, where alkylguanines are known to pair with a thymine residue instead of cytosine. The mispairs are detected via hMLH1, hMSH2 and hMSH6. We monitored the basal expression of these 3 genes and their profiles upon drug exposure. We found that there were no differences in their expression between parent cell line (U87) and resistant cell line (U87CR) with or without drug exposure (data not shown). This suggests that DNA repair processes do not mediate resistance to carmustine.

3.4 DISCUSSION

In the context of chemoresistance, most *in vitro* studies on glioma cell lines have been carried out to characterize the role of a given molecule on the response to a given drug [3, 67]. These studies neglect the effect of heterogeneous genetic background among cell lines and how cells acquire resistance. A more relevant model that has been used, from the therapeutic perspective, is developing resistance *in vitro* through prolonged sublethal exposure to a given chemotherapeutic agent [33, 34, 43, 86, 87].

In spite of being a hurdle in the treatment of gliomas, acquired resistance to carmustine has not been thoroughly investigated. In this study, we have developed resistance to carmustine, *in vitro*, in a panel of glioma cell lines through prolonged exposure to escalating doses. After 11 cycles of treatment, three malignant astrocytoma-derived cell lines (SW1088, A172 and U87) exhibit increased viability subsequent to drug exposure (Figure 3.1). In addition, resistant cells exhibit increased capacity to overcome drug effects and resume proliferation subsequent to drug exposure when compared to parent cell lines, with the exception of U87 cells where the differences between parent cells and resistant cells are minimal (Figure 3.2).

To understand the molecular basis involved in resistance to carmustine, we characterized gene expression profiles upon exposure in parent and resistant cell lines at early times (1 hr). We have chosen early events to in order to monitor changes in the entire population of cells, rather than later time points where only the surviving fraction of cells is examined. This experimental setup highlights the distinct response of parent and resistant cell lines to carmustine exposure, which could ultimately lead to increased efficacy.

Gene expression profiling of parent and resistant cells upon exposure to chemotherapy indicates that NFκB plays a central role in determining the response of gliomas to carmustine. In addition, cell death (as well as survival, growth and proliferation) and cell cycle arrest represent the most statistically significant associations with response to carmustine in most of the cell lines (Table 3.2). It was found that genes associated with these processes were directly linked to networks centered around NFκB (Appendix, Tables A.1-6). This is in agreement with many reports implicating NFκB in

response to radiation [88], alkylating agents, and etoposide [81] in gliomas and other cancer models.

Resistant cells, A172CR and U87CR, exhibited expression profiles that favor increased cell survival and an antiapoptotic outcome (Table 3.3). This expression signature was accompanied with an increased expression of inflammatory response genes—such as IL1A, IL1B, IL8, and LIF—which are induced by NFκB activity (Figure 3.4 and 3.6). Interestingly, Morandi et al. have shown that *in vitro* acquired resistance to camptothecin (CPT) is mediated by increased expression of IL1B and other inflammatory response proteins [34] in U87 cells. In another study, inflammatory response proteins were found to be upregulated at early times (2 hrs) in response to CPT exposure in U87 cells [89]. In SW1088 cells, repression of NFκB activity upon exposure to carmustine was correlated with an increased proapoptotic signal (Table 3.3 and Figure 3.5). In SW1088CR cells, some changes favored cell death while others favored cell survival. Thus, the main difference between the responses of the two cell lines is the status of NFκB activity, where proapoptotic signal is magnified in the absence of NFκB activity as is the case in SW1088 cells. This conclusion is in line with finding that NFκB activity mediates resistance to carmustine and temozolomide in glioma models and correlates with poor prognosis [43].

In agreement with gene expression profiling results, resistant cells exhibit significantly higher levels of survival upon exposure to carmustine as shown by PI exclusion assay (Figure 3.3). This indicates that resistant cells indeed exhibit a lower propensity for cell death, both apoptotic and necrotic, compared to parent cell lines. This result is in agreement with the study performed by Ma et al, where resistance to

alkylating agents has been correlated with decreased activity of proaptotic genes—Bad, Bax, and BCLXS—and upregulation of antiapoptotic genes—BCL2 and BCLXL [90].

As previously discussed, alkylating agents elicit their cytotoxicity through cell cycle arrest. However, there are conflicting reports about the changes in cell cycle arrest that are associated with a given response to carmustine, and alkylating agents in general. A number of studies have shown that resistance to carmustine in glioma models, U87 cells specifically, is associated with increased accumulation of cells in G2/M, which results from inhibition of p53 activity and decrease in accumulation in S phase [15, 91]. In line with these results, Ruan et al show that resistance to carmustine in glioma cell lines is associated with increased cell cycle arrest, as a result of increased activity of p21 [14]. In addition, it has been shown that abrogation of G2/M arrest with PARP inhibitors results in accumulation of cells in S phase and initiation of apoptosis [92]. In other studies, however, G2/M abrogators—caffeine and PTX—were shown to have no specific effect on the response of glioma cell lines to carmustine [16, 93]. These studies were further supported by other reports that show no correlation between cell cycle arrest and response to carmustine [94, 95]. In contradiction with the previous studies, increased accumulation of glioma cell lines in G2/M is associated with sensitivity as cells undergo apoptosis [96, 97]. These results are in line with the general notion that cell cycle arrest corresponds to decreased tumor growth and, thus, represents a therapeutic target in itself [98].

Gene expression profiling upon exposure to carmustine shows that resistant cell lines possess a higher capacity to execute cell cycle arrest, through induction of genes that promote arrest and repression of genes that promote transitions among phases (Table

3.3). Expression profiles of parent cell lines, on the other hand, suggest a balance between promoting progression (and proliferation) and mounting arrest. This heterogeneity in response could explain higher sensitivity to carmustine compared to resistant cell lines, which prioritize the expression of stress response genes and cell cycle arrest.

At the level of cell cycle dynamics (Figures 3.7-3.9), resistant cells (especially U87CR cells) exhibit an increased capacity to arrest in G2/M at earlier times when compared to parent cell lines. However, SW1088CR exhibit more delayed arrest in G2/M, which could be a result of very tight control in G1/S checkpoint, where cells exhibit very slow transition from G1 to S and ultimately slower accumulation in G2/M.

In the case of A172CR and SW1088CR cells, it is evident that cells are capable of resuming proliferation and progressing through cell cycle after exposure to chemotherapy, as evidenced by an increased fraction of cells in G1 and S phases. This conclusion is further supported by the growth inhibition assay (Figure 3.2), which shows increased proliferative capacity of A172CR and SW1088CR compared to their respective parent cell lines. In case of U87CR, cells are not capable of progressing through cell cycle as indicated by the low fraction of cells in G1 and S phases. This is in agreement with results from a similar study where U87 cells are capable of undergoing senescence upon exposure to chemotherapy without loss of viability [89]. Our results indicate that the ability to undergo senescence is preserved in the parent cell line as well as the resistant cell line, given by the comparable proliferative capacity after exposure to carmustine. Taken together, these results indicate that resistant cells have a higher potential to activate cell cycle checkpoints at earlier times, as seen in the case resistant

cell lines, and G2/M arrest; however, they also have a higher capacity to resolve the checkpoint activation at later times, which is an important determinant of cell fate [10, 99].

The fact that resistant cells have a higher capacity to resolve cell cycle checkpoint activation—and exhibit increased survival upon drug exposure—could be related to the DNA damage repair status. As discussed previously, DNA damage proteins, ATM and ATR, tightly control cell cycle arrest and cell death. The capacity to repair DNA damage has been a subject of debate as a predictor of response to carmustine, and other alkylating agents as well. Many studies argue that enhanced DNA repair correlates with resistance to carmustine in gliomas [13-15, 47, 100-103] as well as other tumor models [104-110]. However, the DNA repair status was found to have no direct effect on response to carmustine, and other alkylating agents in many reports [86, 87, 111, 112]. Moreover, it has been shown that evolution of resistance to carmustine is dependent upon a mutator phenotype, which results from decreased DNA damage repair, and drug mutagenicity [113-115]. This has been shown to be the case in cells acquiring resistance to the combination of carmustine and O^6-benzylguanine (OBG), which is an inhibitor of MGMT. These cells developed mutations to an MGMT amino acid sequence resulting in decreased binding of MGMT to OBG.

Our results indicate that resistant cells do not exhibit increased DNA repair capacity upon exposure to carmustine in comparison to parent cell lines, as indicated by single cell electrophoresis (comet) assay results (Figure 3.11). On the contrary, U87 cell lines exhibit a slightly enhanced repair capacity compared to the resistant counterpart (Figure 3.11 E and F). It is worth noting, that parent cell line accumulates more initial DNA

damage however, when compared to U87CR. Decreased initial damage in U87CR indicates less drug availability, which could the results of increased Pgp activity or increased drug detoxification, both of which are known to be absent in U87 cells [87].

Exposure to carmustine results in the formation of monoadducts (90% of damage) and interstrand crosslinks (3-5%) [116]. The repair of monoadducts is mediated by NER and BER [117, 118]. We have chosen the comet assay to detect the level of DNA damage because it assesses the capacity to repair DNA damage through BER and NER[104]. We, also, found the expression of mismatch repair (MMR) genes (hMLH1, hMSH2 and hMSH6) and MGMT not to be differentially expressed (data not shown) by qRT-PCR. This is in agreement with many reports indicating that MMR is not involved in resistance to carmustine [86, 119-121] or MGMT, which is not expressed in U87 and A172 due to promoter hypermethylation [87, 122].

Gene expression profiling of cell lines upon exposure to carmustine show that DNA repair processes are not significantly altered in any of the cell lines except in the case U87 where genes involved in DNA damage response were differentially expressed. These results are in agreement with the comet assay results, which show increased DNA damage repair capacity in U87 compared to other cell lines. However, these results indicate that DNA repair capacity does not promote acquired resistance to carmustine. These results are supported by similar findings, where genes involved in DNA repair process were downregulated in glioma cells upon exposure to CPT at early times [89]. This downregulation is accompanied with a decrease in proliferation and, hence, DNA replication. It is known that many of the genes involved in DNA replication are involved in repair as well. Thus, the apparent downregulation is probably due to the decrease in

proliferative capacity of cells and not necessarily decrease in DNA repair.

Taken together, later times (subsequent to exposure to camusitne) in the cell cycle dynamics of resistant cell lines and comet assay results indicate that A172CR and SW1088CR have an enhanced alkylation tolerance in comparison to parent cell lines as resistant cells resolve the checkpoint activation in G2/M and continue to proliferate. This hypothesis warrants further molecular characterization at later times subsequent to exposure (48 or 72 hours), as our gene expression characterization addressed early response events. It could be of great importance to understand the molecular events underlying alkylation tolerance and resolving checkpoint.

Our results suggest that the primary aspect of acquired resistance to carmustine in a panel of glioma cell lines is enhanced survival and decreased apoptosis and cell death, mediated by NFκB activity. In addition, increased cell cycle arrest and decreased proliferation seem to further confer cells with resistance, although it is not clear how resistant cells acquire tolerance to alkylation and resume proliferation at later times. In addition, DNA damage repair capacity does not seem to play a significant role in resistance to carmustine, at least at early times. These observations indicate that modulation of NFκB activation and cell cycle checkpoint abrogators could increase the efficacy of carmustine in patients afflicted with gliomas.

3.5 TABLES AND FIGURES

Cell Line	F_{resist}	EC_{50} *	N
U87	-3.77 ± 5.37	74.36 ± 4.66	3.46 ± 0.73
U87CR	-15.11 ± 10.38	135.07 ± 10.4	3.65 ± 0.63
SW1088	-2.50 ± 2.12	69.41 ± 1.85	3.06 ± 0.24
SW1088CR	3.38 ± 6.77	115 ± 7.78	7.46 ± 2.48
A172	-5.1 ± 8.51	63.63 ± 7.06	3.22 ± 1.12
A172CR	-17.77 ± 14.8	90.24 ± 13.92	2.45 ± 0.72

Table 3.1: Pharmacological Parameters of Parent and Resistant Cell Lines
*units of μg/mL

Table 3.2: Top 5 Functions of Each Cell Line. Top-Functions associated with response to carmustine exposure in each of the cell lines. Cell death, cell proliferation and survival, and cell cycle are significant in almost all cell lines.

Cell Line	Molecular and Cellular Functions	P-Value	#Molecules
A172	Cell Morphology	5.9E-5 - 4.6E-2	14
	Cellular Assembly and Organization	5.9E-5 - 4.9E-2	18
	Lipid Metabolism	1.8E-4 - 4.6E-2	8
	Molecular Transport	1.8E-4 - 4.6E-2	8
	Small Molecule Biochemistry	1.8E-4 - 4.6E-2	15
A172CR	Cellular Movement	2.7E-7 - 8.7E-3	23
	Cellular Growth and Proliferation	6.2E-7 - 8.7E-3	58
	Cell Cycle	1.2E-5 - 9.5E-3	33
	Lipid Metabolism	1.5E-5 - 9.5E-3	13
	Molecular Transport	1.5E-5 - 8.2E-3	14
SW1088	Cell Death	1.6E-7 - 3.7E-3	58
	Cellular Growth and Proliferation	1.6E-6 - 3.7E-3	54
	Cell Cycle	2.1E-6 - 3.7E-3	33
	Cell Morphology	3.7E-6 - 3.7E-3	20
	Cellular Development	4.1E-6 - 3.7E-3	49
SW1088CR	Cell Death	9.8E-4 - 4.4E-2	19
	Gene Expression	9.8E-4 - 3.8E-2	13
	Cell Cycle	1.6E-3 - 3.8E-2	6
	Cell Signaling	1.6E-3 - 4.9E-2	15
	DNA Replication, Recomb., and Repair	1.6E-3 - 4.4E-2	12
U87	Cell Cycle	3.7E-5 - 2.2E-2	28
	DNA Replication, Recomb., and Repair	1.2E-4 - 2.2E-2	11
	Cellular Growth and Proliferation	2.7E-4 - 2.2E-2	24
	Cellular Development	3.6E-4 - 2.2E-2	27
	Gene Expression	5.4E-4 - 2.2E-2	34
U87CR	Cell-To-Cell Signaling and Interaction	1.1E-4 - 3.9E-2	17
	Cellular Growth and Proliferation	1.1E-4 - 3.9E-2	15
	Cellular Assembly and Organization	2.9E-4 - 3.9E-2	19
	Antigen Presentation	3.2E-4 - 3.9E-2	4
	Cell Death	4.9E-4 - 3.9E-2	15

Table 3.3: Gene Expression Changes Associated with Cell Death and Cell Cycle in Cell Lines. Boldfacing indicates genes that were induced, while underlined genes were repressed. The outcome of expression changes is summarized herein after evaluating gene function based in IPA knowledge base.

Cell	Process	Changes	Outcome
A172	Cell Death	**ADM**, **BAG1**, **BOK**, **CDC42**, **EEF1A**, **G6PD**, **GAS6**, KLF5, LAMA2, **MAP2K1**, **MXD3**, NOL3, **P4HB**, PIAS1, **RARB**, TNFSF10, **TOP1**	Proaptotic and antiapoptotic changes
A172	Cell Cycle	**ADM**, **CDC42**, **CDC45L**, **GAS6**, **MAP2K1**, **MLF1**, **MXD3**, PIAS1, **RARB**, **TIPIN**, TNFSF10, **TOP1**	Changes favoring reentry into and progression through cell cycle
A172CR	Cell Death	**ALDH1A3**, **ANGPTL4**, **B4GALT5**, BIRC3, BIRC5, BNIP3L, CCNI, CDC2, **CSF3**, **CUL1**, **CXCL3**, CYR61, **ESPL1**, FAIM2, **FGF2**, **GATA6**,**GNB1**, **IL8**, **IL24**, **IL1B**, **LAT**, **LIF**, MAP4, **MAPT**, **MCL1**, NAPA, PEG10, **PINK1**, **PMEPA1**, PPP1R15B, **PTGES**, **PTGS2**, PTN, RAD21, S100A4, **S100A8**, **SCG5**, **SLC1A2**, **SMAD3**, **SPHK1**, **ST3GAL1**, TACC3, TOP2A, TOPBP1, UBE2C, USP18	Antiapoptotic changes given by increased inflammatory response
A172CR	Cell Cycle	BIRC5, CCNI, CDC2, COPS2, CP110, **CSF3**, CTNND1, **CUL1**, CYR61, **ESPL1**, **FGF2**, **GATA6**, **IL8**, **IL24**, **IL1B**, KIF23, **LIF**, MAP4, **PFTK1**, PRC1, **PTGS2**, PTN, RAD21, S100A4, **SMAD3**, **SPHK1**, TACC3, TOB2, TOP2A, TOPBP1, TPX2, UBE2C, ZWINT (includes EG:11130)	Changes favoring arrest
SW1088	Cell Death	**ADM**, **ATP6AP1**, BDKRB1, BHLHE40, CCL2, **CDC20**, CDK6, **CRABP2**, **CSF1**, CSF2RB, CTGF, CTNNA1, CXCL1, CXCL2, CYR61, **DDIT3**, **DDIT4**, DUSP6, **EGR1**, **ELAVL1**, EPHX1, F3, FGF2, FIP1L1, GLIPR1, GNA13, **HLA-G**, **ID1**, **ID2**, IL6, IL8, **ITGAV**, **JAK1**, KLF5, KLF10, LIF, **LRDD**, **MSX1**, **NAIF1**, NFKB1, OPN1SW, **PHLDA1**, PMEPA1, **PPAP2A**, PRKDC, **PSAP**, RAD21, RCAN1, SALL1, SH3RF1, SMARCC1, **SNAI1**, SSPN, TACC1, TJP2, **TP53**, TSLP	Proapototic changes accompanied with repression of NFκB components

SW1088	Cell Cycle	**ADM**, ARNTL2, BHLHE40, **CDC20**, CDK6, CDK7, **CSF1**, CYR61, **DDIT3**, **EGR1**, **ELAVL1**, **EPB41L1**, ERRFI1, FGF2, GNA13, **ID1**, **ID2**, IL6, IL8, **ITGAV**, LIF, **MX2**, NFKB1, **PPAP2A**, PRKDC, **PSAP**, RAD21, **SNAI1**, TAF1D, TARDBP, **TP53**, TSLP, ZNF365	Changes favor transition through G1/S and mitosis
SW1088CR	Cell Death	ATP2A2, BCL2L1, CD74, SOCS2, **FCGR2A**, FKBP8, GPR37, **HIP1**, IGFBP3, **NCOA6**, PIK3CA, PLAU, PLSCR3, POT1, **PSEN2**, **PTGER4**, SETMAR, **SP1**, **TRPV1**	Proapoptotic and antiapoptotic changes
SW1088CR	Cell Cycle	BCL2L1, EPB41L1, PLAU, **PSEN2**, RMI1, WRN (includes EG:7486)	Changes favor arrest
U87	Cell Death	**ABCB7**, APBB1, AMIGO2, **ATP6AP1**, **BRE**, **CCDC88A**, **CDC73**, **CDK8**, **CDKN1A**, **CNNM4**, **CSNK1E**, **DDR1**, **DNASE2**, E2F3, **ELAVL1**, **GAB1**, **GSK3B**, **HAS2**, **HSPA2**, ITGA2B (includes EG:3674), **KHDRBS1**,**KRAS**, **MAML2**, MFN1, MITF, MPG, **MSN**, **MT1E**, **MTPN**, MUC2, MXD3, NEK8, NRG1, PIGT, PPP1R8, PURA, RAD54L, **SFRP2**, **SFRS2**, **SMPD1**, **SOAT1**, **SORBS2**, **SP3**, STAT5B, **TBX21**, **TNC**, **TRAF6**, VEGFA	Proapoptotic and antiapoptotic changes
U87	Cell Cycle	APBB1, **AURKB**, **BRE**, **CDKN1A**, **DTD1**, E2F3, **ELAVL1**, **GAB1**, **GSK3B**, **HAS2**, HOXB3, **HSPA2**, **KHDRBS1**, **KIF22**, **KRAS**, MITF, MPG, **MT1E**, MXD3, NRG1, PURA, RAD54L, **SFRS2**, STAT5B, TFE3, **TNC**, TRIM25, VEGFA	Some changes favor arrest while other favor progression through G1/S and Mitosis.
U87CR	Cell Death	APH1B, **CABIN1**, **CAT**, CCNA2,CD40, **CSF2**, EGR1, **MAP4K1**, FKBP8, **IL1A**, MET, PSEN2, SMARCA5, **TAF1B**, WIPF1	Strong antiapoptotic signal accompanied with inflammatory response
U87CR	Cell Cycle	CCNA2, CD40, **CENPC1**, CENPE, CENPH, **CSF2**, EGR1, **IL1A**, MET, PLAC1, PLCG1, PMF1, PSEN2, SSSCA1	Changes favor arrest and limit proliferation.

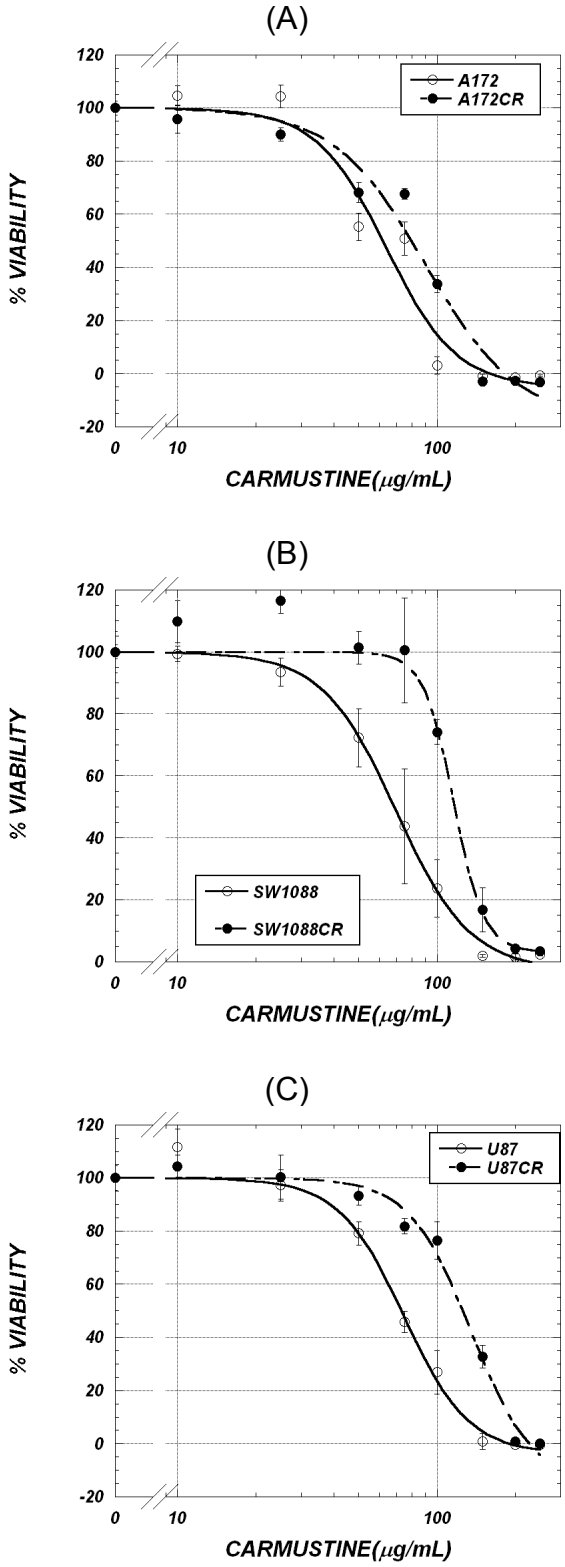

Figure 3.1: Response of Cell Lines to Carmustine Exposure at 72 Hours. Cell viability was determined by MTS assay, which measures metabolic activity of viable cells.

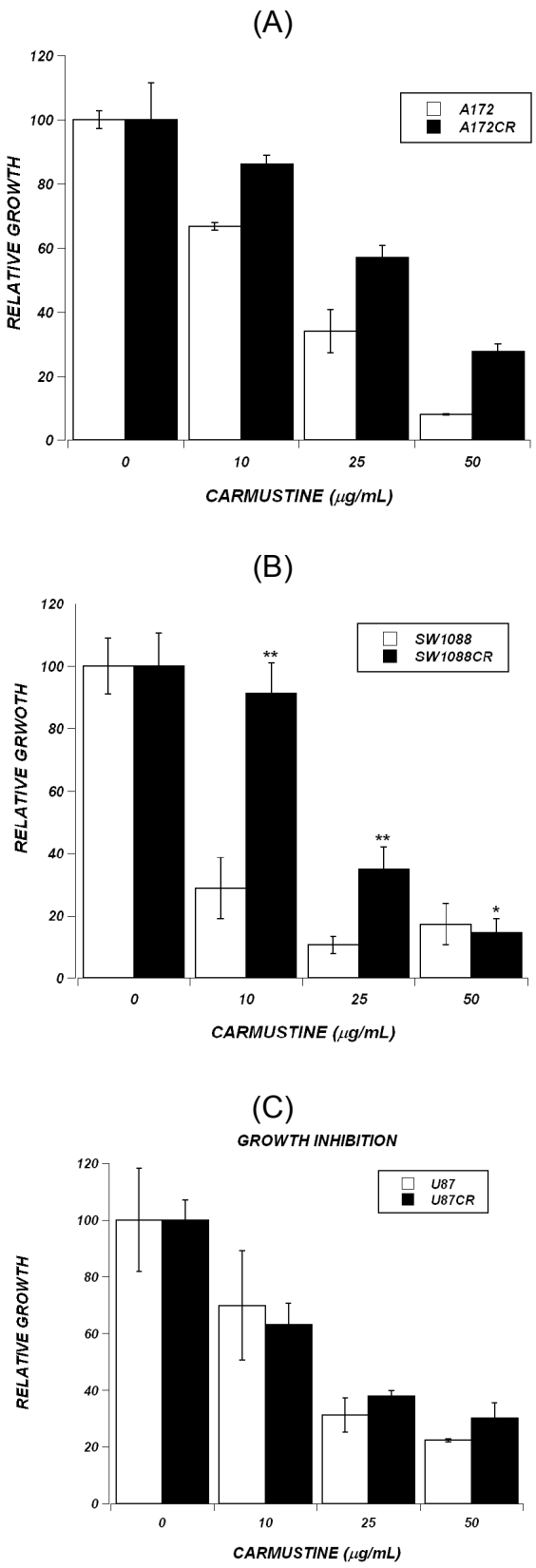

Figure 3.2: Effect of Carmusitne on Cell Growth. Cells were exposed to carmustine for 72 hrs and grown in media for 10 days. Viability was measure by calcein staining.

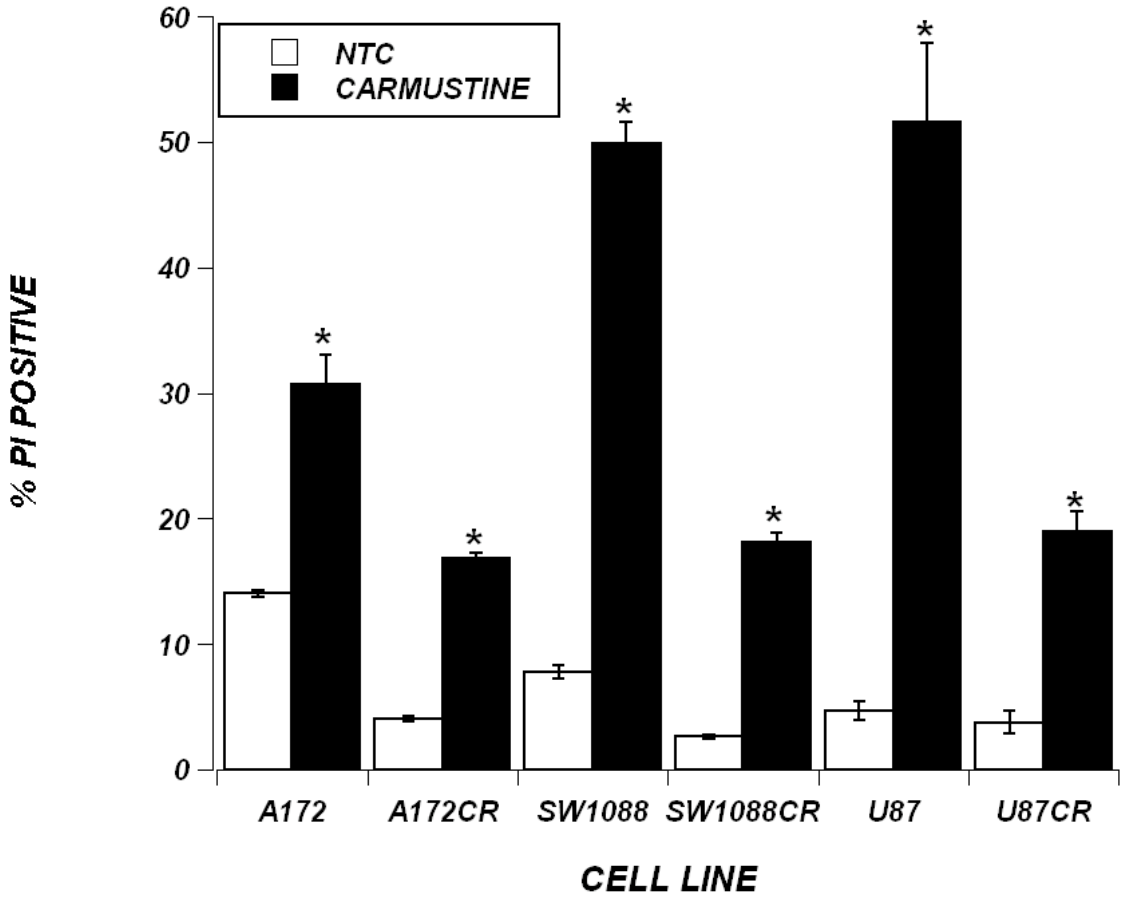

Figure 3.3: Cell Death, Apoptotic and Necrotic, in Response to Carmustine Exposure. Cells were exposed to 100 μg/mL of carmustine for 24 hours. Cell death was measured by PI exclusion assay. PI Positive cells represent fraction of cells with compromised membrane integrity, * indicates $p<0.01$. One-way ANOVA was performed on 6 cell lines treated with carmustine and pairwise comparisons were done using Tukey's HSD. Three resistant cell lines were significantly different from three parent cell lines; however, there were no significant differences among each other. A172 cell line was significantly different form all 5 cell lines.

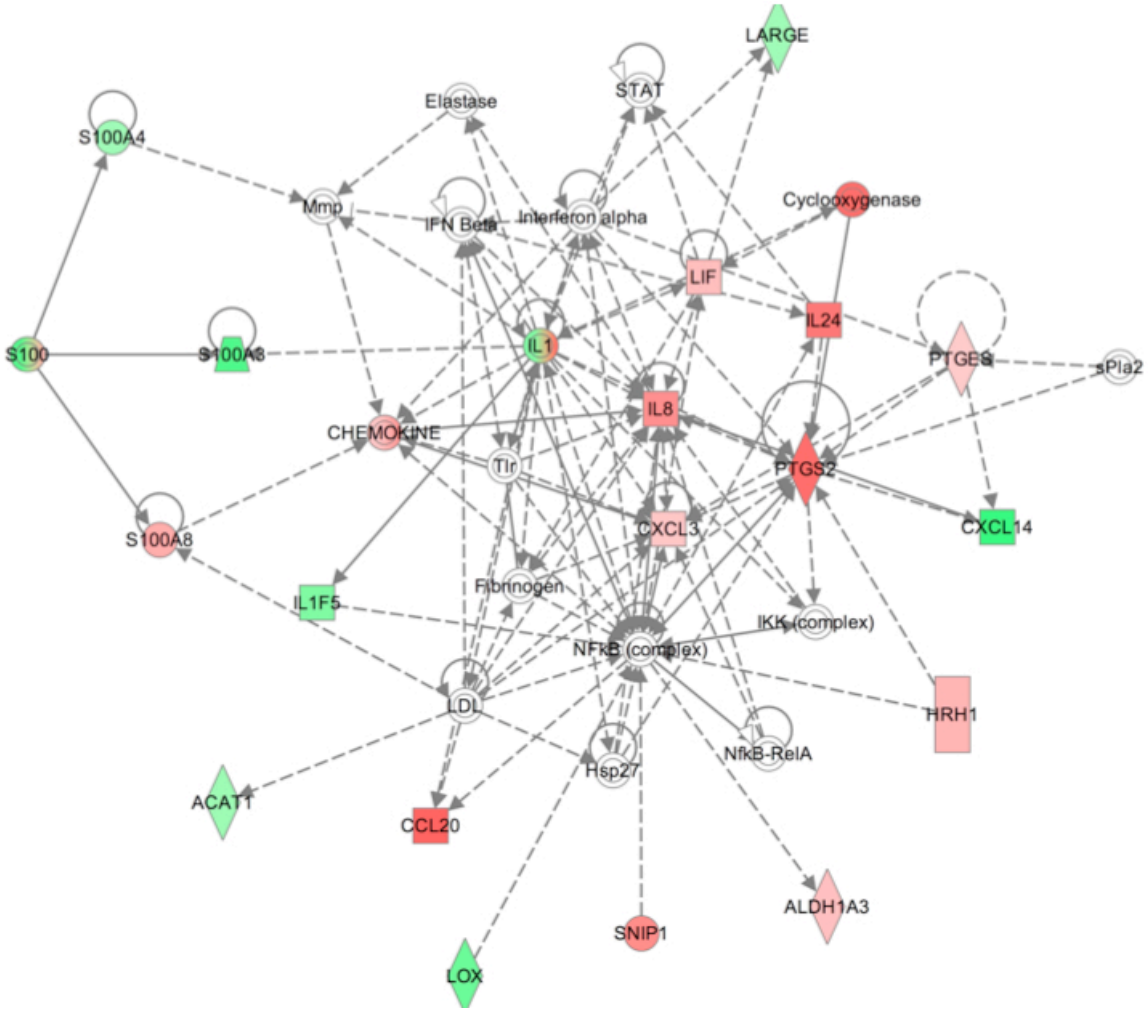

Figure 3.4: A172CR NFκB network implicated in response to carmustine. Inflammatory response gens upregulated, shown in red, in response to drug exposure. This NFκB network is directly connected to other networks involved in cell survival and cell cycle progression. See appendix (Figure A.2) for detailed network legend.

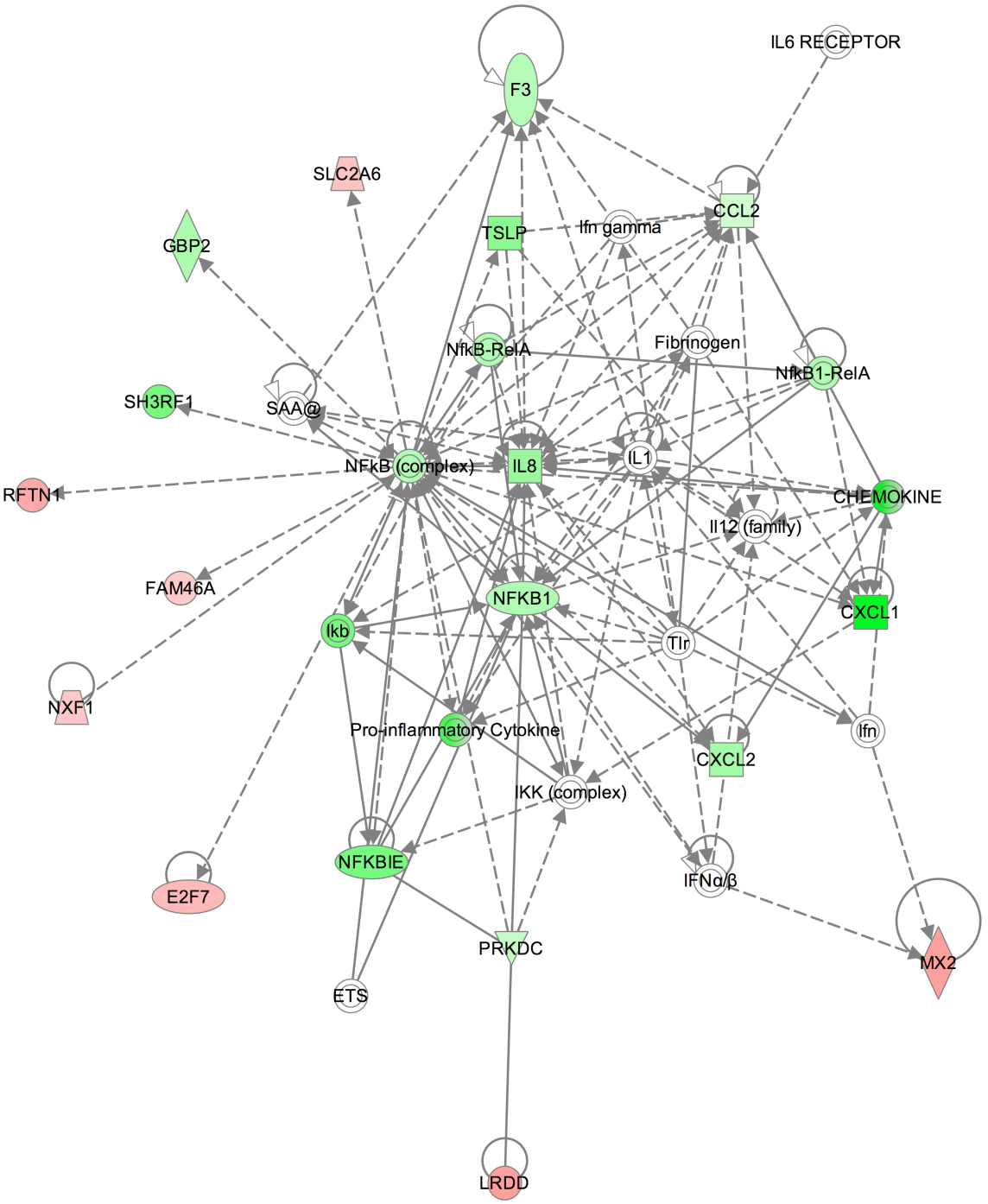

Figure 3.5: SW1088 NFκB network implicated in response to carmustine. Inflammatory response gens downregulated, shown in green, in response to drug exposure. This NFκB network is directly connected to other networks involved in cell survival and cell cycle progression. See appendix (Figure A.2) for detailed network legend.

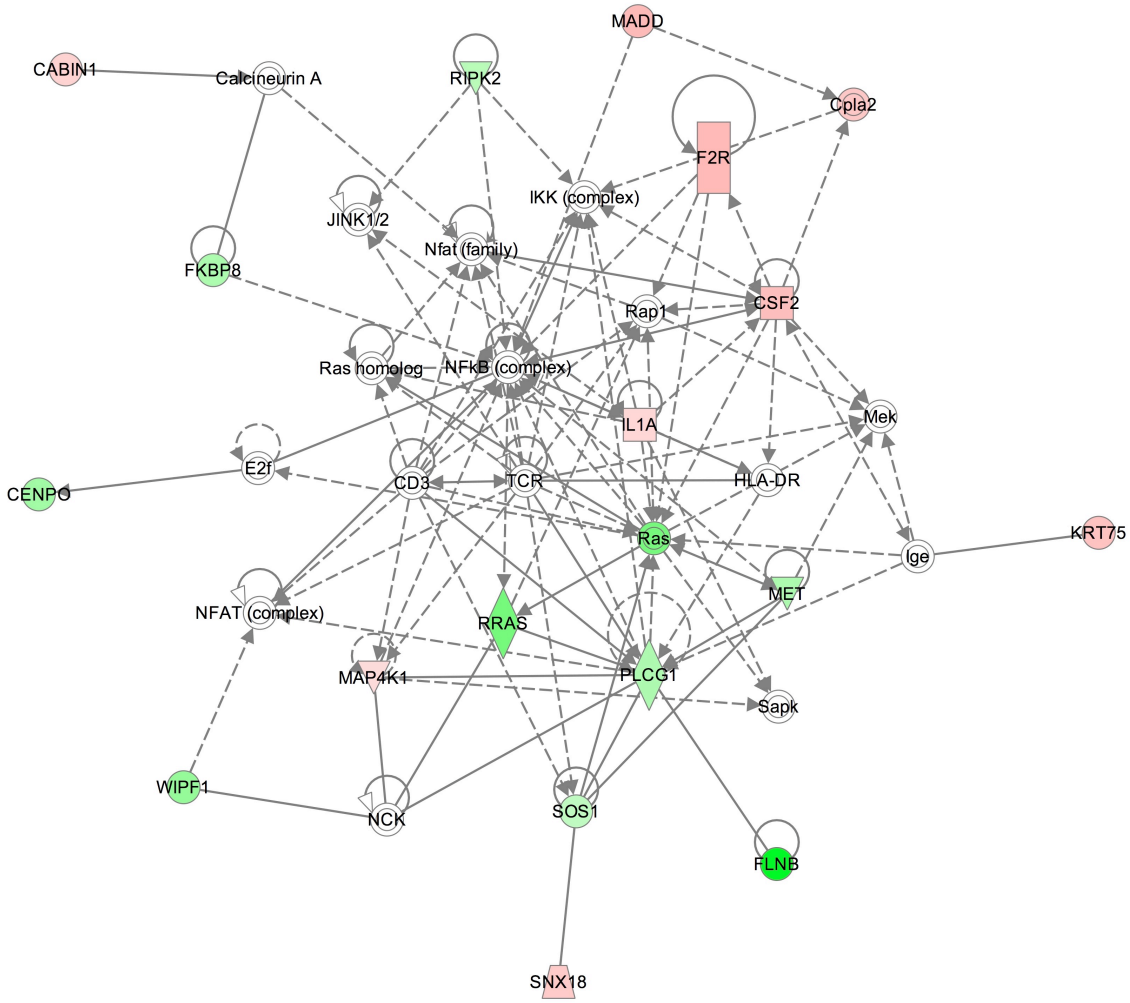

Figure 3.6: U87CR NFκB network implicated in response to carmustine. Inflammatory response gens upregulated, shown in red, in response to drug exposure. This NFκB network is directly connected to other networks involved in cell survival and cell cycle progression. See appendix (Figure A.2) for detailed network legend.

(A)

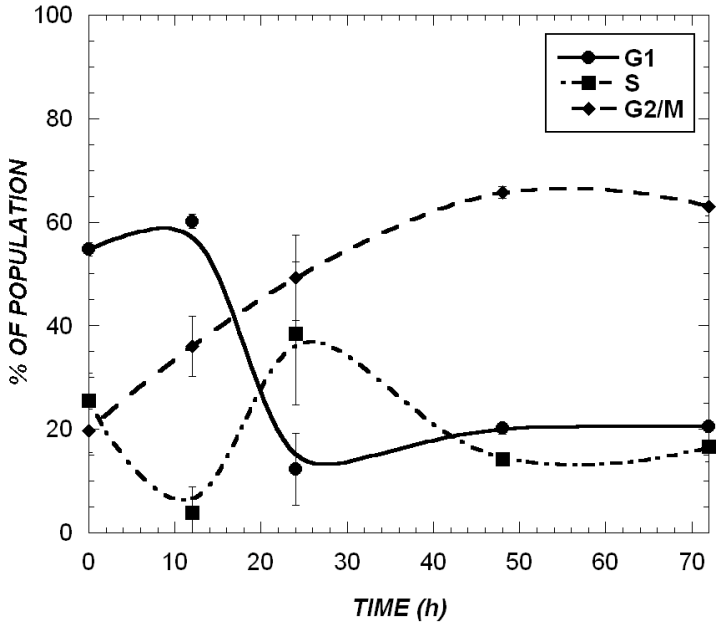

(B)

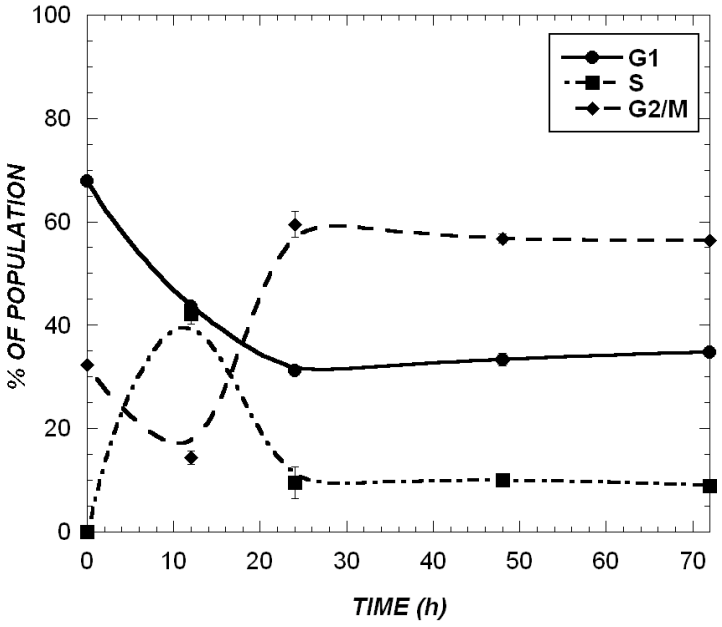

Figure 3.7: Cell Cycle Distribution of (A) A172 and (B) A172CR upon exposure to 25 μg/mL of carmustine.

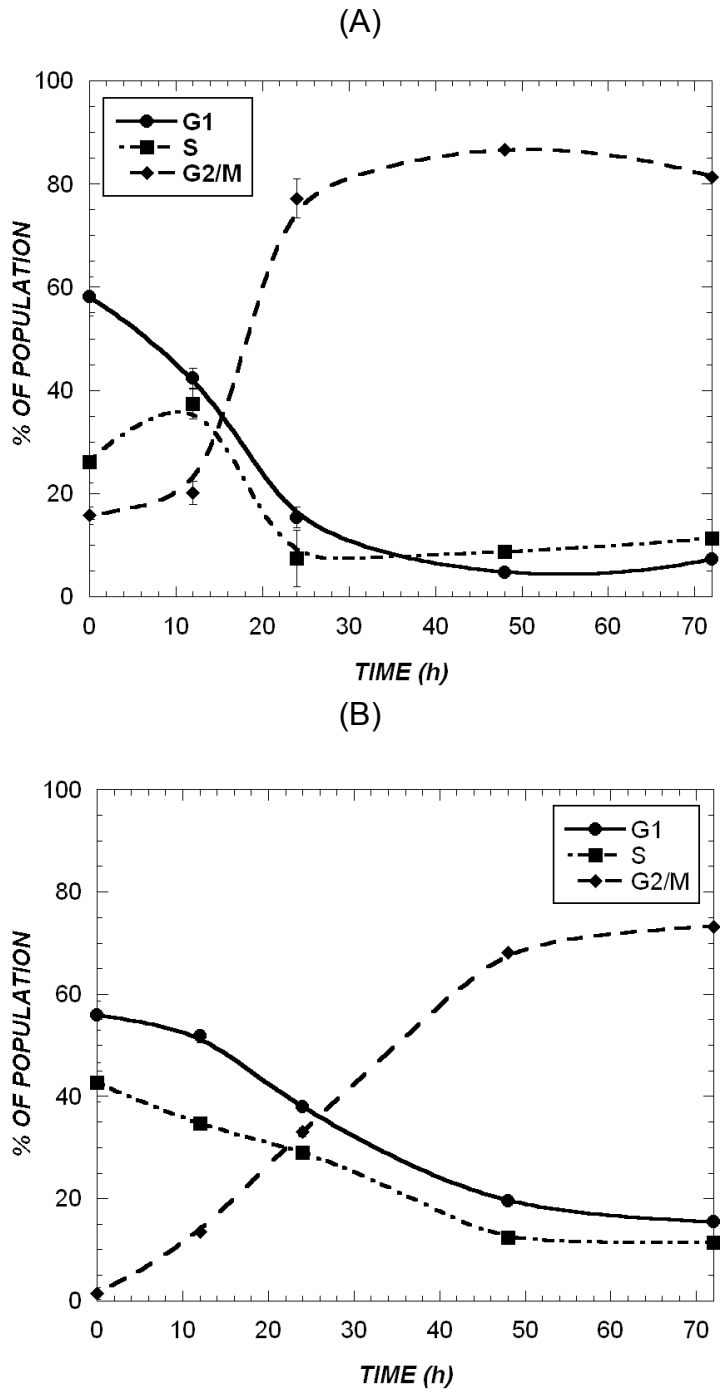

Figure 3.8: Cell Cycle Distribution of (A) SW1088 and (B) SW1088CR upon exposure to 25 μg/mL of carmustine. Examples of cell cycle distribution of untreated cells is provided in Figure A.1

(A)

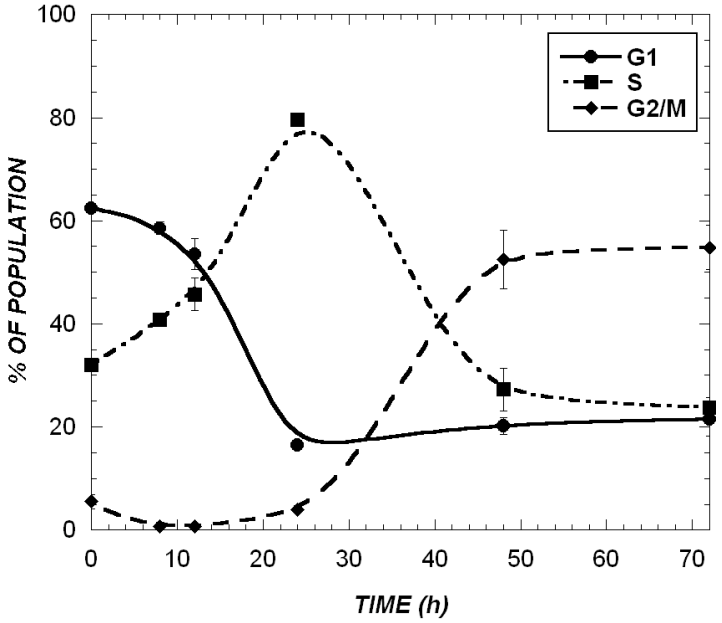

(B)

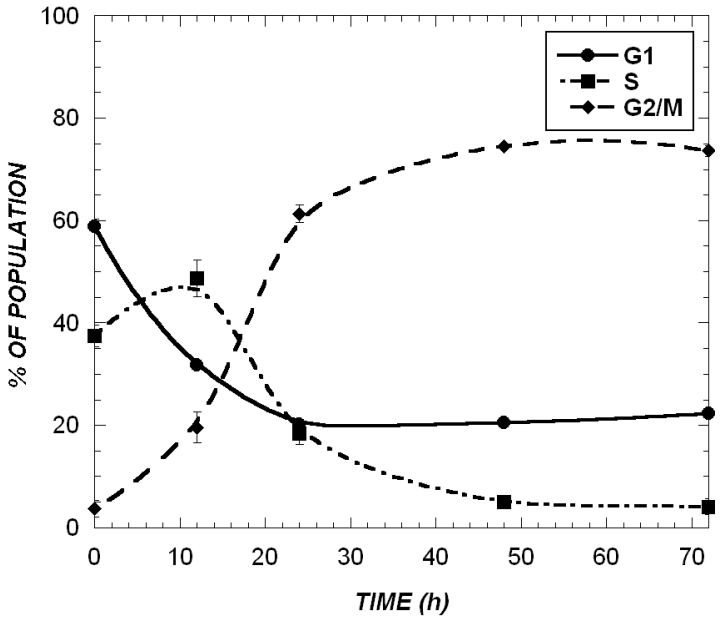

Figure 3.9: Cell Cycle Distribution of (A) U87 and (B) U87CR upon exposure to 25 μg/mL of carmustine.

(A)

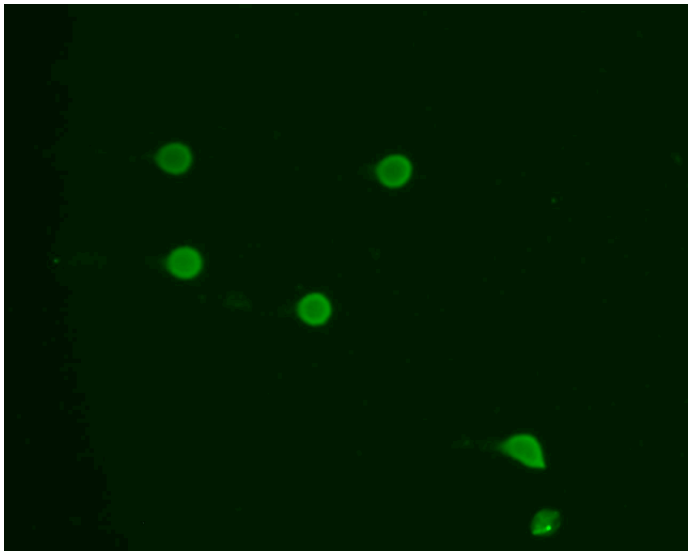

(B)

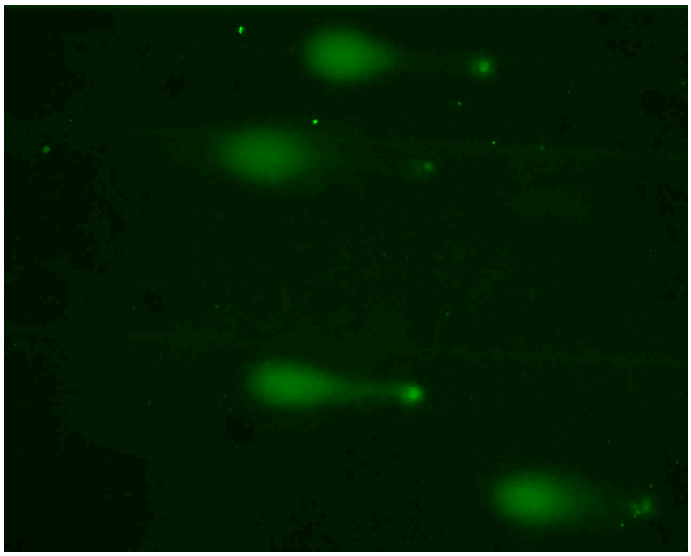

Figure 3.10: Single Cell Alkaline Electrophoresis (comet) Assay. (A)SW1088CR cells treated with DMSO, cells harvested after 2 hours of exposure (t=0) and (B) SW1088CR cells exposed to 50 μg/mL carmustine, cells were harvested after 2 hours of exposure (t=0). Tail moment is an indication of the amount of DNA damage.

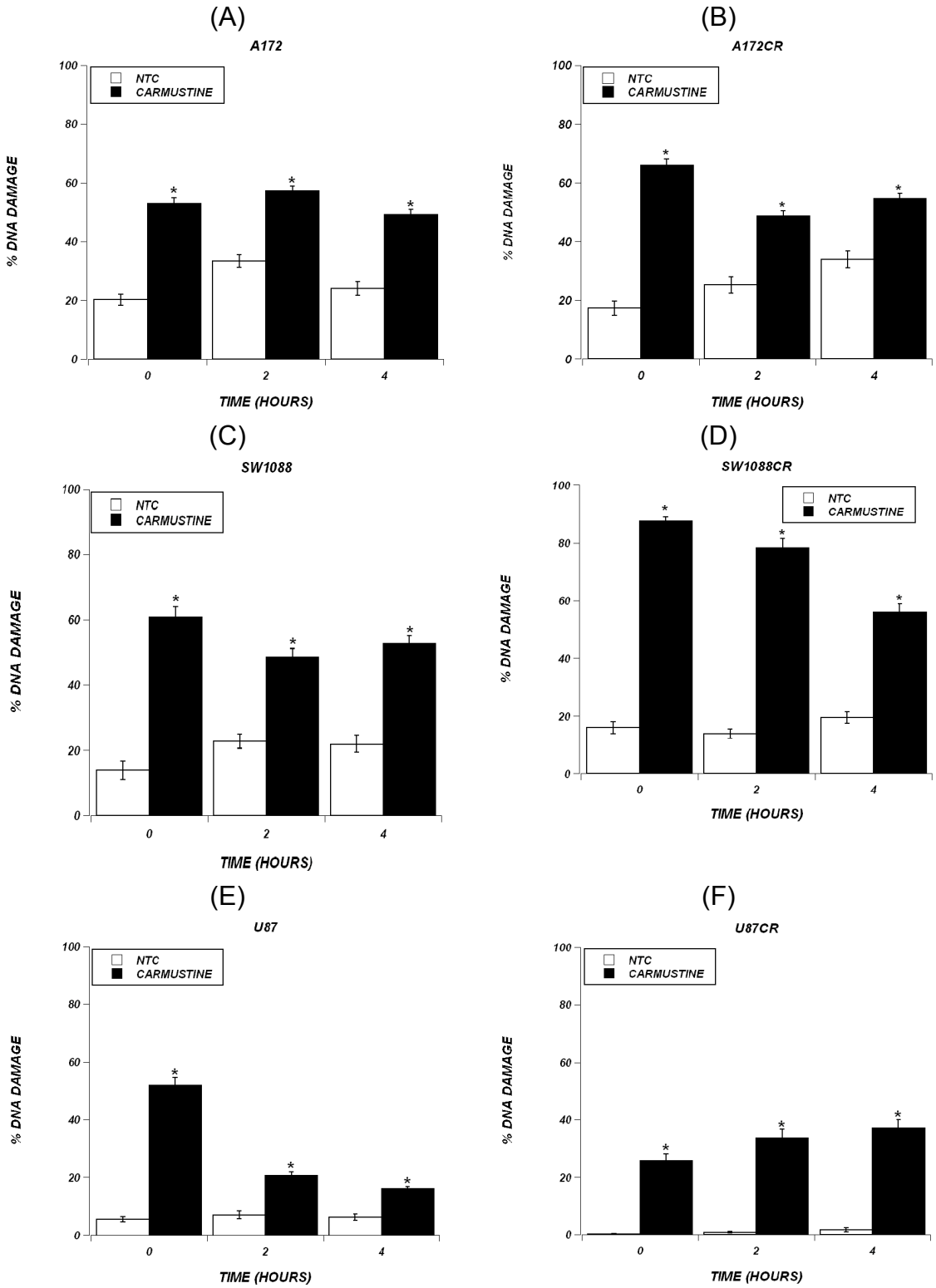

Figure 3.11: DNA Damage Repair in Response to Carmustine exposure. Cells were exposed to 50 mg/mL of carmustine for 2 hours, washed and incubated in drug-free media, and harvested at designated times. Amount of DNA damage was quantified by single cell alkaline electrophoresis (comet) assay. n=100, mean ± S.E. * indicates $p<0.01$.

CHAPTER 4

RESEARCH SUMMARY AND FUTURE DIRECTION

Research Summary and Impact

The main aim of the current work is to understand the mechanisms implicated in acquisition of resistance to chemotherapy in glioma models. First, we characterized the response of a panel of glioma cell lines to two drugs from two distinct classes of chemotherapeutic agents: DNA alkylating agents (carmustine) and topoisomerase II inhibitors (etoposide). We found that the shape and dynamics of the dose response curve of each agent is distinct and dependent on the chemotherapeutic agent rather than the cell line, in spite of the diverse genetic background (see Appendix Tables A.7-A.9). We utilized a cell cycle-structured model as a computational framework to, first, understand the effect of cell cycle arrest and cell death on the shape and dynamics of dose response curves and, subsequently, to estimate the contribution of cell death and cell cycle arrest (model output) from dose response curves obtained experimentally (model input). Our model predicted that the primary mechanism of action of carmustine involves cell death, while the primary mode of action of etoposide is cell cycle arrest. Experimental data obtained from U87 cell lines validated our model predictions.

While our model makes quantitative inferences about the role of cell death and cell cycle arrest in response to a given drug, the structure of the model did not include any molecular details. The importance of these details was highlighted by the fact that cells with diverse genetic background exhibit the same response at level of cell death and cell cycle arrest. Thus, it was important to characterize molecular changes taking place upon drug exposure in order to understand the basis of resistance.

We developed resistance to carmustine in a panel of glioma cell lines through prolonged exposure to sublethal doses. We used an integrated, cellular and genomic, approach to characterize the response of resistant and parent cell lines. To our knowledge, this is the first investigation of both cellular and genomic changes occurring upon exposure to chemotherapy in 6 related cell lines. Gene expression studies performed previously compare basal expression changes between parent and resistant cells. While important, these studies overlook the fact that some changes may not be involved in the response of cells to drugs; moreover, these studies neglect the fact that resistant cells may have an increased capacity to induce pathways upon exposure to drug that are dormant otherwise. The large number of cell lines utilized in this study better emulates the diverse genetic background of actual tumors, thus more meaningful conclusions could be made. In this study, we have tracked the response of parent and resistant cell lines at early and late times subsequent to drug exposure. Our models represents a case of acquisition of resistance through molecular changes as opposed to selection of preexisting fraction with a high level of intrinsic resistance. This was confirmed by testing the sensitivity of many single-cell clonal expansions from each cell line prior to the initiation of treatment; single-cell clonal expansions did not exhibit differences in viability in response to drug exposure.

Our results indicate, in a general sense, that cell survival through NFκB pathway activation coupled with an increased inflammatory response plays a central role in resistance to carmustine. The capacity of resistant cell lines to upregulate immune response through NFκB, perhaps, relates to the physiological function of normal astrocytes. Astrocytes, along with microglia, are involved in mounting a protective

immune response in the central nervous system through NFκB-mediated production of IL-6 subsequent to insult [123]. Thus, increased resistance to chemotherapy could be primarily through the increased activity of an already preexisting molecular mechanism. This notion is not foreign in terms of acquired resistance, especially in brain tumors. It has been shown that Pgp plays an integral role in the physiological function of the blood brain barrier; however, it has been associated with resistance to chemotherapeutic agents [3]. From the therapeutic perspective, acquisition through alterations of a preexisting molecular mechanism could prove challenging as complete silencing or elimination may prove harmful at the level of normal brain physiology. In addition to increased survival, inactivation of proliferation is correlated with resistance. However, changes characterized in our gene expression study are only early response, after only 1 hour of exposure, as cells seem to resume proliferation at later times.

Intuitively, it is important to investigate how cells overcome the proliferation arrest signal and continue dividing in spite of sustained DNA damage. It is also important to investigate the effect of inactivating NFκB signaling and/or components of inflammatory response machinery—such as IL1A, IL1B, IL8 and LIF, which were found to be upregulated in resistant cells—on the response to carmustine. These experiments could be performed, especially with the current advances in siRNA and antisense oligonucleotide technologies, to delineate the contributions of members of these pathways to the resistant phenotype.

Our model of resistance indicates that cells avoid early death by mounting an inflammatory response mediated by NFκB signaling. Subsequently, cells avoid division and cell cycle progession before resuming proliferation again with no evidence of DNA

repair. NFκB system is highly conserved across multiple species indicating it primary role in maintaining cell survival in response to stress [124], and it has been shown to promote cellular proliferation through inducing the expression of cyclin D1, which promotes G1-to-S transition [125]. However, it is observed that halting G1-to-S transition is correlated with increased resistance in our model. This is in agreement with reports indicating that the capacity to arrest in G1 is the more important determinant of response to chemotherapy, compared to G2/M arrest [126]. Thus, it is important from the therapeutic perspective to understand how NFκB activation mediates survival without affecting cell cycle progression (G1 arrest is still maintained).

Our model also points to the therapeutic importance of early response transcription factors, which are present in the cell and are active without the need to be synthesized, such as c-Jun and STATs, nuclear hormone receptors and NFκB [127]. Our results indicate that silencing these survival pathways prior to carmustine exposure could increase drug efficacy and overcome the chemoresistant phenotype. In another context, the future of glioma treatment, and cancer in general, is directed towards the development of molecularly targeted therapies [128, 129]; however, many of these targets are survival and proliferation pathways that are highly redundant, which results in treatment failure in many cases or development of resistance [130-132]. This failure could be attributed to the fact that many of these pathways are involved in the process of tumorigenesis but not necessarily the response of cells to chemotherapy. As an example, cell cycle checkpoint deregulation is a hallmark of cancer, meaning that it is involved in tumorigenesis [7]; however, failure to enforce checkpoint upon exposure to chemotherapy is correlated with sensitivity, as discussed above. In addition, many of these pathways are either

independent or upstream of NFκB, such as PI3K, Akt and, mTOR, which renders capable of survival in spite of the absence of proliferation signals [11].

In our experimental program, we chose to characterize cell death as opposed to apoptosis. Apoptosis, defined as programmed cell death that is caspase dependent, has attracted attention as the primary mode of cellular demise in response to chemotherapy exposure, and resistance has been associated with alterations in pathways controlling this process. There has been, however, compelling evidence that apoptosis may not be the primary mode of cellular demise *in vivo*. These reports argue that apoptosis is induced *in vitro* at high concentrations; however, these concentrations are not attainable *in vivo* [133]. Alternatively, many modes of cell death have been proposed in response to alkylating agents, the most prominent of which is necrosis, which has been associated with increased Poly-ADP Ribose Polymerase activity. In addition, mitotic catastrophe has also been proposed as a mechanism of cellular demise subsequent to exposure to DNA damaging agents *in vivo* as well as *in vitro* [133]. In fact, reports indicate that mitotic catastrophe, characterized by the presence of multinucleated cells, is the more prominent mode of cellular demise in solid tumors compared to apoptosis [134-137]. It is worth noting that our observations are in agreement with the argument that apoptosis may not be the primary mode of death as expression of the executioner caspase 3 was found to be minimal subsequent to drug exposure in all 3 parent cell lines. In addition, there was a significant fraction of cells with multinuclei, a characteristic of mitotic castastrophe (data not shown). Given the lack of detailed molecular characterization and distinction between these 3 processes, we chose to characterize cell death, which is the ultimate goal of therapy, rather than individual modes of cellular demise. These modes of cellular

demise—apoptosis, necrosis, and mitotic catastrophe—can be detected experimentally with propidium iodide staining [133]. Our observations suggest that apoptosis, indeed, may not be the primary mode of cell death as our results show that cells exhibit very low levels of annexin V staining, caspase 3 expression, and caspase 3/7 activity upon exposure to carmustine (data not shown).

In vitro cell culture models play a significant role in the development and evaluation of the cytotoxicity of anti-neoplastic agents. Most of the pre-clinical studies on drug resistance are carried out *in vitro*, where culture conditions and drug dosing are tightly controlled. That is, factors pertaining to patient-to-patient variability and pharmacokinetic parameters—drug absorption, distribution, metabolism, and elimination—do not contribute to the resistant phenotype. Thus, only molecular changes implicated in resistance are delineated, which is of great importance in developing molecularly targeted therapies. The main caveat of utilizing *in vitro* resistance models in lieu of *in vivo* conditions is that cells are removed from their physiological milieu, which has been shown to affect gene expression profiles of glioma cell lines [59] as well as other cell lines, as discussed in details below. As a result, *in vitro* conditions could, in theory, affect proliferation and survival pathways of cell lines. This dichotomy between behavior of cells *in vivo* and *in vitro* could affect the resistant phenotype. In contradiction with this notion, however, the expression profiles of genes correlated with acquired resistance to carmustine and temozolomide *in vivo* and *in vitro* were similar [43]. Bredel et al compared the expression profiles of 4 groups of gliomas: cell lines with *in vitro* acquired resistance, parent cell lines, *in vivo* resistant tumors, and *in vivo* sensitive tumors. The study found that glioma cells were stratified into two distinct groups:

sensitive and resistant, each of which includes a mixture of *in vivo* tumors and *in vitro* cell lines [43]. Thus, while there are significant differences between *in vivo* and *in vitro* resistance models, insights could still be made about the nature of the molecular changes associated with resistance and, ultimately, development of novel therapeutic targets.

Future Direction: More Biologically Relevant Culture Systems

In order to have a better understating of resistant phenotype, culture models that mimic tumor microenvironments should be utilized to characterize drug response and resistant phenotypes. In body tissues, cells connect to each other and to the extracellular matrix (ECM). ECM provides structural support and regulates communication between cells. Receptors on the cell surface, integrins, anchor cells to the ECM and interpret biochemical mediators from immediate surroundings. In 2D culture systems, this interplay between ECM and cells is not present, which alters the biological behavior of cells.

At the gene expression level, microarrays have been used in a number of studies to monitor the differences in expression between cell lines, which have been grown in 2D systems for decades, and tumors from tissue of origin [71, 73, 138-141]. A distinct induction of ribosomal proteins, which are involved in proliferation, was observed in 2D cultures. In addition, induction of genes involved in cell cycling, metabolism and turnover of macromolecules was also observed in cell lines. The group of genes that were found to be downregulated in cell lines was involved in processes such as cell-cell adhesion, cell contact with ECM, and membrane associated signaling proteins. These observations highlight the implications of cellular microenvironment on the gene expression profiles and, thus, phenotype.

Matrix dimensionality has been shown to affect cell morphology as well. Fibroblasts were shown to have an extremely spread morphology in 2D cultures because of the distribution of integrins on the ventral side, while in 3D, integrins were evenly distributed on the entire surface and cell adopted an elongated morphology. The morphology of fibroblasts is known to affect the phosphorylation status of focal adhesion kinase (FAK) [142, 143]. Decreased spreading is known to dephosphorylate FAK, leading to the upregulation of p21, which may be responsible for decreased proliferation of smooth muscle cells cultured in 3D [144]. Culture dimensionality was shown to affect malignant phenotype of epithelial tumors. Mammary epithelial cells were shown to regain polarity and decrease proliferation rates when cultured in 3D [145]. In 2D, however, these cells showed decreased polarity and increased proliferation.

More importantly, dimensionality has been shown to affect response of cell lines to chemotherapy. 3D multicellular tumor spheroids of breast cancer cell line MDA-MB-231 were shown to have lower EC_{50} to cisplatinum compared to cells cultured in 2D monolayers[146].

We investigated the growth rate of gliomas in 3D collagen cultures in comparison to regular 2D monolayers. Cells grown in 3D exhibit slower growth rates, which is agreement with other studies mentioned above. Interestingly, cells grown in 3D were more sensitive to carmustine compared to cells grown in 2D, which is counter intuitive, given the fact that cells with lower proliferative capacity are, generally, less sensitive to chemotherapy. Thus, it is of great importance to characterize the molecular events involved in response to drug in 3D cultures.

In order to develop a detailed understanding of acquired resistance to carmustine, the response of resistant cells in 3D upon drug exposure should investigated at the cellular and molecular level in order to validate conclusions made from the current study, performed on 2D monolayers.

REFERENCES

1. Reardon, D.A., et al., *Recent advances in the treatment of malignant astrocytoma*, in *J Clin Oncol*. 2006. p. 1253-65.
2. Devita, V.T., S. Hellman, and S. Rosenberg, *Principles & Practice of Oncology*. 7th ed. 2004, Philadelphia: Lippincott Wilkins & Williams.
3. Bredel, M., *Anticancer drug resistance in primary human brain tumors.* Brain Res Brain Res Rev, 2001. **35**(2): p. 161-204.
4. Roos, W.P., et al., *The translesion polymerase Rev3L in the tolerance of alkylating anticancer drugs.* Mol Pharmacol, 2009. **76**(4): p. 927-34.
5. Beljanski, V., L.G. Marzilli, and P.W. Doetsch, *DNA damage-processing pathways involved in the eukaryotic cellular response to anticancer DNA cross-linking drugs.* Mol Pharmacol, 2004. **65**(6): p. 1496-506.
6. Roos, W.P. and B. Kaina, *DNA damage-induced cell death by apoptosis.* Trends Mol Med, 2006. **12**(9): p. 440-50.
7. Hanahan, D. and R.A. Weinberg, *The hallmarks of cancer.* Cell, 2000. **100**(1): p. 57-70.
8. Paulovich, A.G., D.P. Toczyski, and L.H. Hartwell, *When checkpoints fail.* Cell, 1997. **88**(3): p. 315-21.
9. Stewart, Z.A., M.D. Westfall, and J.A. Pietenpol, *Cell-cycle dysregulation and anticancer therapy.* Trends Pharmacol Sci, 2003. **24**(3): p. 139-45.
10. O'Brien, V. and R. Brown, *Signalling cell cycle arrest and cell death through the MMR System.* Carcinogenesis, 2006. **27**(4): p. 682-92.
11. Damia, G. and M. Broggini, *Improving the selectivity of cancer treatments by interfering with cell response pathways.* Eur J Cancer, 2004. **40**(17): p. 2550-9.
12. Maddika, S., et al., *Cell survival, cell death and cell cycle pathways are interconnected: implications for cancer therapy.* Drug Resist Updat, 2007. **10**(1-2): p. 13-29.
13. Batista, L.F., et al., *p53 mutant human glioma cells are sensitive to UV-C-induced apoptosis due to impaired cyclobutane pyrimidine dimer removal.* Mol Cancer Res, 2009. **7**(2): p. 237-46.
14. Ruan, S., et al., *Overexpressed WAF1/Cip1 renders glioblastoma cells resistant to chemotherapy agents 1,3-bis(2-chloroethyl)-1-nitrosourea and cisplatin.* Cancer Res, 1998. **58**(7): p. 1538-43.
15. Xu, G.W., et al., *Inactivation of p53 sensitizes U87MG glioma cells to 1,3-bis(2-chloroethyl)-1-nitrosourea.* Cancer Res, 2001. **61**(10): p. 4155-9.
16. Borbe, R., J. Rieger, and M. Weller, *Failure of taxol-based combination chemotherapy for malignant glioma cannot be overcome by G2/M checkpoint abrogators or altering the p53 status.* Cancer Chemother Pharmacol, 1999. **44**(3): p. 217-27.
17. Zheng, L.T., et al., *Down-regulation of lipocalin 2 contributes to chemoresistance in glioblastoma cells.* J Neurochem, 2009. **111**(5): p. 1238-51.
18. Furnari, F.B., et al., *Malignant astrocytic glioma: genetics, biology, and paths to treatment.* Genes Dev, 2007. **21**(21): p. 2683-710.

19. Gardner, S.N. and M. Fernandes, *New tools for cancer chemotherapy: computational assistance for tailoring treatments.* Mol Cancer Ther, 2003. **2**(10): p. 1079-84.
20. Norton, L. and R. Simon, *Tumor size, sensitivity to therapy, and design of treatment schedules.* Cancer Treat Rep, 1977. **61**(7): p. 1307-17.
21. Coldman, A.J. and J.H. Goldie, *Impact of dose-intense chemotherapy on the development of permanent drug resistance.* Semin Oncol, 1987. **14**(4 Suppl 4): p. 29-33.
22. Gardner, S.N., *A mechanistic, predictive model of dose-response curves for cell cycle phase-specific and -nonspecific drugs.* Cancer Res, 2000. **60**(5): p. 1417-25.
23. Sherer, E., et al., *Analysis of resonance chemotherapy in leukemia treatment via multi-staged population balance models.* J Theor Biol, 2006. **240**(4): p. 648-61.
24. Panetta, J.C., W.E. Evans, and M.H. Cheok, *Mechanistic mathematical modelling of mercaptopurine effects on cell cycle of human acute lymphoblastic leukaemia cells.* Br J Cancer, 2006. **94**(1): p. 93-100.
25. Dan, S., et al., *An integrated database of chemosensitivity to 55 anticancer drugs and gene expression profiles of 39 human cancer cell lines.* Cancer Res, 2002. **62**(4): p. 1139-47.
26. Komatani, H., et al., *Identification of breast cancer resistant protein/mitoxantrone resistance/placenta-specific, ATP-binding cassette transporter as a transporter of NB-506 and J-107088, topoisomerase I inhibitors with an indolocarbazole structure.* Cancer Res, 2001. **61**(7): p. 2827-32.
27. Ross, D.T., et al., *Systematic variation in gene expression patterns in human cancer cell lines.* Nat Genet, 2000. **24**(3): p. 227-35.
28. Scherf, U., et al., *A gene expression database for the molecular pharmacology of cancer.* Nat Genet, 2000. **24**(3): p. 236-44.
29. Staunton, J.E., et al., *Chemosensitivity prediction by transcriptional profiling.* Proc Natl Acad Sci U S A, 2001. **98**(19): p. 10787-92.
30. Zembutsu, H., et al., *Genome-wide cDNA microarray screening to correlate gene expression profiles with sensitivity of 85 human cancer xenografts to anticancer drugs.* Cancer Res, 2002. **62**(2): p. 518-27.
31. Bao, L., T. Guo, and Z. Sun, *Mining functional relationships in feature subspaces from gene expression profiles and drug activity profiles.* FEBS Lett, 2002. **516**(1-3): p. 113-8.
32. Butte, A.J., et al., *Discovering functional relationships between RNA expression and chemotherapeutic susceptibility using relevance networks.* Proc Natl Acad Sci U S A, 2000. **97**(22): p. 12182-6.
33. Bacolod, M.D., et al., *Mechanisms of resistance to 1,3-bis(2-chloroethyl)-1-nitrosourea in human medulloblastoma and rhabdomyosarcoma.* Mol Cancer Ther, 2002. **1**(9): p. 727-36.
34. Morandi, E., et al., *A cDNA-microarray analysis of camptothecin resistance in glioblastoma cell lines.* Cancer Lett, 2006. **231**(1): p. 74-86.
35. Levenson, V.V., I.A. Davidovich, and I.B. Roninson, *Pleiotropic resistance to DNA-interactive drugs is associated with increased expression of genes involved in DNA replication, repair, and stress response.* Cancer Res, 2000. **60**(18): p. 5027-30.

36. Vikhanskaya, F., et al., *P73a overexpression is associated with resistance to treatment with DNA-damaging agents in a human ovarian cancer cell line.* Cancer Res, 2001. **61**(3): p. 935-8.
37. Yamanaka, R., et al., *Identification of expressed genes characterizing long-term survival in malignant glioma patients.* Oncogene, 2006. **25**(44): p. 5994-6002.
38. Naumann, U., et al., *PCTAIRE3: a putative mediator of growth arrest and death induced by CTS-1, a dominant-positive p53-derived synthetic tumor suppressor, in human malignant glioma cells.* Cancer Gene Ther, 2006. **13**(5): p. 469-78.
39. Baldwin, R.M., et al., *Protection of glioblastoma cells from cisplatin cytotoxicity via protein kinase Ciota-mediated attenuation of p38 MAP kinase signaling.* Oncogene, 2006. **25**(20): p. 2909-19.
40. Bandres, E., et al., *Gene expression profile induced by BCNU in human glioma cell lines with differential MGMT expression.* J Neurooncol, 2005. **73**(3): p. 189-98.
41. Ma, Y., et al., *Identification of genes that modulate sensitivity of U373MG glioblastoma cells to cis-platinum.* Anticancer Drugs, 2006. **17**(7): p. 733-51.
42. Natsume, A., et al., *IFN-beta down-regulates the expression of DNA repair gene MGMT and sensitizes resistant glioma cells to temozolomide.* Cancer Res, 2005. **65**(17): p. 7573-9.
43. Bredel, M., et al., *Tumor necrosis factor-alpha-induced protein 3 as a putative regulator of nuclear factor-kappaB-mediated resistance to O6-alkylating agents in human glioblastomas.* J Clin Oncol, 2006. **24**(2): p. 274-87.
44. Goffe, W.L., G.D. Ferrier, J. Rogers, *Global Optimization of Statistical Functions with Simulated Annealing.* Journal of Econometrics, 1994. **60**: p. 65-100.
45. Florian, J.A., Jr., J.L. Eiseman, and R.S. Parker, *Accounting for quiescent cells in tumour growth and cancer treatment.* Syst Biol (Stevenage), 2005. **152**(4): p. 185-92.
46. Kozusko, F., et al., *A mathematical model of in vitro cancer cell growth and treatment with the antimitotic agent curacin A.* Math Biosci, 2001. **170**(1): p. 1-16.
47. Batista, L.F., et al., *Differential sensitivity of malignant glioma cells to methylating and chloroethylating anticancer drugs: p53 determines the switch by regulating xpc, ddb2, and DNA double-strand breaks.* Cancer Res, 2007. **67**(24): p. 11886-95.
48. Basse, B., et al., *Modelling cell death in human tumour cell lines exposed to the anticancer drug paclitaxel.* J Math Biol, 2004. **49**(4): p. 329-57.
49. Ribba, B., T. Colin, and S. Schnell, *A multiscale mathematical model of cancer, and its use in analyzing irradiation therapies.* Theor Biol Med Model, 2006. **3**: p. 7.
50. Venkatasubramanian, R., M.A. Henson, and N.S. Forbes, *Integrating cell-cycle progression, drug penetration and energy metabolism to identify improved cancer therapeutic strategies.* J Theor Biol, 2008. **253**(1): p. 98-117.
51. Das, C.M., et al., *Valproic acid induces p21 and topoisomerase-II (alpha/beta) expression and synergistically enhances etoposide cytotoxicity in human glioblastoma cell lines.* J Neurooncol, 2007. **85**(2): p. 159-70.

52. Khoshyomn, S., et al., *Synergistic effect of genistein and BCNU on growth inhibition and cytotoxicity of glioblastoma cells.* J Neurooncol, 2002. **57**(3): p. 193-200.
53. Yan, L., J.R. Donze, and L. Liu, *Inactivated MGMT by O6-benzylguanine is associated with prolonged G2/M arrest in cancer cells treated with BCNU.* Oncogene, 2005. **24**(13): p. 2175-83.
54. Yin, D., N. Tamaki, and T. Kokunai, *Wild-type p53-dependent etoposide-induced apoptosis mediated by caspase-3 activation in human glioma cells.* J Neurosurg, 2000. **93**(2): p. 289-97.
55. Sarkaria, J.N., et al., *Mechanisms of chemoresistance to alkylating agents in malignant glioma.* Clin Cancer Res, 2008. **14**(10): p. 2900-8.
56. Mayo, L.D., et al., *PTEN protects p53 from Mdm2 and sensitizes cancer cells to chemotherapy.* J Biol Chem, 2002. **277**(7): p. 5484-9.
57. Law, M.E., et al., *Molecular cytogenetic analysis of chromosomes 1 and 19 in glioma cell lines.* Cancer Genet Cytogenet, 2005. **160**(1): p. 1-14.
58. Iwadate, Y., et al., *Promising survival for patients with glioblastoma multiforme treated with individualised chemotherapy based on in vitro drug sensitivity testing.* Br J Cancer, 2003. **89**(10): p. 1896-900.
59. Camphausen, K., et al., *Influence of in vivo growth on human glioma cell line gene expression: convergent profiles under orthotopic conditions.* Proc Natl Acad Sci U S A, 2005. **102**(23): p. 8287-92.
60. Ogunnaike, B.A., *Elucidating the digital control mechanism for DNA damage repair with the p53-Mdm2 system: single cell data analysis and ensemble modelling.* J R Soc Interface, 2006. **3**(6): p. 175-84.
61. Gurkan, E., et al., *Probabilistic modeling of DNA mismatch repair effects on cell cycle dynamics and iododeoxyuridine-DNA incorporation.* Cancer Res, 2007. **67**(22): p. 10993-1000.
62. Haberichter, T., et al., *A systems biology dynamical model of mammalian G1 cell cycle progression.* Mol Syst Biol, 2007. **3**: p. 84.
63. Ma, L., et al., *A plausible model for the digital response of p53 to DNA damage.* Proc Natl Acad Sci U S A, 2005. **102**(40): p. 14266-71.
64. Toettcher, J.E., et al., *Distinct mechanisms act in concert to mediate cell cycle arrest.* Proc Natl Acad Sci U S A, 2009. **106**(3): p. 785-90.
65. Hart, M.G., et al., *Chemotherapeutic wafers for High Grade Glioma.* Cochrane Database Syst Rev, 2008(3): p. CD007294.
66. Bartek, J. and J. Lukas, *Chk1 and Chk2 kinases in checkpoint control and cancer.* Cancer Cell, 2003. **3**(5): p. 421-9.
67. Bredel, M., C. Bredel, and B.I. Sikic, *Genomics-based hypothesis generation: a novel approach to unravelling drug resistance in brain tumours?* Lancet Oncol, 2004. **5**(2): p. 89-100.
68. Evans, W.E. and M.V. Relling, *Pharmacogenomics: translating functional genomics into rational therapeutics.* Science, 1999. **286**(5439): p. 487-91.
69. Evans, W.E. and M.V. Relling, *Moving towards individualized medicine with pharmacogenomics.* Nature, 2004. **429**(6990): p. 464-8.
70. Nutt, C.L., et al., *Differential expression of drug resistance genes and chemosensitivity in glial cell lineages correlate with differential response of*

oligodendrogliomas and astrocytomas to chemotherapy. Cancer Res, 2000. **60**(17): p. 4812-8.

71. Schaner, M.E., et al., *Gene expression patterns in ovarian carcinomas.* Mol Biol Cell, 2003. **14**(11): p. 4376-86.
72. Wallqvist, A., et al., *Establishing connections between microarray expression data and chemotherapeutic cancer pharmacology.* Mol Cancer Ther, 2002. **1**(5): p. 311-20.
73. Welsh, J.B., et al., *Analysis of gene expression identifies candidate markers and pharmacological targets in prostate cancer.* Cancer Res, 2001. **61**(16): p. 5974-8.
74. Segal, E., et al., *From signatures to models: understanding cancer using microarrays.* Nat Genet, 2005. **37 Suppl**: p. S38-45.
75. Stears, R.L., R.C. Getts, and S.R. Gullans, *A novel, sensitive detection system for high-density microarrays using dendrimer technology.* Physiol Genomics, 2000. **3**(2): p. 93-9.
76. Wu, H., Kerr, K., Cui X., Chruchill, G.A., *MAANOVA: a Software Package for The Analysis of Spotted cDNA Micrarray Experiments*, in *The Analysis of Gene Expression Data: Methods and Software*, G. Parmigiani, Garett, E.S., Irizarry, R.A., et al, Editor. 2003, Springer: Heidelberg. p. 313-341.
77. Cui, X., et al., *Improved statistical tests for differential gene expression by shrinking variance components estimates.* Biostatistics, 2005. **6**(1): p. 59-75.
78. Benjamini, Y., Hochbery, Y., *Controlling the False Discovery Rate: a Practical and Powerful Appraoch to Multiple Testing.* J R Statist Soc B, 1995. **57**: p. 289-300.
79. Abramoff, M.D., Magelhaes, P.J., Ram, S.J., *Image Processing with ImageJ.* Biophotonics International, 2004. **11**(7): p. 36-42.
80. Wolff, J.E., et al., *Chemosensitivity of glioma cells in vitro: a meta analysis.* J Cancer Res Clin Oncol, 1999. **125**(8-9): p. 481-6.
81. Weaver, K.D., et al., *Potentiation of chemotherapeutic agents following antagonism of nuclear factor kappa B in human gliomas.* J Neurooncol, 2003. **61**(3): p. 187-96.
82. Bernardi, A., et al., *Nonsteroidal anti-inflammatory drugs inhibit the growth of C6 and U138-MG glioma cell lines.* Eur J Pharmacol, 2006. **532**(3): p. 214-22.
83. Oberkovitz, G., L. Regev, and A. Gross, *Nucleocytoplasmic shuttling of BID is involved in regulating its activities in the DNA-damage response.* Cell Death Differ, 2007. **14**(9): p. 1628-34.
84. Aghi, M., S. Rabkin, and R.L. Martuza, *Effect of chemotherapy-induced DNA repair on oncolytic herpes simplex viral replication.* J Natl Cancer Inst, 2006. **98**(1): p. 38-50.
85. Gomi, A., et al., *Elevated expression of DNA polymerase beta gene in glioma cell lines with acquired resistance to 1-(4-amino-2-methyl-5-pyrimidinyl)methyl-3-(2-chloroethyl)-3- nitrosourea.* Biochem Biophys Res Commun, 1996. **227**(2): p. 558-63.
86. Auger, N., et al., *Genetic alterations associated with acquired temozolomide resistance in SNB-19, a human glioma cell line.* Mol Cancer Ther, 2006. **5**(9): p. 2182-92.

87. Gaspar, N., et al., *Acquired resistance to 17-allylamino-17-demethoxygeldanamycin (17-AAG, tanespimycin) in glioblastoma cells.* Cancer Res, 2009. **69**(5): p. 1966-75.
88. Wang, C.Y., et al., *Control of inducible chemoresistance: enhanced anti-tumor therapy through increased apoptosis by inhibition of NF-kappaB.* Nat Med, 1999. **5**(4): p. 412-7.
89. Morandi, E., et al., *Gene expression time-series analysis of camptothecin effects in U87-MG and DBTRG-05 glioblastoma cell lines.* Mol Cancer, 2008. **7**: p. 66.
90. Ma, J., et al., *Biochemical changes associated with a multidrug-resistant phenotype of a human glioma cell line with temozolomide-acquired resistance.* Biochem Pharmacol, 2002. **63**(7): p. 1219-28.
91. Xu, G.W., J.S. Mymryk, and J.G. Cairncross, *Pharmaceutical-mediated inactivation of p53 sensitizes U87MG glioma cells to BCNU and temozolomide.* Int J Cancer, 2005. **116**(2): p. 187-92.
92. Winter, S. and M. Weller, *Poly(ADP-ribose) polymerase-independent potentiation of nitrosourea cytotoxicity by 3-aminobenzamide in human malignant glioma cells.* Eur J Pharmacol, 2000. **398**(2): p. 177-83.
93. Winter, S. and M. Weller, *Potentiation of CD95L-induced apoptosis of human malignant glioma cells by topotecan involves inhibition of RNA synthesis but not changes in CD95 or CD95L protein expression.* J Pharmacol Exp Ther, 1998. **286**(3): p. 1374-82.
94. Trepel, M., et al., *Chemosensitivity of human malignant glioma: modulation by p53 gene transfer.* J Neurooncol, 1998. **39**(1): p. 19-32.
95. Bartussek, C., U. Naumann, and M. Weller, *Accumulation of mutant p53(V143A) modulates the growth, clonogenicity, and radiochemosensitivity of malignant glioma cells independent of endogenous p53 status.* Exp Cell Res, 1999. **253**(2): p. 432-9.
96. Bocangel, D.B., et al., *Multifaceted resistance of gliomas to temozolomide.* Clin Cancer Res, 2002. **8**(8): p. 2725-34.
97. Biroccio, A., et al., *Increase of BCNU sensitivity by wt-p53 gene therapy in glioblastoma lines depends on the administration schedule.* Gene Ther, 1999. **6**(6): p. 1064-72.
98. Blagosklonny, M.V., *Prospective strategies to enforce selectively cell death in cancer cells.* Oncogene, 2004. **23**(16): p. 2967-75.
99. Tannock, I.F., *Cell Kinetics and Chemotherapy: a Critical Review.* Cancer Treat Rep, 1978. **62**: p. 1117-1133.
100. Dhandapani, K.M., V.B. Mahesh, and D.W. Brann, *Curcumin suppresses growth and chemoresistance of human glioblastoma cells via AP-1 and NFkappaB transcription factors.* J Neurochem, 2007. **102**(2): p. 522-38.
101. Chen, C.C., T. Taniguchi, and A. D'Andrea, *The Fanconi anemia (FA) pathway confers glioma resistance to DNA alkylating agents.* J Mol Med, 2007. **85**(5): p. 497-509.
102. Chen, H., et al., *Single nucleotide polymorphisms and expression of ERCC1 and ERCC2 vis-a-vis chemotherapy drug cytotoxicity in human glioma.* J Neurooncol, 2007. **82**(3): p. 257-62.

103. Rhee, C.H., et al., *Characterization of cellular pathways involved in glioblastoma response to the chemotherapeutic agent 1, 3-bis(2-chloroethyl)-1-nitrosourea (BCNU) by gene expression profiling.* Oncol Rep, 1999. **6**(2): p. 393-401.
104. Yamauchi, T., Y. Kawai, and T. Ueda, *Alkylator-induced DNA excision repair in human leukemia CCRF-CEM cells in vitro, measured using the single-cell gel electrophoresis (comet) assay.* Int J Hematol, 2002. **76**(4): p. 328-32.
105. Yamauchi, T., Y. Kawai, and T. Ueda, *Inhibition of nucleotide excision repair by fludarabine in normal lymphocytes in vitro, measured by the alkaline single cell gel electrophoresis (Comet) assay.* Jpn J Cancer Res, 2002. **93**(5): p. 567-73.
106. Yamauchi, T., Y. Kawai, and T. Ueda, *Enhanced DNA excision repair in CCRF-CEM cells resistant to 1,3-bis(2-chloroethyl)-1-nitrosourea, quantitated using the single cell gel electrophoresis (Comet) assay.* Biochem Pharmacol, 2003. **66**(6): p. 939-46.
107. Yamauchi, T., M.J. Keating, and W. Plunkett, *UCN-01 (7-hydroxystaurosporine) inhibits DNA repair and increases cytotoxicity in normal lymphocytes and chronic lymphocytic leukemia lymphocytes.* Mol Cancer Ther, 2002. **1**(4): p. 287-94.
108. Yamauchi, T., M. Ogawa, and T. Ueda, *Carmustine-resistant cancer cells are sensitized to temozolomide as a result of enhanced mismatch repair during the development of carmustine resistance.* Mol Pharmacol, 2008. **74**(1): p. 82-91.
109. Bobola, M.S., et al., *Apurinic/apyrimidinic endonuclease activity is associated with response to radiation and chemotherapy in medulloblastoma and primitive neuroectodermal tumors.* Clin Cancer Res, 2005. **11**(20): p. 7405-14.
110. Bobola, M.S., et al., *O6-methylguanine-DNA methyltransferase, O6-benzylguanine, and resistance to clinical alkylators in pediatric primary brain tumor cell lines.* Clin Cancer Res, 2005. **11**(7): p. 2747-55.
111. Naumann, S.C., et al., *Temozolomide- and fotemustine-induced apoptosis in human malignant melanoma cells: response related to MGMT, MMR, DSBs, and p53.* Br J Cancer, 2009. **100**(2): p. 322-33.
112. Bacolod, M.D., et al., *BCNU-sequestration by metallothioneins may contribute to resistance in a medulloblastoma cell line.* Cancer Chemother Pharmacol, 2009. **63**(4): p. 753-8.
113. Reyes, S., et al., *Quinacrine enhances carmustine therapy of experimental rat glioma.* Neurosurgery, 2001. **49**(4): p. 969-73.
114. Liu, L., et al., *Chemotherapy-induced O(6)-benzylguanine-resistant alkyltransferase mutations in mismatch-deficient colon cancer.* Cancer Res, 2002. **62**(11): p. 3070-6.
115. Bacolod, M.D., et al., *Brain tumor cell lines resistant to O6-benzylguanine/1,3-bis(2-chloroethyl)-1-nitrosourea chemotherapy have O6-alkylguanine-DNA alkyltransferase mutations.* Mol Cancer Ther, 2004. **3**(9): p. 1127-35.
116. Wiencke, J.K. and J. Wiemels, *Genotoxicity of 1,3-bis(2-chloroethyl)-1-nitrosourea (BCNU).* Mutat Res, 1995. **339**(2): p. 91-119.
117. Muller, M.R., et al., *Drug resistance and DNA repair in leukaemia.* Cytotechnology, 1998. **27**(1-3): p. 175-185.
118. Muller, M.R., et al., *DNA repair and cellular resistance to alkylating agents in chronic lymphocytic leukemia.* Clin Cancer Res, 1997. **3**(11): p. 2055-61.

119. Calatozzolo, C., et al., *Expression of drug resistance proteins Pgp, MRP1, MRP3, MRP5 and GST-pi in human glioma.* J Neurooncol, 2005. **74**(2): p. 113-21.
120. Friedman, H.S., et al., *Methylator resistance mediated by mismatch repair deficiency in a glioblastoma multiforme xenograft.* Cancer Res, 1997. **57**(14): p. 2933-6.
121. Trivedi, R.N., et al., *The role of base excision repair in the sensitivity and resistance to temozolomide-mediated cell death.* Cancer Res, 2005. **65**(14): p. 6394-400.
122. Ueda, S., et al., *Induction of the DNA repair gene O6-methylguanine-DNA methyltransferase by dexamethasone in glioblastomas.* J Neurosurg, 2004. **101**(4): p. 659-63.
123. Spooren, A., et al., *Cooperation of NFkappaB and CREB to induce synergistic IL-6 expression in astrocytes.* Cell Signal. **22**(5): p. 871-81.
124. Prasad, S., J. Ravindran, and B.B. Aggarwal, *NF-kappaB and cancer: how intimate is this relationship.* Mol Cell Biochem, 2009.
125. Hinz, M., et al., *NF-kappaB function in growth control: regulation of cyclin D1 expression and G0/G1-to-S-phase transition.* Mol Cell Biol, 1999. **19**(4): p. 2690-8.
126. Carrassa, L., et al., *Chk1, but not Chk2, is involved in the cellular response to DNA damaging agents: differential activity in cells expressing or not p53.* Cell Cycle, 2004. **3**(9): p. 1177-81.
127. Lodish, H., Baltimore, D., Berk, A., Zipursky, S.L., Matsudaira, P. and Darnell, J., *Molecular Cell Biology*. Third ed. 1995, New York: W.H. Freeman and Company.
128. Guha, A. and J. Mukherjee, *Advances in the biology of astrocytomas.* Curr Opin Neurol, 2004. **17**(6): p. 655-62.
129. Drappatz, J. and P.Y. Wen, *Non-cytotoxic drugs as potential treatments for gliomas.* Curr Opin Neurol, 2004. **17**(6): p. 663-73.
130. Milojkovic, D. and J. Apperley, *Mechanisms of Resistance to Imatinib and Second-Generation Tyrosine Inhibitors in Chronic Myeloid Leukemia.* Clin Cancer Res, 2009. **15**(24): p. 7519-7527.
131. Gramza, A.W., C.L. Corless, and M.C. Heinrich, *Resistance to Tyrosine Kinase Inhibitors in Gastrointestinal Stromal Tumors.* Clin Cancer Res, 2009. **15**(24): p. 7510-7518.
132. Banck, M.S. and A. Grothey, *Biomarkers of Resistance to Epidermal Growth Factor Receptor Monoclonal Antibodies in Patients with Metastatic Colorectal Cancer.* Clin Cancer Res, 2009. **15**(24): p. 7492-7501.
133. Portugal, J., M. Bataller, and S. Mansilla, *Cell death pathways in response to antitumor therapy.* Tumori, 2009. **95**(4): p. 409-21.
134. Mansilla, S., W. Priebe, and J. Portugal, *Mitotic catastrophe results in cell death by caspase-dependent and caspase-independent mechanisms.* Cell Cycle, 2006. **5**(1): p. 53-60.
135. Eom, Y.W., et al., *Two distinct modes of cell death induced by doxorubicin: apoptosis and cell death through mitotic catastrophe accompanied by senescence-like phenotype.* Oncogene, 2005. **24**(30): p. 4765-77.

136. Chang, B.D., et al., *Molecular determinants of terminal growth arrest induced in tumor cells by a chemotherapeutic agent.* Proc Natl Acad Sci U S A, 2002. **99**(1): p. 389-94.
137. Chang, B.D., et al., *A senescence-like phenotype distinguishes tumor cells that undergo terminal proliferation arrest after exposure to anticancer agents.* Cancer Res, 1999. **59**(15): p. 3761-7.
138. Alizadeh, A.A., et al., *Distinct types of diffuse large B-cell lymphoma identified by gene expression profiling.* Nature, 2000. **403**(6769): p. 503-11.
139. Alon, U., et al., *Broad patterns of gene expression revealed by clustering analysis of tumor and normal colon tissues probed by oligonucleotide arrays.* Proc Natl Acad Sci U S A, 1999. **96**(12): p. 6745-50.
140. Perou, C.M., et al., *Distinctive gene expression patterns in human mammary epithelial cells and breast cancers.* Proc Natl Acad Sci U S A, 1999. **96**(16): p. 9212-7.
141. Virtanen, C., et al., *Integrated classification of lung tumors and cell lines by expression profiling.* Proc Natl Acad Sci U S A, 2002. **99**(19): p. 12357-62.
142. Beningo, K.A., M. Dembo, and Y.L. Wang, *Responses of fibroblasts to anchorage of dorsal extracellular matrix receptors.* Proc Natl Acad Sci U S A, 2004. **101**(52): p. 18024-9.
143. Cukierman, E., et al., *Taking cell-matrix adhesions to the third dimension.* Science, 2001. **294**(5547): p. 1708-12.
144. Li, S., et al., *Genomic analysis of smooth muscle cells in 3-dimensional collagen matrix.* Faseb J, 2003. **17**(1): p. 97-9.
145. Weaver, V.M., et al., *Reversion of the malignant phenotype of human breast cells in three-dimensional culture and in vivo by integrin blocking antibodies.* J Cell Biol, 1997. **137**(1): p. 231-45.
146. Ohmori, T., et al., *Blockade of tumor cell transforming growth factor-betas enhances cell cycle progression and sensitizes human breast carcinoma cells to cytotoxic chemotherapy.* Exp Cell Res, 1998. **245**(2): p. 350-9.
147. Sallinen, S.L., Sallinen, P., Ahlstedt-Sionim, M., Haapasalo, H., Helin, H., Isola, J., Karhu, R., *Arm-Specific mutlicolor flourescence in situ hybridization reveals widespread chromosomal instability in glioma cell lines.* Cancer Genetics and Cytogenetics, 2003. **144**(1): p. 52-60.
148. Badie, B., et al., *Combined radiation and p53 gene therapy of malignant glioma cells.* Cancer Gene Ther, 1999. **6**(2): p. 155-62.
149. Sato, Y., et al., *Diversity of DNA damage response of astrocytes and glioblastoma cell lines with various p53 status to treatment with etoposide and temozolomide.* Cancer Biol Ther, 2009. **8**(5): p. 452-7.
150. Poulos, N.E., et al., *Design of a novel bicistronic expression vector with demonstration of a p16INK4-induced G(1)-S block(1).* Cancer Res, 1996. **56**(8): p. 1719-23.
151. Poch, E., et al., *RhoE interferes with Rb inactivation and regulates the proliferation and survival of the U87 human glioblastoma cell line.* Exp Cell Res, 2007. **313**(4): p. 719-31.

152. Chalmers, A.J., et al., *Cytotoxic effects of temozolomide and radiation are additive- and schedule-dependent.* Int J Radiat Oncol Biol Phys, 2009. **75**(5): p. 1511-9.
153. Hermes, M., et al., *Alterations in S-adenosylhomocysteine metabolism decrease O6-methylguanine DNA methyltransferase gene expression without affecting promoter methylation.* Biochem Pharmacol, 2008. **75**(11): p. 2100-11.
154. Huber, K.R., et al., *Human tumor cells resistant to verapamil.* Biochem Biophys Res Commun, 1989. **161**(3): p. 1312-8.
155. Kondo, S., et al., *mdm2 gene mediates the expression of mdr1 gene and P-glycoprotein in a human glioblastoma cell line.* Br J Cancer, 1996. **74**(8): p. 1263-8.

APPENDIX

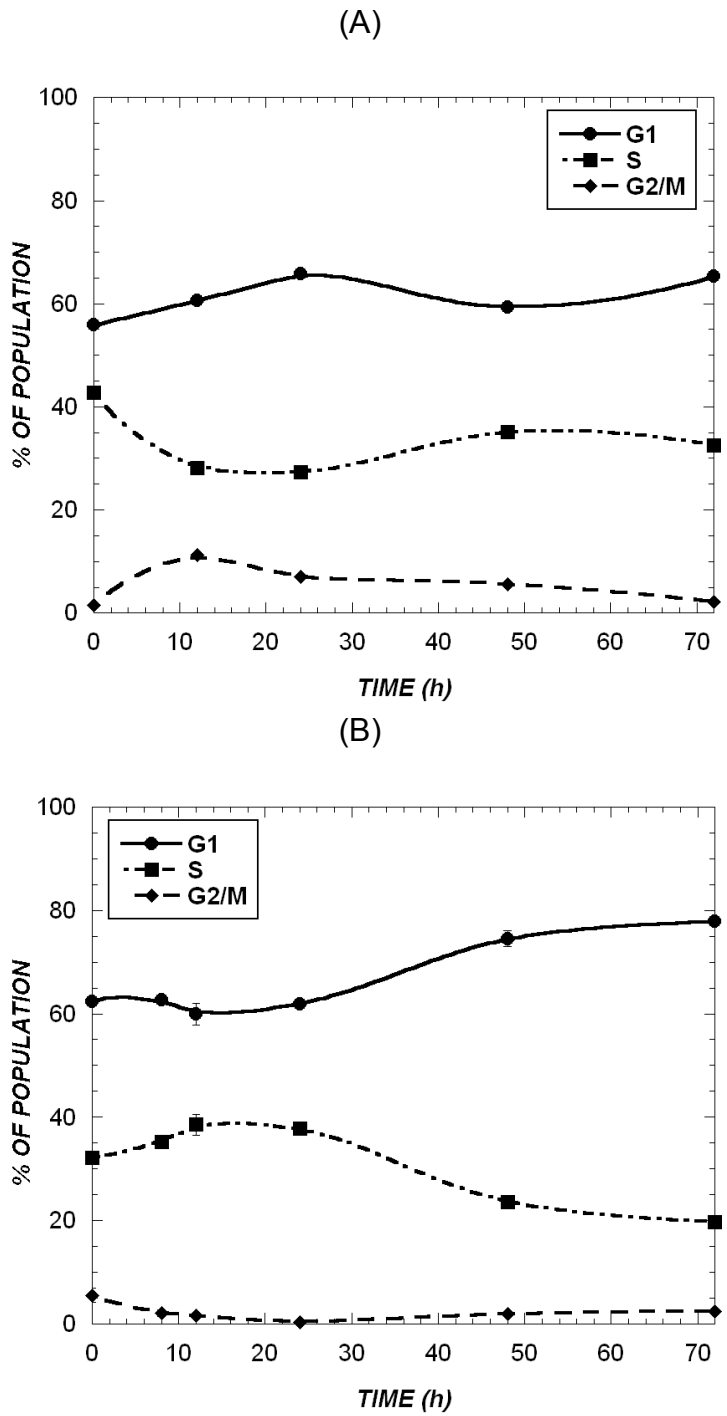

Figure A.1: Cell Cycle Phase Distribution of DMSO-Treated Cells. (A) SW1088CR cells and (B) U87 Cells, as well as, other cell lines do not show alterations in phase distribution upon exposure to vehicle control (DMSO).

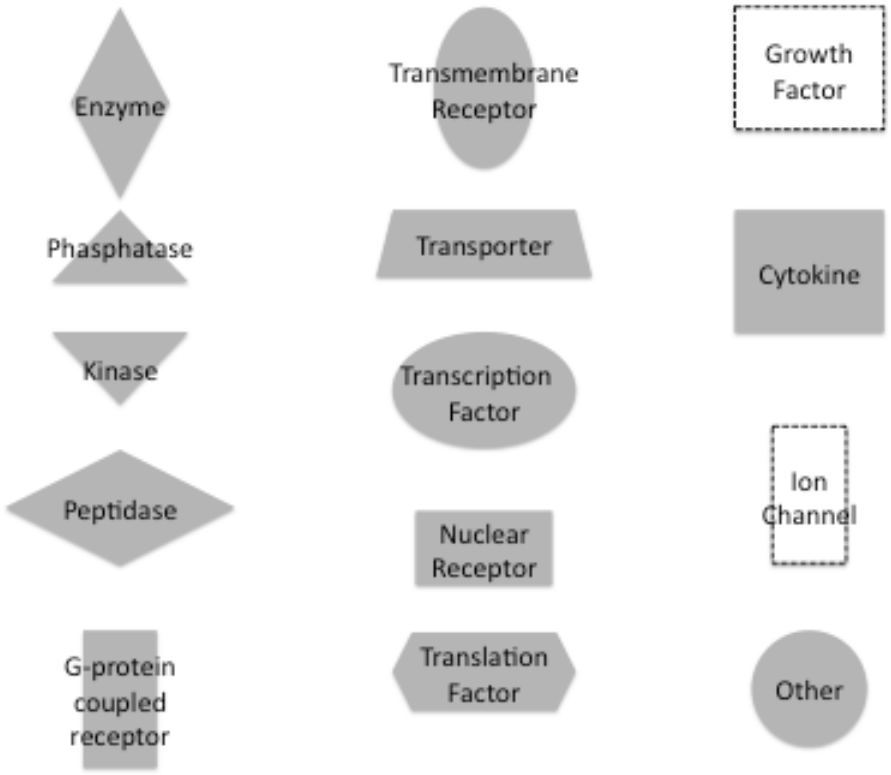

Figure A.2: Lengend representing molecular functions of genes in datasets. Genes in datasets of interest were associated with cellular functions, from IPA knowledge base, and used to construct networks in figures 3.4-3.6

Table A.1: A172 Top-scoring Networks. Boldfacing indicates overexpressed gene. Genes that are underexpressed are underlined. Genes in plain type are gene that were connected to differentially expressed genes by IPA to form network

ID	Molecules in Network	Score	Focus Mol.	Top Functions
1	**ADM**, ARHGEF7, Caspase, **CBR3**, **CDC42**, CRADD, CXCL16, DNAJA2, DNAJC4, **DNAJC14**,EIF2S1, ERK, **G6PD**, **GAS6**, Hsp22/Hsp40/Hsp90, Insulin, Jnk, KLF5, LDL, MAP2K1, Mapk, **MAPK8IP2**, NFkB (complex), P38 MAPK, Pdgf, PI3K, Pkc(s), PRSS23, Rac, Raf, Ras, SLC25A12, STK3, **TMPO**, TNFSF10	37	20	Cell Death Cellular Assembly & Organization Nervous System Dev. and Func.
2	ARHGEF7, ASXL1, ASXL2, ASXL3, **C12ORF49**, Cbp/p300-Hd-Taf4-Taf9b-Tbp, CBX2, CLCN3, DOCK11, EED,HIST3H3 (includes EG:8290), Histone h3, HMP19, HSPD1,HTT, LARP1B, MIR1, MPST, MTOR, PCGF1, **PCGF6**, PHF19, RNF138, RUNX1T1, SAMD8, SEC22B, **STX18**, SUZ12, Taf, **TAF9B**, **TELO2**, TGFBR1, **TRIM52**, TRPM7, **ZNF264**	26	15	Protein Trafficking Neurological Disease Cell-To-Cell Signaling and Interaction
3	ADAM10, amino acids,**BOK**, Ca2+, **CBR3**, **CSRP1**, CTDP1, CXCL16, DBP, **EEF1A2**, **ELMO2**, **F8**, GEFT, Ho, **JAZF1**, JUN, LAMA2, **MFSD5**, MGC29506, MIR23A (includes EG:407010), **MLF1**, **MXD3**, NET1, NFKB1, NR3C1, NRBP1, P2RX4, P2RX6, progesterone, S100B, **SNAPC5**, STK38, TGFB1, TNFAIP2, TNFRSF11A	26	15	Cell-To-Cell Signaling and Interaction Tissue Development Cellular Development

4	ACIN1, **ACN9**, ACOT2, ATL1, BAT1, CXCL3, EAF1, ELL, EPO, FUZ, FYCO1, **HMOX2**, HNF4A, **HNRNPA0**, IL15, MLXIPL, MRPL44, **NFKBIL1**, **OAZ2** (includes EG:4947), ONECUT1, PPP1R3B, PYGL, SEPSECS, SETDB1, SMARCA5, SPAST, SSSCA1, TFPT, TMEM48, TRAPPC3,TRAPPC4, **TRAPPC6A**, **TRNAU1AP**, ZNF277	24	14	Cell Cycle Cellular Development Hematological System Develop. and Fun.
5	Actin, ACTR1A, **C11ORF75**, **C12ORF68**, **CDC45L**, CDKN1A, CEACAM1, DCTN1, DCTN2, DCTN3, DCTN4, DCTN6, DLGAP4,FGF13, **GINS1**, IL6, ITGB3, **KNTC1**, MIR17 (includes EG:406952), MIR214 (includes EG:406996), MKI67, **MUC15**, NSMCE1, PLK2, **POLDIP2**, RABGAP1, **RBM33**, SMC5, SMC6, SUMO3, TFDP2, UBE2C, Ubiquitin, ZNF804A, ZW10	24	14	Cellular Assembly and Organization Cell Cycle Organismal Functions
6	**AKAP8**, ASNS, BAT1, BAZ1A, BOP1, CHRAC1, CSRP2, DDX17, EIF2S1, EIF4G1, ETF1, FBL, GSPT2, HRAS, **KIAA1524**, KPTN, MED26, MYC, MYO9A, MYO9B, NOP58, P4HA1, **P4HB**, PABPC1, PES1, **PIN4**, POLE3, **PTGES2**, RPAP2, SMARCA5, SMC3, SYNGAP1, **TSPAN7**, ULK2, ZXDB	21	13	Cellular Assembly and Organization DNA Replication, Recombination, and Repair Amino Acid Metabolism
7	AChR, Adaptor protein 1, APOD, ARG1, ARL6IP5, BGN, **C10ORF35**, CDX1, CREB1, CSRP2, CTNNB1, **CTSZ** (includes EG:1522), EIF2S1, FRMD6, **GAS6**, GM2A, GPR126, **GRINL1A**, **HEXA**, IER3, IFITM1, KLF5, MYO9A, MYO9B, PSMC2, RPL7A (includes EG:6130), SEC22B, SERPIND1, SLC26A2,SLC2A4, SMAP1, SMURF2, TCF7L1, **TIMM44**, TNF	20	13	Amino Acid Metabolism Molecular Transport Small Molecule Biochemistry

8	ACIN1, ALPL, **APOBEC3C**, ARHGDIB, ASNS, CYP4F3, deoxyuridine, **DYRK4**, **FAM153A**, FBLN1, **FLOT1**, IFIT1, IFITM1, IFITM2, Igfbp, MMP11, **NOTCH2NL**, **NOV**, PAX3, PRAME (includes EG:23532), **RAB11B**, retinoic acid, RPA1, RPA4, SFRS3, SFRS2IP, SHBG, SMARCA4, thymidine, TIMELESS, **TIPIN**, **TK2**, tyrosine kinase, ZEB2	17	11	Lipid Metabolism Small Molecule Biochemistry DNA Replication, Recombination, and Repair
9	ACP5, ALPL, APOBEC3G, ARL6IP5, **BAG1**, **CYB561**, DPY19L1, ERK1/2, FSH, IFIT1, Interferon alpha, KDM5B, KIAA1797,Lh, MOS, NKX3-1, NOL3, NR2C1, P4HA2, PIAS1, PRAME (includes EG:23532), Proteasome, PTPRN, **RAP1GDS1**, **RARB**,SP100, TBL1XR1,TCF7, **TOP1**, TOPBP1, TOPORS, TRIB1, TYRO3, USP18, VCL	15	10	Genetic Disorder Metabolic Disease Cellular Growth and Proliferation
10	ABCA2, Acid Phosphatase, ACP5, ALB, **AMBRA1**, AR, CNOT1, ERLEC1, GH1, GSN, hydrocortisone, IFI16, Igfbp, IGFBP5, IGHG1, IL4, ITGA2, KLK3, MAPKAPK2, MUC1, NKX3-1, NUP160, PA2G4, PIAS4, PPAPDC2, PSMC2, RANBP2, RP2, RXRB, SELE, SPAST, TF, TNFRSF11B, TRA@	10	7	Cellular Development Cellular Growth and Proliferation Inflammatory Disease
11	C8ORF30A, **TRIT1**	2	1	Cellular Growth and Proliferation
12	**IMP4**, MPHOSPH10	2	1	RNA Post-Transcriptional Modification
13	**GLT8D2**, Hexosyltransferase	2	1	
14	CCDC85B, PPIL3, SLU7	2	1	RNA Post-Transcriptional Modification

Table A.2: A172CR Top-scoring Networks. Boldfacing indicates overexpressed gene. Genes that are underexpressed are underlined. Genes in plain type are gene that were connected to differentially expressed genes by IPA to form network

ID	Molecules in Network	Score	Focus Mol.	Top Functions
1	ABCC2, BIRC3, COL1A2, Collagen Alpha1, Collagen(s), **CSF3**, Cyclin E, CYR61, DOCK3, Focal adhesion kinase, **HAS1**, **HCCS**, Ige, **IL1B**, Laminin, **LAT**, N-cor, NFAT (complex), Pdgf, PDGF BB, PIAS3, Pld, **PTPRN**, Rar, RDH5, Rxr, **SLC1A2**, **SLC20A2**, Smad, **SPHK1**, STAT5a/b, Tgf beta, **ULBP2**, USP18, YPEL3	32	19	Cellular Development Cellular Growth and Proliferation Hematological System Development and Function
2	ACAT1, **ALDH1A3**, **CCL20**, CHEMOKINE, **CXCL3**, CXCL14, Cyclooxygenase, Elastase, Fibrinogen, **HRH1**, Hsp27, IFN Beta, IKK (complex), IL1, **IL8**, **IL24**, IL1F5, Interferon alpha, LARGE, LDL, **LIF**, LOX, Mmp, NFkB (complex), NfkB-RelA, **PTGES**, **PTGS2**, S100, S100A3, S100A4, **S100A8**, **SNIP1**,sPla2, STAT, Tlr	30	18	Cellular Movement Inflammatory Response Antigen Presentation
3	14-3-3, ALP, Alpha catenin, APC, **CCDC76**, Cdc2, CDC2, Creb, CTNND1, Cyclin A, Cyclin B, E2f, ERK, Fgf, **FGF2**, **GPNMB**, **GRB14**, Gsk3, Histone h3, Histone h4, KPNB1, LOXL1,MAP4, MAP2K1/2,**MAPT**, Mek, **PFTK1**, PLC γ, POLD3, PTN, Rb, RPA2, TOP2A, TPX2, UBE2C	26	17	Cell Morphology Reproductive System Development and Function Cellular Assembly and Organization
4	ADAMTS5, **AGBL5**, ALDH7A1, ALPL, beta-estradiol, CDKN3, ERLIN2, GAD2, HIST2H2BE, ICOSLG, IER2, IFI44, IFNG, ILK, **KIAA1199**, MEFV, MIRN338, **MORC2**, OAS2, **OTUD4**, PARP9,PEG10, PRC1, PRIM1, PRSS23, PTGIS, **PTPRN**, retinoic acid, **SCG5**, SP110, STT3A, TGFB1, TNFAIP2, TYMP, ZWINT (includes EG:11130)	23	15	Cell Cycle Lipid Metabolism Small Molecule Biochemistry

5	ACTB, ACTR10, **ACTR1B** (includes EG:10120), **ANGPTL4**,ARHGAP17, **CALD1**, CDC42SE2, CDKN1A, CIT, CNTNAP1, **COG1**, COG2, **COG3**, COG4, **DOCK7** (includes EG:85440), EPB41L3, F2, GMPPB, I kappa b kinase, IKBKB, IL32, **PITPNC1**, PLA2G6, PNPT1, PROS1, RAC1, **TAGLN3**, TMSB4, TPX2, ZFP36, **ZNF692**	21	14	Genetic Disorder Metabolic Disease Amino Acid Metabolism
6	ABR, ADCY, Akt, Ap1, APLN, BIRC5, BNIP3L, Caspase, **CDC42SE1**, DHCR7, **DHRS3**, **DR1**, ERK1/2, FSH, **GATA6**, **GNB1**, hCG, Hsp70, Insulin, Jnk, Lh, **MCL1**, Nfat (family), P38 MAPK, p70 S6k, Pka, Pkc(s), Proteasome, Rac, Ras, RHOQ, **SMAD3**, **SVEP1**, TOPBP1, Vegf	20	15	Infection Mechanism Cell Cycle Tumor Morphology
7	AR, BRF2, **C10ORF18**, **CCDC59**, CCNH, CDK9, CTSO, CYP1A2, **DUSP11**, FAIM2, GRIP1, GSN, HNF4A, HSP90B1, MUT, NCOA2, NHP2L1, NONO, NR0B1, NR0B2, NR2C2, NUFIP1, PAK7, **PINK1**, PPP1R15B, **RRP9**,**RTN4IP1**, RXRB, SULT2A1, TCF4, TCF7L2 (includes EG:6934), TEAD3, **TIGD6**, **UBL7**, **USMG5**	19	13	Gene Expression Infection Mechanism Cell Morphology
8	**ABHD6**, C11ORF48, C4ORF43, CENPN, CETN3, CP110, CTSZ (includes EG:1522), DDX27, HNF4A, HNRNPUL1, HRAS, KIAA1217, **LYAR**, MIPEP, MTDH, NAT10, ONECUT1, PDE6D, PIN1, PNMA1, PPP1R1B, PWP1, ROBO2, RSL24D1, **SDSL**, TACC3, TP53, TUBGCP3, TUBGCP4, TUBGCP5, TUBGCP6, **UBA6**, UTP3, YPEL3, **ZMIZ2**	19	14	Cellular Assembly and Organization Cellular Function and Maintenance Cell Cycle

9	ATXN2L, BCOR, CDCA3, CIDEC, COPS2, CTSZ (includes EG:1522), **CUL1**, ELK1, EPO, **ESPL1**, **FBXL12**, Ferritin, GBP2, GPS1 (includes EG:209318), GPS1 (includes EG:2873), IER2, IL1F9, IL3RA, JAM2, L-carnitine, **LTBP2**, MIR298 (includes EG:723832), MOAP1, NLRP3, NR3C1, PTCD3, RAD21, SENP8, SMC1B, TGTP, TIE1, TNF, TNFAIP2, UGCG, **USP31**	17	12	Organismal Injury & Abnormalities Lipid Metabolism Molecular Transport
10	12-hydroxyeicosatetraenoic acid, AK3L1, **AKR1C1**, ANXA11, **B4GALT5**, **CCL20**, CDH23, DOK5, DUSP5, EDN2, EGFR, Egfr-Erbb2, EREG, FLOT2, **FUT8**, GCNT1, GPC1, IL18BP, INPP5D, ITFG3, MAPK3, MATN2, MME, prostaglandin E2, PTGER1, PTGFR, PTGIS, SH2D2A, SNX6, **ST3GAL1**, TFF3, TIE1, TREM1, VEGFA, **ZNF7**	17	12	Drug Metabolism Lipid Metabolism Small Molecule Biochemistry
11	CAPZB, CCNI, CDC7, CDC45L, CDK4, CDKN2A, **CHORDC1**, CHTF18, CNOT7, CSDE1, CSF2RB, CYP2E1,EIF3I (includes EG:8668), ERLEC1, FAM70A, GCLC, GH1,HSP90AA1, HUWE1, IGFBP7,IPO7, IQUB, IRS2, **LGMN**, **MAGMAS**, MIR129-2 (includes EG:406918), MYC, **NOL12**, RPS19, S100A6, SCPEP1, THY1, TOB2, TOP1, **ZNF592**	14	10	Cellular Growth and Proliferation Endocrine System Development and Function Cell Cycle
12	ACAD9, BCKDK, BEAN, **BEX1**, BNIP1, C17ORF101, **FAM98B**, FGF1, FOXC2, GLG1, GOSR2, LEPRE1, LRRC17, MTDH, NAPA, NEDD4, neuroprotectin D1, NFkB (complex), NR1D1, **PMEPA1**, PPARG, RPL18A, SCNN1B, SCNN1G, SGK1, SLC2A2, SLC2A4, SNAP25, SNAP29, Snare, STX6, STX7, STX12, STX18, STXBP6	14	10	Molecular Transport Cellular Assembly and Organization Cell Signaling

13	Actin, ANXA11, ARF3, ARHGEF18, BTC, **CALD1**, CCL1, Ck2, CLTB, CNR2, **CORO2B**, **CTSLL3**, F Actin, Fascin, FUT7, HIP1R, IgG, IL25, IL31, IL12 (complex), KIF23, LGALS3, Mapk, MARCKS (includes EG:4082), MAZ, MIR1, MST1, PI3K, PIK3C2B, PQBP1, PRC1, Profilin, RABL2A, RNA polymerase II, **XPO6**	10	8	Cellular Assembly and Organization DNA Replication, Recombination, and Repair Antigen Presentation
14	APEX2, CCDC85B, EFEMP2, ENDOD1, GFI1B, MIR124, MIR124-1, MIR124-2, MIR124-3, **MON1A**, NME4, SLC30A7	10	6	Cell-mediated Immune Response Cellular Development Cellular Function and Maintenance
15	C1ORF168, FDFT1	2	1	Developmental Disorder Genetic Disorder Skeletal and Muscular Disorders
16	SSNA1, STAT2	2	1	Cancer Neurological Disease Infection Mechanism
17	hyaluronic acid, LAYN	2	1	Cellular Compromise Cellular Movement Carbohydrate Metabolism
18	ANP32E, MIR195	2	1	Cellular Compromise Cardiovascular Sys. Dev.&Func. Organ Development
19	ATG4A, GABARAPL2 (includes EG:11345)	2	1	Protein Degradation Protein Synthesis Cardiac Arteriopathy
20	LOC339047, NANOG	2	1	Cellular Development Cellular Growth and Proliferation Embryonic Development
21	EFNB3, RHBDL2	2	1	Cell-To-Cell Signaling and Interaction Cellular Assembly & Organiz. Nervous System Dev. and Func.
22	HPS1, HPS4	2	1	Genetic Disorder Cellular Assembly & Organiz. Cellular Development
23	3-oxoacyl-[acyl-carrier-protein] synthase, **OXSM**	2	1	Lipid Metabolism Small Molecule Biochemistry Nucleic Acid Metabolism
24	DIRAS3, Mannose-6-phosphate isomerase, **MPI**	2	1	Cancer Reproductive System Disease Cellular Development

Table A.3: SW1088 Top-scoring Networks. Boldfacing indicates overexpressed gene. Genes that are underexpressed are underlined. Genes in plain type are gene that were connected to differentially expressed genes by IPA to form network

ID	Molecules in Network	Score	Focus Mol.	Top Functions
1	AASDHPPT, AMPK, Caspase, **CDC20**, **CRABP2**, Creatine Kinase, CTDSP2, **DDIT4**, DNAJA2, Estrogen Receptor, GLIPR1, Hdac, Histone h4, **HLA-G**, Hsp27, Hsp70, Hsp90, HSPB3, **ID1**, **ID2**,IFN Beta, INSIG1, MHC CLASS I (family), NKX2-2, Nuclear factor 1, PDLIM5, PMEPA1, Proteasome,SMARCC1, **SMARCC2** (includes EG:6601), **SNAI1**,SP4, **TP53**, **BA2**, Ubiquitin	34	21	Cell Cycle Connective Tissue Development and Function Cellular Function and Maintenance
2	**ADM**, ALP, BDKRB1, BHLHE40, Cbp/p300, CDK6, Collagen(s), **CSF1**, CSF2RB, Cyclin E,CYR61, DUSP6,ELAVL1,Eotaxin,ERRFI1, **HOMER3**, IL6, **ITGAV**, JAK, **JAK1**, KLF10, Laminin, LIF, **MSX1**, p70 S6k, Pdgf, PDGF BB, **PHLDA1**, **PSAP**, **RDBP**, Shc, SOCS, STAT, STAT5a/b, Tgf beta	34	20	Hematological System Development and Function Hematopoiesis Organismal Development
3	CCL2, CHEMOKINE, CXCL1, CXCL2, **E2F7**, ETS, F3, **FAM46A**, Fibrinogen, GBP2, Ifn,Ifn gamma, IFNα/β, Ikb, IKK (complex), IL1, IL8, Il12 (family), IL6 RECEPTOR, **LRDD**, **MX2**, NFKB1, NFkB (complex), NfkB-RelA, NfkB1-RelA, NFKBIE, **NXF1**, PRKDC, Pro-inflammatory Cytokine, **RFTN1**, SAA@, SH3RF1, **SLC2A6**, Tlr, TSLP	29	18	Infection Mechanism Infectious Disease Cellular Movement

4	ARRDC3, ATAD2, C14ORF4, C3ORF59, CDKN1A, E2F1, **EAPP**, EIF2C1, FBXO22, HPGD, JAG1, KIAA0101, KLF10, MIR103-1 (includes EG:406895), MIR98 (includes EG:407054), MIRLET7A1, MIRN338, NUSAP1, **PCDH7**, PDCD1, **PHF8**, PLEKHA3, PTPN12, RASIP1, SDCBP2, SERTAD2, SOCS5, SSPN, TIFA, TM4SF1, TNF, TNRC6B, TTK, ZMAT2, ZNF365	23	15	Cellular Assembly and Organization Cellular Compromise Cell Death
5	ACIN1, BTBD10, **C17ORF70**, CPSF2, CPSF3, CPSF4, CPSF6, EWSR1, FA, FANCB, FANCE, FANCL, FANCM, FIP1L1,GGN, **HMG20A**, KLF12, MAGOHB, **NLE1**, PAK4, PIK3C3, **PIK3R4**, PLSCR1, PRPF38B, PRPF40A, RNPS1, SFRS4, SKIL, SMAD4, **SMCR7L**, STK11, **TCTA**, **YIPF3**, YWHAG, **ZBTB3**	21	14	Gastrointestinal Disease Genetic Disorder Hematological Disease
6	**ATP6AP1**, BCL2L14, BTK, CDC40, **CENPT**, CREBBP, DACH1, EXOC1, EXOC2, EXOC3,EXOC5, EXOC6, EXOC8, Exocyst, FKBP2, FNTA, HDAC1, HGS, IL1F9, ITGB6, **KCMF1**, **KIAA1731**, KLF5, MAPK3, **NAGK**, NR3C1, **NUDT14**, RAF1, RAP2A, SALL1, SMAD2, SS18L1, TADA2L, TNFRSF8, **ZNF7**	19	13	Cell Morphology Cellular Assembly and Organization Hair and Skin Development and Function
7	AGAP2, ARHGAP18, ARHGAP29, ARHGEF1, BLZF1, BMP6, BMPR1A, DAD1, DLX5, ELF4, **EPB41L1**, EPHX1, ERRFI1, **FAM153A**, FGF3, FGF8, FST, **HM13**, HOXB7, ITM2B, **LHX8**, **MGAT2**, MIR124-1, MIR214 (includes EG:406996), PLOD3, RAP2A, RARG, retinoic acid, **RNF169** (includes EG:254225), SMAD5, SMARCA1, SPPL2A, **TBC1D13**, XBP1, **ZNF608**	19	13	Organismal Development Cellular Development Connective Tissue Development and Function

8	AFF4, AGT, **ANKRA2**, ARNTL2, BACH1, BANP, C11ORF82, CASP3, CD48, CLEC4E, **CPNE8**, CSH2, **CTBS**, CTSS, ERAP1, ESPL1, **GEMIN7**, **GNPAT**, GPNMB, **HIGD1A**, hydrogen peroxide, IFNG, IL13, KAT5, Mlc, MYC, **MYL5**, MYL9 (includes EG:98932), progesterone, RAD21, SLC14A2, SLC15A3, STK17A, TIPARP, TRAF2	18	14	DNA Replication, Recombination and Repair Lipid Metabolism Molecular Transport
9	Alcohol group acceptor phospho-transferase, Calcineurin protein(s), CDK7, Creb,CTGF, DAAM1, **DCAF7**, **DDIT3**, DYRK1A, **EGR1**, Elastase, ERK, ERMP1, FGF2, Focal adhesion kinase, GNA13, Igfbp, Integrin, KLF5, LDL, MAP2K1/2, Mek, Mmp, Nfat (family), P38 MAPK, Pkc(s), Pld, **PPAP2A**, Rac, Ras, Ras homolog, RCAN1, Rsk, TACC1, Vegf	18	14	Nervous System Development and Function Cell Signaling Vitamin and Mineral Metabolism
10	ADRB2, **C18ORF55**, CALCOCO2, CCDC49, CCDC85B, CCNH, CDC45L, **DEM1**, DKFZP761E198, FTSJ1, **GIN1**, GTF2B, HLA-B, HNF4A, **MICAL3** (includes EG:57553), NCOA1, NCOA3, ONECUT1, PNKP, POLB, POLE3, POLR2A, PSMA1, PSMA3, PSMA5, RAB1B (includes EG:81876), RFC3, **TACO1**, TAF1D, TP53RK (includes EG:112858),TRMT6, TRMT61A, **TSEN34**, YBX1, **ZFAND2A**	15	11	Gene Expression DNA Rep., Recomb., & Repair Dermatological Diseases and Conditions
11	AHSG, ATP6V1H, CA9, CCDC59, CCDC101, CIDEC, CPB2, GSTA5, **HACL1**, **HIST1H2BC**, HNF1A, HNF4A, IDH1, IGF1, IGFBP6, MAP3K7, MTTP, **MUTYH**, NBR1, NLK, PHF2, POLE3, POLR1C, POLR3E, PPARG, **PTPRG**, RPL10, SCAND1, SLC10A1, SLC2A2, TBPL1, **TRPV2**, UGT2B15, VHL, **YEATS2**	15	11	Cellular Growth and Proliferation Connective Tissue Development and Function Tissue Morphology

12	ANXA9, **ARHGEF10L**, ARSA, ARSB, ARSD, ARSE, ARSF, ARSG, ARSI, ARSJ, ATF7IP, ATXN1, ATXN1L, **CALY**, FNG, **HCFC2**, IFIT1L, Ifnar, IL10RA, IL18RAP, IL1B, MT1F, NOTCH1, NR4A1, PELI2, **RFNG**, **SENP3**, STAT4, SULF1, SULF2, **SUMF1**, TAL1, VSNL1, ZC3H12A, ZNF804A	13	10	Skeletal and Muscular System Development and Function Infection Mechanism Molecular Transport
13	ACBD3, **ACCN3**, AKAP, AKAP3, AKAP11, AKAP13, CDKN2A, EXO1, GHRH, Gpcr,**GPRASP2**, GRIA4, KIAA0101, KLK4, MAP2, **MELK**, MLH1, NFYB, PCNA, POLD2, POLD3, POLH, **POLM**, PRKACA, PRKAR1A, PRKAR2A, PSD3, RAC1, RFC1, RFC3, RFC4, S1PR2, SYNJ2, TARDBP, **ZNF323**	13	10	DNA Replication, Recombination and Repair Post-Translational Modification Cell Cycle
14	ADCY, Akt, Ap1, ARL4C, C1q, CEBP-AP-1, Ck2, Collagen type I, CTNNA1, Cyclin A, EIF5, ERK1/2, FMOD, FSH, hCG, Histone h3, IgG, IL12 (complex), Insulin, Interferon alpha, Jnk, KIAA0895, Lh, Mapk, MED28, MIR124, OPN1SW, PI3K, Pka, PLC gamma, Rb, RGS20, RNA polymerase II, **STEAP1**, TJP2	12	9	Cellular Assembly and Organization Skeletal and Muscular System Development and Function Gene Expression
15	DPP4, **GPC2**	2	1	Cell Cycle Cellular Development Developmental Disorder
16	butyric acid, SPHAR	2	1	Cell Cycle Cell Death Cellular Development
17	**D2HGDH**, RAB25	2	1	
18	CLCC1, MIR197	2	1	
19	**FAM188A**, RPL8	2	1	
20	BRD2, **RAB24**	2	1	Cancer Immunological Disease Cell Death
21	CSGALNACT2, Glucuronylgalactosyl-proteoglycan beta-1,4-N-acetyl-galactosaminyltransferase	2	1	Carbohydrate Metabolism Small Molecule Biochemistry

22	HLA-A, UGGT1, UGGT2	2	1	Neurological Disease Ophthalmic Disease Dermatological Diseases and Conditions
23	acad, ACADSB, Acyl-CoA dehydrogenase, phosphate	2	1	Cardiovascular Disease Hematological Disease Carbohydrate Metabolism
24	POP1, POP4, POP7, RPP14, RPP21, RPP30, RPP38, **RPP40**	1	1	RNA Damage and Repair RNA Post-Transcriptional Modification

Table A.4: SW1088CR Top-scoring Networks. Boldfacing indicates overexpressed gene. Genes that are underexpressed are underlined. Genes in plain type are gene that were connected to differentially expressed genes by IPA to form network

ID	Molecules in Network	Score	Focus Mol.	Top Functions
1	26s Proteasome, ABCD3, **APBA3**, **APOL3** (includesEG:80833), ATP2A2, ATPase, **AUTS2** (includes EG:26053), BCL2L1, **CARD8**, CD74, **CDH22**, **CLPX**, CXCL16, **FCGR2A**, FKBP8, IFN β, IL12 (complex), Interferon α, MHC Class II, MUC2, NFkB (complex), peptidase, POT1, **PSEN2**, RAD23B, **RFXAP, SKIV2L**, **STAM2**, **TLR3**, UBE2E2, UBE2E3, Ubiquitin, **VAV3**, VCP, WRN (includes EG:7486)	48	26	Cell Signaling Vitamin and Mineral Metabolism Molecular Transport
2	ABI2, ACTG2 (includes EG:72), Ap1, Coup-Tf, Creb, **CYFIP2** (includes EG:26999), DUSP3, EFNB2, ERK, FSH, hCG, Histone h3, HMBS, IGFBP3, ITGAX, LDL, Lh, LRP, LRPAP1, Mek, MKNK1, **MZF1**, NR2F2, OLFM2, P38 MAPK, PKM2, PLAU, PROCR, RPS6KA4, SLC39A8,**SMARCC2** (includes EG:6601), **SP1**, Tgf beta, **TRPV1**, Vegf	35	21	Gene Expression Organismal Injury and Abnormalities Neurological Disease
3	**ABCC2**, Akt, ARHGDIB, BRAP, Calmodulin, Clathrin, **CLTCL1**, ERK1/2, Estrogen Receptor, **HIP1**, Hsp90, Insulin, Mapk, **NCOA6**, **NRGN**, Pdgf, PDGF BB, PI3K, PIK3C2A, PIK3CA, Pkc(s), PLC γ, PROS1, Proteasome, QARS, Rac, Ras, **RXRA**,SLC3A2, SOCS2, STAT, STAT5a/b, **TNK2**, tyrosine kinase, UBE3A	24	16	Carbohydrate Metabolism Lipid Metabolism Small Molecule Biochemistry

4	ABCG2, ACAA1, ACTN2, β-estradiol, **CCDC24** (includes EG:149473), CD44, CENPM, COLEC12, DDR1, DISC1, DLG1, EXOC1, **HEATR6**, HSD17B7, **HYAL2**, KCTD12, LRP12, **METTL2B**, MPP5, MPP7,NFYB, NHP2, PDGF BB, PDLIM1, **PGS1**, PTPN11, RFX5, RG9MTD1, **RHPN2**, SH3BP5, TMBIM6, TRAF6, TUFM, ZFP36, **ZNF692**	22	15	Drug Metabolism Molecular Transport Small Molecule Biochemistry
5	AK2, ARFIP1, ARPC1B, BNIP1, CTNNB1, CTSA, DHRSX, ELOVL1, FKBP10, GPR37, HNF4A, LSR, MFSD1, MIR124, **NUFIP1**, Oxidoreductase, PDE1C, PDIA5, PIH1D1, PKM2, PRPF31, RAB10, RECQL4, RNU2-1, RNU4-1, **RNU5A**, RNU6-1, SCFD1, SLC2A4, SNX17, STOM, TTC19, UPF3B, VAMP7, YKT6	21	15	Molecular Transport Protein Trafficking Lipid Metabolism
6	ARNT2, BCL9, Bcl9-Cbp/p300-Ctnnb1-Lef/Tcf, CCND1, CCNDBP1, CCS, CDC27, CDC73, CUL3, Cyclin D, DNAJB11, EGFR, EPHA2, ERI3, GRAP2, Histone h3, HOXC10, hydrogen peroxide, MIR198, MIR188 (includes EG:406964), MLL2, MRPS9, NDRG3, NT5E, PPFIA3 (includes EG:8541), PTPRD, **PTPRS** (includes EG:5802), RIMS3, SCAMP1, SETMAR, TMEM55A, **UBR1**, WDR1, **ZDHHC14**, **ZNF445**	20	14	Cell Morphology Cellular Development Cellular Growth & Proliferation
7	ALDH2, ATF6B, C14ORF1, CCDC21, CDKN1A, **CLCN6**, FAS, HELQ, HIST1H2BF, HMGB1 (includes EG:3146), HNF1A, HNF4A, HSPA5, HYLS1, LRCH2, MAT2A, MEPCE, MIR30C1, MIR30C2, **N4BP2L2**, NAT10, NFYA, NSF, ONECUT1, POLRMT, RMI1, RPA2, SEC23A, SEC23IP, SFRS1, **TBC1D15**, **TBCK**, TFB2M, ZFP64	20	14	Cell Morphology Cellular Assembly and Organization Gene Expression

8	**ANKRD32**, ATP2A2, ATXN1, B2M, BAG1, **C20ORF7**, CD40LG, CIITA, DAXX, DMPK, **ELMOD2**, ESRRA, **FASTKD2**, **FAT4**, GMEB1, **GMEB2**, HMGB2, **IDI1**, MIR133A1, MIR133A2, MIR133A-1, MIR92A1, MIR92A2, MYH6, MYH7, NR3C1, NRIP1, RNF38, **SFRS18**,SMARCA4, **SMARCC2** (includes EG:6601), TNFSF13, U2AF2 (includes EG:11338), UBTD2, UVRAG	19	13	Cellular Assembly and Organization Cellular Compromise Cardiovascular Disease
9	ABCC1, **AHSA2** (includes EG:130872), AIP, ATP, BIK, Ca2+, **CCNL2**, Ck2, DMBT1, DNAJB6, **EIF5**, EIF2AK1, Endothelin, ENTPD4, F2RL3, HSP90AA1, MIR1, MTX1 (includes EG:4580), MUC2, NCOA4, NETO2, NLRP3, NRTN, **PBX4**, PDCD6, PLSCR3, **RABL2A**, **RABL2B**, RRAD, SFRS5, **SLC9A5**, **SNAPC4**, SRPK1, STAT4, TNF	18	13	Drug Metabolism Molecular Transport Amino Acid Metabolism
10	APOBEC3C, ASS1, B2M, BCL7B, **C8ORF38**, CD38, CECR5, CKMT1B, CTSD, CX3CL1, CYP24A1, **ERAP1**, **ERAP2**, HDC, HLA-DQA1, IFNG, Ige, KPNB1, MIR25 (includes EG:407014), MTHFD1L, NUP98, PAPPA, PLTP, POLG, **PSEN2**, SHBG, SPHK2, TCF7L2 (includes EG:6934), TERF2, TERT, TNFSF13, TP53, UBE3A, ZAP70, **ZNF140**	18	13	Cell-To-Cell Signaling & Interaction Drug Metabolism Lipid Metabolism
11	ABL1, ACCN1, **ACCN3**, **ATP11C**, **ATP8B2** (includes EG:57198), BRCA1, C7ORF20, **CABLES1**, CCR7, CDC27, CDK3, CDKN1A, CIT, CTNNBIP1, DDB2, EID2, geranylgeranyl pyrophosphate, HNRNPR, IL1A, Il8r, **KIFC2**, Mg2+-ATPase, PTGER4, RAGE, Ras homolog, RHOB, RHOG, RHOH,RHOT1, RPA3, RTKN, **SUV39H2**, TRIO, WRN (includes EG:7486)	17	12	Cell Cycle Cell Morphology Reproductive System Development and Function

12	ABCC1, ADNP, **ANKRD17**, ANPEP, BIRC2, BTRC, C1ORF107, CD38, CX3CL1, DDX19B, **DGCR14**, EFNB2, FAF1, FBXO22, FBXO32, FBXW11, HGF, HLA-DR, IL11, **KLHL15**, LDHA, MAGEA11, MIR103-1 (includes EG:406895), MIR33A, NfkB-RelA, NFKBIE, OTUB2, RWDD2B, SKP1, TNF, Ube3, **WDR90**, WEE1, WT1, **ZNF7**	15	11	Cellular Development Cardiovascular System Development and Function Cell Morphology
13	BANF1, BCLAF1, **BDH1**, BET1, BET1L, C3ORF10, CCDC85B, CD99 (includesEG:673094), EMD, **FAM53B**, GCNT1, GMCL1L (includesEG:64396), GOLGA2, GOLGB1, GOSR1, GOSR2, **KIAA1688**, LEMD3, LMNA, LMNB1, MEAF6, **PILRB** (includes EG:29990), **PRPF3**, RAC1, SCFD1, SEC22A, **SLU7**, SYNE2, TGFB1, TOR1A, TOR1AIP1, USO1, VPS72, WISP1, YKT6	15	11	Cellular Assembly and Organization Cellular Function and Maintenance Molecular Transport
14	2-oxoglutaric acid, ALK, ALKBH1, BCL2L10, BID, BNIP3L, CASP3, CASP8AP2, Caspase, CHKA, CHRNA7, Cytochrome c, DBN1, **EGR2**, EPB41L1, HN, HSH2D (includes EG:84941), HTRA2, HTT, IKBKG, Jnk, MOAP1, **PACS2**, RIC3 (includesEG:79608), SRP72, STEAP3, TAOK1, tauroursodeoxycholic acid, THAP11, **TMEM90A**, TPP1, USO1, **UTP20**, **ZNF598**, ZNF675	13	11	Cell Death Embryonic Development Nervous System Development and Function
15	**ANGEL1**, ANK2, ANKRD12, APP, C10ORF71, DNAJC18, E2F3, EFNB1, EZR, FAM49B, FRMPD3, **HECTD2**, HNRNPU, HOXA1, HUWE1, IL6, KPNA4, MAP2K4, MARCH6, MECP2, MIR202 (includes EG:387198), MIR34A (includes EG:407040), MIRLET7D (includesEG:406886), MIRLET7F1 (includesEG:406888), MIRLET7F2 (includesEG:406889), NAV3, NEDD4L, NR4A2, **PABPC1L**, POU4F1, **SCN3A**, TMEM25, TMEM104, TRIP10, ZZZ3	6	6	Cellular Movement Nervous System Development and Fucntion Cellular Development

16	**DHX34**, POLA2	2	1	Molecular Transport Protein Trafficking DNA Rep., Recomb., & Repair
17	**D2HGDH**, RAB25	2	1	
18	**TRMU**, tRNA(5-methylaminomethyl-2-thiouridylate)-methyltransferase	2	1	Auditory Disease
19	HLA-A, **KDM5D**	2	1	Neurological Disease Ophthalmic Disease Dermatological Diseases & Conditions
20	DUB, **USP35**	2	1	
21	KNTC1, ZW10, ZWILCH	2	1	Cell Cycle DNA Rep., Recomb., & Repair Cellular Assembly & Organization
22	Cpt, CPT1, **CPT1C**	2	1	Digestive Sys. Dev. & Func. Lipid Metabolism Small Molecule Biochemistry
23	MIR204 (includes EG:406987), MIRN326, MIRN343, **PRR7**	2	1	Cellular Development Cellular Growth & Proliferation

Table A.5: U87 Top-scoring Networks. Boldfacing indicates overexpressed gene. Genes that are underexpressed are underlined. Genes in plain type are gene that were connected to differentially expressed genes by IPA to form network

ID	Molecules in Network	Score	Focus Mol.	Top Functions
1	ANXA13, **BRE**, Collagen type I, Cyclin A, Cyclin E, **DDR1**, **DDX17**, DOT1L, E2f, E2F3, GNA15, **HAS2**, Hdac, Histone h4, **KRAS**, **KRT17**, **MCM6**, MFHAS1, MUC2, NCOR1, NFkB (complex), **NPTXR**, PURA, Rb, Rxr, Smad2/3, SNW1, **SP3**, SPINK1, **STAP2**, TFE3, Thyroid hormone receptor, **TNC**, **TRIP11**, VSNL1	45	24	Cell Cycle Connective Tissue Development and Function Cellular Assembly and Organization
2	ADAM17, **AGTRAP**, Calpain, CK1, Creb, **CSNK1E**, **CSNK1G3**, **ELAVL1**, ERK, Focal adhesion kinase, **GAB1**, **GSK3B**, **HEXA**, LDL, Mek, MITF, MT1E, NRG1, Pdgf, PDGF BB, PHLPP1, Pkc(s), Ras, **RPN2**, Rsk, **SART3**, **SFRS2**, Smad, STAT, STAT5a/b, STAT5B, **TBX21**, Tgf beta, Vegf, VEGFA	30	18	Cell Cycle Cardiovascular System Development and Function. Cellular Development
3	ADIPOR1, Akt, Alpha tubulin, Ap1, APBB1, **AURKB**, Calmodulin, **CCDC88A**, **CDK8**, **CDKN1A**, Estrogen Receptor, **HAX1**, hCG, HISTONE, Histone h3, Insulin, **KHDRBS1**, **KIF22**, **LRRN3**, Mapk,**MSN**, P38 MAPK, **PHKB**, PI3K, Proteasome, Rac, Ras homolog, RNA polymerase II, Rock, **SMPD1**,**SNRPN**, SNX9 (includes EG:51429), **SORBS2**, **UBE3A**, Ubiquitin	27	17	Cancer Genetic Disorder Lipid Metabolism
4	BBC3, **C3ORF19**, **C6ORF170**, CBFB, CDKN3, CENPF, **CHRNB1**, CLMN, DDB2, DTL, FBXL18, FERMT2, **IFIT3**, ITGA2B (includes EG:3674), **KLHL3**, MGMT, NFYB, PLK2, retinoic acid, RFC4, **RWDD2A**, SERPINB2,SLC22A18, SLC39A8, **SLIT3**, SNX19, SSRP1, TGFB1, TNFAIP6, TP73, TPSB2, TYMS, UTP3, **YIPF4**, ZFP36	22	14	Cell Cycle Embryonic Development Tissue Development

5	BAI2, CDC42EP3, CHMP4A, DKK1, DLST, **EDEM3**, EXOSC8, EXOSC10, **FEM1C**, GTF2E1, HBP1, HEY1, HIST1H2BO, HMGB2, HMGB1 (includes EG:3146), HNF4A, HOXB3, HOXD11, ING3, JINK1/2, **LPPR2**, LSM3, MDM2, MIRN101B, **MOCS3**, **MYPOP**, **NOB1**, **PPIG**, PSMA3, SCFD1, STAMBP, TARDBP, UMPS, UPF2, **XRN2**	20	14	Gene Expression Infection Mechanism Infectious Disease
6	ABCC9, ATAD2, BLK, CCND1, **CDC73**, CEP192, **CHST10**, CKS1B, **CUEDC2**, CXCL14, DECR1, DOCK2, EML1 (includes EG:2009), ERBB2, ESR1, FGF2, GPAA1, GPC1, H19, HEXDC, **ISG20L2**, KCNJ1, magnesium-adenosine triphosphate, MIF, MKI67, MXD3, **NOMO1**, **RILPL2**, RNF149, SHBG, SRC, TUBB4, VAV1, WWC1, ZBTB17	18	12	Cancer Reproductive System Disease Cell Cycle
7	ABCB7, BAX, BBC3, CCL3L1, CCNE2, DDX1, **DNASE2**, EAF1, **EPC2**, GPAA1, HIGD1A, IL6, **KIAA1217**, KIF11, MAZ, MFN1, MFN2, **MPHOSPH8**, MYC, PEG3, PIGK, PIGS, PIGT, PIN1, PLSCR4, PNPT1, PRPH, **RMND5A**, RUVBL2, SMAD9, **TRIP12**, UBE2C, **VPS72**, YEATS4, ZNHIT1	17	12	Cellular Assembly and Organization Cancer Cellular Compromise
8	ABCB1B, ACAT1, AHNAK, AIMP1, ALDH3A1, APP, arachidonic acid, ATP5O, **ATP6AP1**, **BCAS4**, CCDC93, CDH13, CH25H, **CLSTN3**, DNAJB4, ETFA, F2RL3, GOT2, MIRLET7A1, MPG, **MT1E**, PDIA6, **PHF8**, PHGDH, PRPSAP2, RTN3, SAA2, **SCPEP1**, SLC2A4, SND1, **SOAT1**, SOD2, STXBP3, STXBP5, TNF	17	12	Molecular Transport Lipid Metabolism Small Molecule Biochemistry

9	APOD, beta-estradiol, CALCR, CLDN6, CLDN14, **CNNM4**, CTNNB1, CXADR, **DGCR6L**, DLG4, DVL1L1, **ERLEC1**, **FBXO45**, FZD8, HSPA2, HSPA5, HSPA12A, KRT5, KRT19, LDHB, MIR24-1 (includes EG:407012), MYF5, NEK8, NPTX1, NRCAM, OS9, PTP4A2, **SAV1**, SFN, **SFRP2**, SIPA1L1, STK3, TRIM25, TUBG1, WNT3	17	12	Cell Cycle Cell Morphology Cellular Assembly and Organization
10	ACSS2, ADAM21 (includes EG:8747), ATYPICAL PROTEIN KINASE C, **BEST1**, **C12ORF30**, **C17ORF63**, C7ORF16, CDK2, cholesterol, CSHL1,HEY1,MAML1, **MAML2**, MAPK1, MAZ, Metalloprotease, MIR23B (includes EG:407011), NOTCH1, NOTCH3, PPM1A, PPP1R8, PPP2CA, **PREB**, PRKCH, PRL, PTPN18, putrescine, RHBDF2, **SFRP2**, ST8SIA1, TK1, **TNRC6B**, TSPYL2, TTK, WNT4	16	11	Gene Expression Cell-To-Cell Signaling and Interaction Hematological System Development and Function
11	ADCK4, AK1, AMIGO2, BRD2, CNTN2, COMT, DBF4, ELL, **ENOX1**, FHL2, **GPR158**, **HCFC2**, Histone-lysine N-methyltransferase, ING1, MDM4, MEN1, MGMT, NR3C1, POLH, POLK, PPA1, PPP5C, RAB24, RAD54L, REV1, RNF38, SETD7, SPHK2, TADA3L, TK1, TP53, UBC, Ube3, ZBTB16, ZNF346	15	11	Cell Cycle DNA Replication, Recombination, and Repair Cell Morphology
12	ACT1, BTG3, Caspase, CTLA2A, **CYB561**, DDB2, **DDR1**, ECSIT, ERK1/2, FGF13, **FGF19** (includes EG:9965), GAS2, GAS5, **GCGR**, HRSP12, IL1, IL12 (complex), IL17RA, Interferon α, Jnk, KCTD12, KLB, Lh, MIR124, **MTPN**, Nfat (family), **RYK**, **SPOP**, TLR11, TMEM109, **TRAF6**, VEGFB (includes EG:7423), ZNF274, ZNF675, ZNRF3	12	10	Lipid Metabolism Molecular Transport Small Molecule Biochemistry
13	CTSLL3, LGALS3	2	1	Cell Morphology Cellular Assembly and Organization Cellular Development

14	ERMAP, MIR146A	2	1	Inflammatory Disease Genetic Disorder Skeletal & Muscular Disorders
15	PGAP1, SIRT3	2	1	Amino Acid Metabolism Post-Translational Modification Small Molecule Biochemistry
16	Methionyl-tRNA formyltransferase, **MTFMT**	2	1	
17	AR, **CTSO**	2	1	Cell Cycle Cellular Development Cellular Function & Maintenance
18	ATXN7L1, ZNF862	2	1	
19	**GRAMD1C**, MIR292	2	1	
20	**ANKRD7**, MARK3	2	1	Organ Development Reproductive Sys. Dev. & Funct.
21	COG8, **NBPF10**	2	1	Genetic Disorder Metabolic Disease
22	EFHD2, MIR126, RAD51L3	2	1	Cardiovascular Disease Cardiovascular Sys. Dev. & Funct. Organismal Development
23	HTN1, MUC7, MUC5B	2	1	Genetic Disorder Inflammatory Disease Respiratory Disease
24	**ISY1**, MIR1, MIR1-1 (includes EG:406904), MIR1-2 (includes EG:406905)	2	1	Cardiovascular Disease Cardiac Arteriopathy Genetic Disorder

Table A.6: U87CR Top-scoring Networks. Boldfacing indicates overexpressed gene. Genes that are underexpressed are underlined. Genes in plain type are gene that were connected to differentially expressed genes by IPA to form network

ID	Molecules in Network	Score	Focus Mol.	Top Functions
1	Actin, Akt, ATPase, **C20ORF20**, Caspase, **CCR1**, CD40, **CHMP7**, DNMBP, HISTONE, Histone h3, Histone h4, Hsp70, Hsp90, IL1, IL12 (complex), Interferon alpha, Jnk, **MCM3**, **MED28**, MYO9B, **NUMA1**, P38 MAPK, PI3K, PRX, **RDBP**, RNA polymerase II, RNU4-1, RNU5A, **SLC30A7**, SMARCA5, Ubiquitin, USP8, VPS72, **ZNF668**	30	18	Cell Death Cellular Development Cellular Growth and Proliferation
2	26s Proteasome, Ap1, APBA2, APH1B, CAPN1, CAPN3, **CAT**, CCNA2, EGR1, ELOVL2, ERK, ERK1/2, **FAM189B**, **FERMT2**, **FJX1**, Focal adhesion kinase, GIPC1, GTF2H1, hCG, Integrin, LDL, Mapk, Pdgf, PDGF BB, peptidase, Pkc(s), PLC, PLC gamma, **PLEKHA1**, PSEN2, SENP6, STAT, **TAF1B**, Tgf beta, Vegf	28	17	Post-Translational Modification Gene Expression Cell Cycle
3	AKIRIN1, **APIP**, **ARID4A**, **BFSP1**, **C10ORF2**, CDC2, CRADD, CRCT1 (includes EG:54544), DNAJC7, E4F1, EDN1, **FERMT2**, FN1, FRYL, **HEG1**, ITGB3, ITGB6, ITGB8, MIR292, MIR27B (includes EG:407019), MORF4L1, MORF4L2, NCOA2, **PPFIA1**, PPFIA2, **PPP2R5E**, **RABGAP1**, RB1, **RBBP9**, **RIF1**, RNF121, SMAD9, **UBE4A**, VIM, ZNF638	28	17	Cellular Movement Reproductive System Development and Function Cell Cycle
4	**CABIN1**, Calcineurin A, CD3, CENPO, Cpla2, **CSF2**, E2f, **F2R**, FKBP8, FLNB, HLA-DR, Ige, IKK (complex), **IL1A**, JINK1/2, **KRT75**, **MADD**, **MAP4K1**, Mek, MET, NCK, NFAT (complex), Nfat (family), NFkB (complex), PLCG1, Rap1, Ras, Ras homolog, RIPK2, RRAS, Sapk, **SNX18**, SOS1, TCR, WIPF1	25	17	Cellular Development Cellular Growth & Proliferation Hematological System Development and Function

5	ALDH3A2, ALPP, COL7A1, CTSC, **CYP11B1**, **DMXL1**, EGLN1, ELOVL7, EPAS1, EPHX1, **FERMT2**, GCLC, glutathione, HIST1H2AC, **HIVEP3**, IKBKG, ITGB6, ITGB8, ITPR2, JUN, KIAA1310, LAMP2, MIA3, MVD, **NAT1**, PCYT1A, RDH5, retinoic acid, SLC16A3, SREBF1, TGFB1, TGFB3, TSPAN2, Type II Receptor, **UTP20**	24	15	Drug Metabolism Molecular Transport Gene Expression
6	ACAA2, AHNAK, APOD, arachidonic acid, beta-estradiol, Calmodulin, CDH15, Ck2, CKB, **CREB3L2**, **DEPDC1**, DMD, EPB41L3, **FARSA**, GMFB, HADHB, **IRX5**, ITGBL1, **KANK1**, KCND2, LITAF, **LYPLA2**, MIR124, NOP2, OSTF1, PCYT1A, **PLA2G2E**, PLA2G4A, PPFIBP1, PSEN2, PTP4A1, STXBP1, **TSFM** (includes EG:10102), YWHAZ, **ZCCHC24**	24	15	Lipid Metabolism Molecular Transport Small Molecule Biochemistry
7	AIFM2, **ANKRD32**, **ARL4C**, BLM, **C12ORF5**, **CHD7**, CLIC1, CREB1, DAGLB, EP400, ERCC3, ERCC5, GH1, IKBKE, ING1, **JMJD1C**, MAGMAS, **METTL11A**, MPHOSPH6, MYO9B, PACRGL, PCNA, PPARG, PSENEN, PSMC2, RAD18, RECQL5, SEPT2, **SHPRH**, SMARCA4, SMARCA5, TAF1C, TMEM33, TOP3A, TP53	23	15	DNA Replication, Recombination and Repair Nucleic Acid Metabolism Small Molecule Biochemistry
8	ACOX3, BMP2K (includes EG:55589), **C14ORF147**, CCNG1, COPS8, **COPS7A**, COPS7B, **CTDSPL2**, DDX41, FHIT, **FYCO1**, **GDAP2**, GPT, HNF4A, HSD11B1, **HSDL2**, IGF1, INADL, IRS4, LCN2, **MAK16**, MAPK7, palmitoylcoenzyme A, PI4KB, PTPN4,RAB11A, SERPINA3, **SULT1C2**, **TIGD6**, TNFRSF11B, TUBB3, TUBB4, VEGFC, VTN, **ZZEF1**	22	14	Connective Tissue Development and Function Skeletal and Muscular System Development and Function Tissue Morphology

9	ACT1, APP, BAT2, CCDC33, CCDC101, CCR10, CPSF3, Filamin, FLNA, FLNB, FOLR1, GMFB, GNB5, GRB2, GSTK1, HSPA1L, KCND2, **MADD**, MAP3K7, NCBP1, NOC4L, **OPN4**, **RHPN2**, **RTN3**, SEPT9, **SEPT11**, SH3PXD2A, SNX17, SSSCA1, TRAF2, TRAF6, TRAIP, VTA1, **XPO4**, **YEATS2**	21	14	Protein Synthesis Cell Signaling Cellular Assembly and Organization
10	**AKD1**, ARF3, BUB1B, CD274, **CENPC1**, CENPE, CENPH (includes EG:64946), CRADD, E2F1, GABPB1 (includes EG:2553), GCA, GCAT, GPR176, **HIVEP2**, KIF2C, MIR17 (includes EG:406952), NAPEPLD, NDC80, PCYT1A, PEA15, **PHF13**, Pld, **POLA2**, PRIM1, PRIM2, PTEN, RALGDS, **RMND5A**, RRM1 (includes EG:6240), STXBP1, TNF, TNFRSF4, YY1, ZFP36, ZFP36L1	18	12	Cellular Assembly and Organization DNA Replication, Recombination, and Repair Immunological Disease
11	26s Proteasome, ADCYAP1, ANAPC5, ANAPC7, APC, ATF3, CASP6, Cbp/p300, CD80, CDC6, CDC20, CHGB, CREBBP, Cytochrome c, DHFR, EGR1, EPAS1, FZR1, **GALNT7**, GNRHR, MAF, MIR24-1 (includes EG:407012), MLL, NFE2L2, NKX2, NR5A1, PMF1, RAB4B, SAT1, SERPINA3, SLC2A1, SS18L1, TK1, **ZDHHC5**	9	7	Cancer Gene Expression Cell Death
12	**ARMCX5**, ZNF217	2	1	Cellular Development Cardiovascular Sys. Dev. & Funct. Cellular Function & Maintenance
13	**PARS2**, Proline-tRNA ligase	2	1	
14	ASNSD1, Asparagine synthase (glutamine-hydrolysing)	2	1	
15	**RBM33**, SUMO3, ZNF143	2	1	Gene Expression Post-Translational Modification Infection Mechanism
16	AKAP3, **ROPN1L**, YBX2	2	1	Cellular Development Reproductive Sys. Dev. & Funct. Cell Signaling
17	FBXW12, FIGLA, LOC728622	2	1	Cellular Compromise Organ Development Reproductive Sys. Dev. & Funct.

Chromosome	A172	SW1088	U87
1	+		+
2	+		
3	+		
4	-		
5	+		
6			
7	+		
8	+		
9	+	+	
10	+		
11	+		
12	-		
13	-	-	-
14	-		-
15	-	-	
16	+		
17	+		
18	+	-	
19	+	-	
20	+	+	
21	+		
22	-		
X			
X/Y	+	+	
Total	**66-80**	**63-63**	**44**

Table A.7: Gross chromosomal gains (+) and losses (-) reported for 3 parent cell lines. Chromosomal gains and losses are presented relative to ploidy of parent cell line. Blank cells indicate no changes. Data adopted from reference [147].

Cell	Chromosomal Changes
A172	XXY, i(X)(p10)[18], +Y[15], +1[15], der(1)t(1;18)(q?;q?)[17], der(1)t(1;17;14)(1qter→cen→1q?::17p?::14q?→14qter)[20], der(1)t(9;1;17;14)[5], ider(1)t(X;1;18;1)(Xp?::1q?::18::1q?→cen→1q?::18::1q::Xp?)[20], +2[10], der(2;5)(q33;q13)[22]×2[11], +3[10], der(3)t(3;9)(q27;p13)[17], 4[5],+5[12], del(6)(q12)[20],+7×2[18], del(7)(q32)[2], der(7)t(6;7)(q?;q11)[19], der(7;19)[3], +8[12], del(8)[18], +9[13], der(9)inv(9)t(9;16)(16q?::9p?11→cen→9q34::9p?11→9pter)×2[19], dic(9;14)(9qter→cen::14q21→cen→14pter)×2[22], +10[11], der(10)t(1;10)×4[11], der(10)t(1;10)×3[5], der(10)t(1;10)×2[6],+11[11], der(11)t(1;11)[17], der(1;11)[17], 12[5], del(12)(p11)[19], 13[11], 14×3[22], 15[5], +16[18], +17[17], +18[12], der(18)t(1;18)×3[11], der(18)t(1;18)×2[11], del(18)[2], +19[13], der(7;19)×2[4], der(7;19)[2], der(19)t(10;19)(?;p13)×2[10], der(19)t(10;19)[8],+20[16], +21[13], der(21)t(2;21)[12], 22[16][cp22]
SW1088	XXY, +Y[12], +del(1)[15],der(1)t(1;18)[13], del(3)[2], der(6)t(6;19)[5], der(7)t(3;7)[3],r(8)[2], +der(9)t(7;9)[17], der(7;9)[3], der(10)t(4;10)[2], der(10)t(10;15)[5], 13[9], 15[21], 18[10], 19[7],+20[17][cp21]
U87	X, X, der(1)t(1;13)(p13;q?)×2, +der(1;20)t(1;14)(p?;q?)t(1;20)(p10;q10), der(6)t(6;7)(p12;p?), der(6)t(6q;18;6q;12q), ins(9;13)(p13;q?), del(10)(q11), del(11)(q12), der(12)t(6;12)(q?;q?), 13, 14, der(16)t(1;16)(p?;p?), del(20), der(22)t(10;22)(q?;p?)[10]/44, idem, ins(2;16)(p?;?)[10]

Table A.8: Detailed chromosomal aberrations reported in 3 parent cell lines. Table adopted as reported in reference [147].

Gene	A172	SW1088	U87
P53	Mutant Function[148]	Not Reported	Wild-type Function[148]
P21	Wild-type Function [149]	Not Reported	Wild-type Function[14]
P16 (INK4A)	Wild-Type Function [149]	Not Reported	Homozygous Deletion[150]
RB	Not Reported	Not Reported	Wild-type Function[151]
Chk1	Not Reported	Not Reported	Wild-type Function[152]
Chk2	Not Reported	Not Reported	Wild-type Function[152]
Mgmt	No Activity[85]	Not Reported	No Activity[153]
P-glycoprotein	No Activity[154]	Not Reported	No Activity[155]

Table A.9: Genetic alterations and activity status of genes involved in cell cycle regulation and drug resistance reported in literature for the three parent cell lines. Reference indicated in parenthesis**.**

CURRICULUM VITA

SALAHELDIN S. HAMED

EDUCATION:

2000-2003 B.S. Biomedical Engineering, Rutgers, The State University of New Jersey, Piscataway, NJ

1997-2000 A.A.S Natural Sciences and Mathematics, Bergen Community College, Paramus, NJ

RESEARCH:

2003-Present **Graduate Fellow,** Dept. of Biomedical Engineering, Rutgers University, Piscataway, NJ

Summer 2008 **Summer Intern**, Center for Research in Biomedicine, University of The West of England, Bristol, U.K.

Summer 2003 **Summer Intern**, Metabolic Research Dept., Bristol-Myers Squibb, Hopewell, NJ

2002-2003 **Research Assistant**, Dept. of Biomedical Engineering, Rutgers University, Piscataway, NJ

PUBLICATIONS:

Hamed SS and Roth CM, "Modeling Chemotherapeutic Dose Response Curves via Cell Cycle Dynamics". Submitted to Journal of Pharmacokinetics and Pharmacodynamics, Jan 2010.

Hamed SS and Roth CM, "Understanding Changes Associated with Acquired Resistance to Carmustine in Glioma Cell Lines Through Gene Expression Profiling". To be submitted, Feb 2010.